ENFOQUE

UTE

REVISTA

Facultad Ciencias de la Ingeniería e Industrias
elSSN:13906542

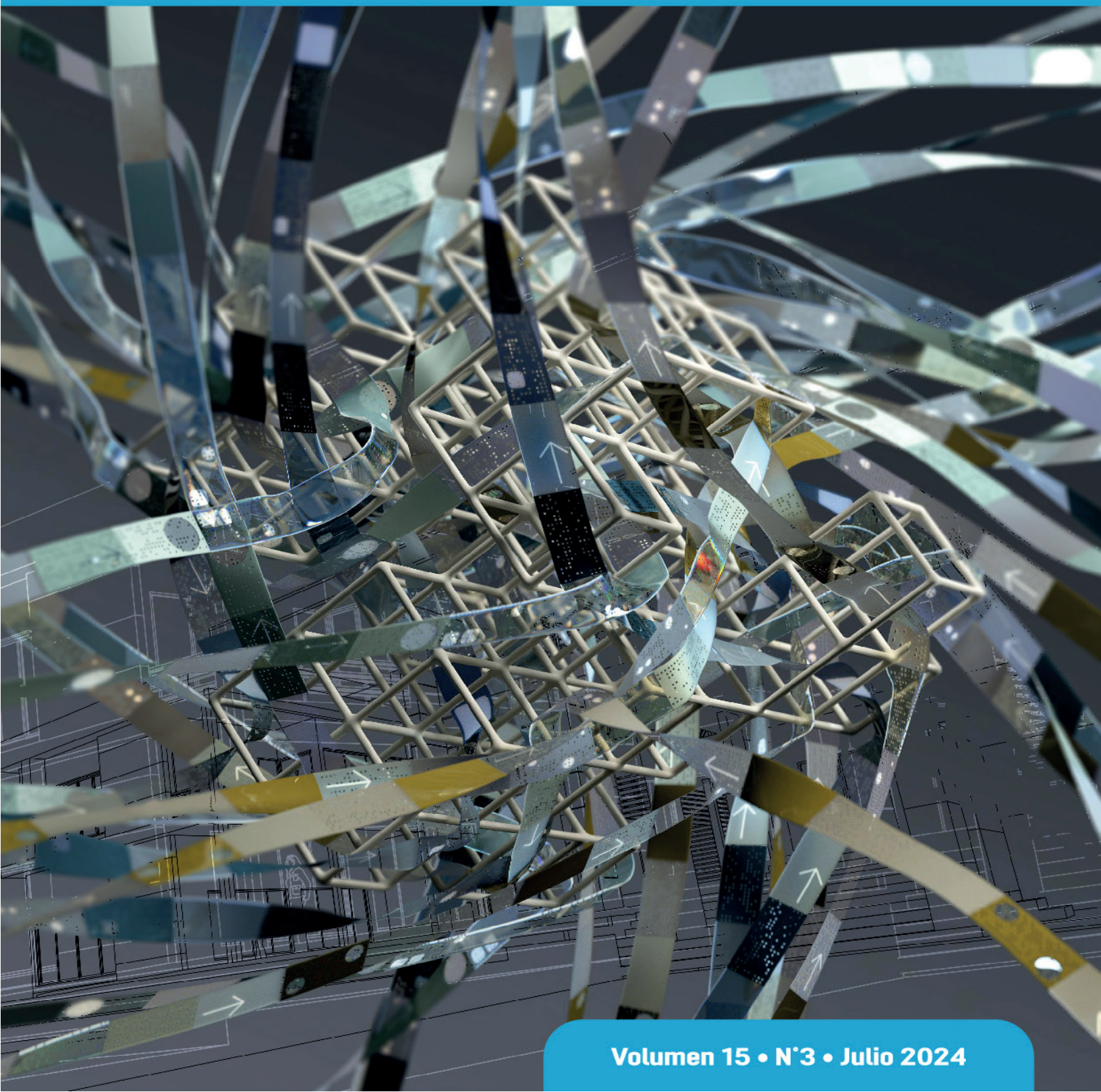

Volumen 15 • N°3 • Julio 2024

Sumario

ENFOQUE UTE REVISTA
Facultad Ciencias de la Ingeniería e Industrias
eISSN:13906542

Editorial

Estimadas y estimados lectores:

Nos complace presentarles la edición del tercer número del volumen 15, correspondiente a los meses de julio-septiembre de 2024 de la *Revista Enfoque UTE.* En esta ocasión, hemos reunido una selección de artículos que reflejan los avances y desarrollos más recientes en diversos campos de la ingeniería. Estos trabajos representan el esfuerzo y la dedicación de investigadores de diferentes instituciones, quienes han aportado sus conocimientos y descubrimientos para el enriquecimiento de la comunidad científica.

Como siempre, los artículos incluidos en esta edición han pasado por una rigurosa revisión por pares de expertos nacionales e internacionales.

Tras este exhaustivo proceso, hemos seleccionado seis artículos que conforman el presente número, donde se incluyen investigaciones destacadas como "Analysis of Ultra-Dense Wavelength Division Multiplexing (UDWDM) in a Passive Optical Network (PON)" por Nubia Mancha y su equipo de la Escuela Politécnica Nacional del Ecuador. Este estudio ofrece una visión innovadora sobre la implementación de tecnologías ópticas avanzadas en redes pasivas, proporcionando una perspectiva crucial para el futuro de las telecomunicaciones.

Desde México, el equipo liderado por Megchun-García Juan Valente del Instituto Nacional de Investigaciones Forestales, Agrícolas y Pecuarias nos presenta el artículo "Thiamethoxam Residuality in Papaya Plant and Fruit (Carica papaya Linnaeus) Cultivated in Rotation with Watermelon (Citrullus lanatus)", una investigación fundamental para comprender la residualidad de pesticidas en cultivos rotativos y sus implicaciones para la seguridad alimentaria.

La innovación en transporte y medio ambiente es abordada en "Ecological Motorcycle Taxi, incorporation of an electrolyzer as an alternative for the suppression of pollutants and noise reduction" por Manuel Rodríguez-Perez y su equipo de la Universidad de Trujillo, Perú. Este trabajo explora nuevas tecnologías para la reducción de emisiones contaminantes y ruido en el transporte urbano, proponiendo soluciones ecológicas prácticas y efectivas.

El artículo "CFD simulation of the surface pumping of heavy crude oil in eastern Ecuador", de José Cabrera-Escobar y su equipo de la Universidad Nacional de Chimborazo, presenta una simulación detallada del bombeo superficial de crudo pesado, contribuyendo significativamente a la optimización de procesos en la industria petrolera.

Desde la Universidad Autónoma de Ciudad Juárez, Omar Celis-Gracia y su equipo nos presentan "Reduction of Setup Times in a Metal Fabrication Company Using a Lean-Sigma Approach". Este estudio se enfoca en la implementación de metodologías Lean-Sigma para la mejora de la eficiencia en la fabricación de metales, ofreciendo estrategias clave para la industria manufacturera.

Finalmente, Roberto Luis López Ferras y su equipo de la Universidad Central "Marta Abreu" de Las Villas en Cuba, nos presentan "Intensity-Duration-Frequency Curves for Manicaragua city, Cuba", trabajo que proporciona herramientas esenciales para la gestión de recursos hídricos y la planificación urbana en áreas propensas a eventos climáticos extremos.

Estamos convencidos de que estos artículos serán una valiosa adición a sus investigaciones y contribuirán significativamente al avance del conocimiento en sus respectivos campos.

Agradecemos su continuo apoyo y les invitamos a disfrutar de esta nueva edición de la *Revista Enfoque UTE.*

Atentamente,

Dr. Oscar Martínez Mozos
Universidad Politécnica de Madrid
Editor en Jefe

Dr. Diego Guffanti Martínez
Universidad UTE
Editor en Jefe

ENFOQUE UTE REVISTA
Facultad Ciencias de la Ingeniería e Industrias
elSSN:13906542

Editorial

Dear Readers,

We are pleased to present the volume 15, number 3 edition for the months of July-September 2024 of the Enfoque UTE Journal. On this occasion, we have compiled a selection of articles that reflect the latest advancements and developments in various fields of engineering. These works represent the effort and dedication of researchers from different institutions, who have contributed their knowledge and discoveries for the enrichment of the scientific community.

It is worth mentioning that the articles included in this edition have undergone a rigorous peer review process by national and international experts. After this thorough process, we have selected six articles that make up the current issue.

In this issue, we include noteworthy research such as "Analysis of Ultra-Dense Wavelength Division Multiplexing (UDWDM) in a Passive Optical Network (PON)" by Nubia Mancha and her team from the Escuela Politécnica Nacional del Ecuador. This study offers an innovative perspective on the implementation of advanced optical technologies in passive networks, providing crucial insights for the future of telecommunications.

From Mexico, the team led by Megchun-García Juan Valente from the Instituto Nacional de Investigaciones Forestales, Agrícolas y Pecuarias presents the article "Thiamethoxam Residuality in Papaya Plant and Fruit (Carica papaya Linnaeus) Cultivated in Rotation with Watermelon (Citrullus lanatus)", a fundamental investigation for understanding pesticide residuality in rotational crops and its implications for food safety.

Innovation in transportation and the environment is addressed in "Ecological Motorcycle Taxi, incorporation of an electrolyzer as an alternative for the suppression of pollutants and noise reduction" by Manuel Rodríguez-Perez and his team from the Universidad de Trujillo, Peru. This work explores new technologies for reducing pollutant emissions and noise in urban transportation, proposing practical and effective ecological solutions.

The article "CFD simulation of the surface pumping of heavy crude oil in eastern Ecuador" by José Cabrera-Escobar and his team from the Universidad Nacional de Chimborazo presents a detailed simulation of surface pumping of heavy crude oil, significantly contributing to the optimization of processes in the oil industry.

From the Universidad Autónoma de Ciudad Juárez, Omar Celis-Gracia and his team present "Reduction of Setup Times in a Metal Fabrication Company Using a Lean-Sigma Approach". This study focuses on the implementation of Lean-Sigma methodologies to improve efficiency in metal fabrication, offering key strategies for the manufacturing industry.

Finally, Roberto Luis López Ferras and his team from the Universidad Central "Marta Abreu" de Las Villas in Cuba present "Intensity-Duration-Frequency Curves for Manicaragua city, Cuba". This work provides essential tools for water resource management and urban planning in areas prone to extreme weather events.

We are confident that these articles will be a valuable addition to your research and will significantly contribute to the advancement of knowledge in their respective fields.

We appreciate your continued support and invite you to enjoy this new edition of the Enfoque UTE Journal.

Sincerely,

Dr. Oscar Martínez Mozos
Universidad Politécnica de Madrid
Editor-in-Chief

Dr. Diego Guffanti Martínez
Universidad UTE
Editor-in-Chief

Analysis of Ultra-Dense Wavelength Division Multiplexing (UDWDM) in a Passive Optical Network (PON)

Nubia Manchay[1], Christian Tipantuña[2], Germán V. Arévalo[3], Berenice Arguero[4], Carla Parra[5]

***Abstract*—Passive Optical Networks (PONs) are essential in optical communications to meet the increasing demand for network capacity and connected users, ensuring reliable and adaptable connections for data transmissions. These networks also simplify infrastructures and efficiently utilize energy by eliminating the need for active devices. In this context, Ultra-Dense Wavelength Division Multiplexing (UDWDM) is one of the most prominent solutions for data transmission. This technology uses the narrow separation between channels from 25GHz and even as small as 6.25GHz to increase the transmission capacity. This document analyzes the performance of UDWDM considering the transmission of three simultaneous channels in a PON network for which three different scenarios have been considered for the analysis with the following parameters: i) transmission speed from 10 Gbps to 17 Gbps, ii) the distance from 10 km to 20 km and iii) the separation between channels of 15GHz, 20GHz, and 25GHz. The performance metrics for the analyzed scenario are the bit error rate and the eye diagram. To ensure the reception of the transmitted channel, an analysis of raised cosine and Gauss filters is also discussed. Including these filters allows for verifying whether their use enhances the performance of the channels compared to transmission without a filter. This is crucial for understanding how filters can optimize the quality and reliability of data transmission in a PON, which is of great importance in environments where high efficiency and connection quality are required.**

***Keywords* - optical communications; UDWDM; PON; multiplexing; optSim; BER.**

***Resumen*—Las redes ópticas pasivas (PON) son esenciales en las comunicaciones ópticas para satisfacer la creciente demanda de capacidad de red y usuarios conectados, garantizando conexiones fiables y adaptables para la transmisión de datos. Estas redes también ofrecen un uso eficiente de la energía y la simplificación de las infraestructuras, eliminando la necesidad de dispositivos activos. En este contexto, la multiplexación por división de longitud de onda ultradensa (UDWDM) es una de las soluciones más destacadas para la transmisión de datos; esta tecnología aprovecha la estrecha separación entre canales a partir de 25GHz e incluso de tan solo 6,25GHz para aumentar la capacidad de transmisión. Este documento analiza el rendimiento de UDWDM considerando la transmisión de tres canales simultáneos en una red PON para la que se han considerado tres escenarios diferentes para el análisis con los siguientes parámetros: i) velocidad de transmisión de 10 Gbps a 17 Gbps; ii) la distancia de 10 km a 20 km; y iii) la separación entre canales de 15GHz, 20GHz, y 25GHz. Las métricas de rendimiento para el escenario analizado son la tasa de errores de bit y el diagrama de ojo. Para garantizar la recepción del canal transmitido, también se analiza la utilización de filtros coseno elevado y Gauss. La inclusión de estos filtros permite comprobar si su uso mejora el rendimiento de los canales en comparación con la transmisión sin filtro. Esto es crucial para entender cómo los filtros pueden optimizar la calidad y fiabilidad de la transmisión de datos en una PON, lo que es de gran importancia en entornos donde se requiere una alta eficiencia y calidad de conexión.**

***Palabras Clave* - comunicaciones ópticas; UDWDM; PON; Multiplexación; OptSim; BER.**

Authors acknowledge the support provided by Escuela Politécnica Nacional.
Corresponding author: christian.tipantuna@epn.edu.ec.

[1]Nubia Manchay is with the Departamento de Electrónica, Telecomunicaciones y Redes de Información at Escuela Politécnica Nacional, Quito 170517, Ecuador. Email: nubia.manchay@epn.edu.ec, ORCID: https://orcid.org/0009-0002-4886-2876.

[2]Christian Tipantuña is with the Departamento de Electrónica, Telecomunicaciones y Redes de Información at Escuela Politécnica Nacional, Quito 170517, Ecuador. Email: christian.tipantuna@epn.edu.ec, ORCID: https://orcid.org/0000-0002-8655-325X.

[3]Germán V. Arévalo is with the Carrera de Ingeniería en Telecomunicaciones, Universidad Politécnica Salesiana, Quito 17001, Ecuador. Email: garevalo@ups.edu.ec, ORCID: https://orcid.org/0000-0001-7034-5774.

[4]Berenice Arguero is with the Departamento de Electrónica, Telecomunicaciones y Redes de Información at Escuela Politécnica Nacional, Quito 170517, Ecuador. Email: jarguero@ups.edu.ec, ORCID: https://orcid.org/0000-0003-3054-6883.

[5]Carla Parra is with NuCom, Nuevas Comunicaciones Iberia S.A., Barcelona, Spain. Email: carla.parra@nucom.es, ORCID: https://orcid.org/0000-0002-7974-471X.

Manuscript Received: 02/04/2024
Revised: 18/05/2024
Accepted: 03/06/2024
DOI: https://doi.org/10.29019/enfoqueute.1049

I. Introduction

In recent years, access networks have evolved significantly to cater to the high demand for widely available and high-speed connectivity. These networks are characterized by their reach from the optical network terminal to the user premises. To address the growing number of users and ensure long-distance, high-speed information transmission, new wavelength multiplexing techniques have been explored to improve global connectivity. Emerging technologies must provide quality data, video, and voice services while being economical, scalable, and offering appropriate bandwidth to meet user requirements.

Passive optical networks (PONs) play a fundamental role in the growth and improvement of optical networks. They employ multiplexing techniques to share bandwidth and transmit multiple signals simultaneously over a single fiber. Multiplexing techniques are constantly evolving through various variants. These include techniques such as wavelength division multiplexing (WDM), Coarse Wavelength Division Multiplexing (CWDM), and Dense Wavelength Division

Multiplexing (DWDM), each offering an increased number of channels per fiber and improved bandwidth.

Ultradense Wavelength Division Multiplexing (UDWDM) is the latest advancement in this field, an emerging technology with significant potential for next-generation access networks demanding higher bandwidth.

UDWDM is characterized by its ability to reduce the wavelength spacing between channels, enabling the utilization of an even higher bandwidth in PONs. This capability provides a solution to the stringent requirements of 5G technologies [1]. With channel spacings as narrow as 6.25GHz, UDWDM can accommodate up to 1022 wavelengths over a single fiber optic channel, achieving cost savings and improving spectral efficiency.

This paper investigates the performance of UDWDM on a PON, building on previous studies of UDWDM systems. These studies focus attention on the analysis of non-linear effects that can degrade transmission in UDWDM-PON networks, such as stimulated Raman scattering (SRS), stimulated Brillouin scattering (SBS), four-wave mixing (FWM) and cross-phase modulation (XPM). In addition, software simulations were carried out using 7 channels, comparing BER values and received power and eye diagrams. The results indicate that these nonlinear effects limit the transmission of information to a BER rate greater than $10^{-}9$ at distances greater than 55 km, with a transmission power greater than 25 mW and at a speed of 10 Gbps. Furthermore, a maximum received power is observed at a transmission speed of 5 Gbps up to a maximum distance of 45 km. This research considers only a channel spacing of 25 GHz and a transmission rate of 10 Gbps [2].

In addition, studies by Sales, Segarra, Polo, and Prat (2015) have explored the operation of UDWDM-PON in conditions of low laser tuning, highlighting its operational viability in environments with limited resources. In another research, the same authors (2014) propose a half-duplex transmission technique to avoid Rayleigh backscatter crosstalk in UDWDM-PON using coherent receivers. These previous studies have significantly advanced knowledge in the efficient design and operation of UDWDM-PON networks, offering valuable information on key challenges such as laser tuning, transceiver cost, and crosstalk mitigation, thereby improving their performance and feasibility in practical environments [3].

A review of the theoretical foundation of UDWDM and PON networks is carried out to carry out this work. This includes knowing the basic concepts, spacing between channels, transmission capacity, and effects of channel separation, among others. Once the theoretical foundation has been reviewed, the study's specific objectives are defined. Link budget calculation is then performed to determine if data transmission will be successful in the communications system. Subsequently, different scenarios are simulated in Optsim, using filters to limit the signal bandwidth and reduce interference between adjacent channels. Finally, the graphs of the results obtained in different scenarios are presented to compare the best performance.

II. Background

This section begins by reviewing the concepts related to a PON network, its structure, and its operation. Then, the different types of multiplexing are described, such as WDM, DWDM, CWDM, and UDWDM, the latter of which is the main technology used in developing this work. For each of them, their main characteristics are mentioned regarding the capacity to transmit, a separation between channels, and advantages, among others.

Information is collected regarding the types of multiplexing, the most relevant information is extracted, and a comparative table of the four technologies is prepared. In addition, the standard, wavelengths per fiber, distance, spacing between channels, capacity, and cost are presented.

Subsequently, the design of the PON network using UDWDM technology is carried out. To do this, the current transmission standards and the analysis of requirements regarding the network elements are considered.

Three simulation scenarios are developed using a raised cosine filter, a Gaussian filter, and no filter. This study analyzes each channel's individual performance, considering phenomena such as chromatic dispersion and attenuation. The objective is to determine the optimal configuration of the three evaluated channels.

Finally, the analysis of the results of the different simulation scenarios for each channel is carried out, where the BER vs. distance is compared for the different channel separations, varying the distance and transmission speed.

A. Theoretical framework

A passive optical network, as shown in Fig. 1, consists of a fiber optic distribution network that does not use active components to distribute the signal. In a PON network, point-to-point and point-to-multipoint architecture is used. Passive is understood when it does not require a power supply for the splitters, fiber, and combiners, unlike an Active Optical Network (AON: Active Optical Network), which does require it [4].

A PON network comprises the optical line terminal (OLT: Optical Line Terminal), optical splitter, and various optical network terminals (ONT: Optical Network Terminal). In principle, a distinction can be made between point-to-point and point-to-multipoint PON. With a point-to-point PON, each subscriber is connected to the central OLT through its optical fiber. Therefore, each subscriber needs its connection port in the central office. With point-to-multipoint architecture, the subscriber's optical fiber only extends from its ONT to the next switching point. From there, a shared optical fiber with multiple connections leads to the OLT of the switching center to connect users with the network operations centers, as is the case of fiber to the home (FTTH).

Splitters distribute the optical signal from the OLT to multiple users in a PON network. The OLT is the active

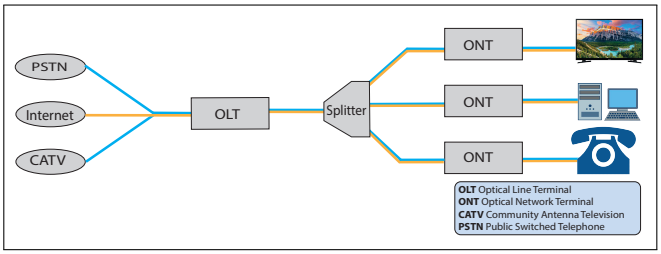

Fig. 1. Structure of a PON network, based on [5].

network equipment at the central edge of the PON network that provides the termination point for optical fiber and manages data traffic between end users and the network. Splitters are placed at different points in the PON network to split the optical signal into multiple paths, which are then transmitted to the end users. By distributing the optical signal from the OLT, splitters allow a single fiber optic line to provide high-speed connectivity to multiple homes or businesses, thereby reducing the costs and complexity of network infrastructure [6].

PON technology has recently been the subject of significant research, standardization, and development efforts. Compared to other technologies, such as WDM, it is one of the preferred and best-positioned technologies for future broadband access. They are low energy consumption networks and reduce problems in the last mile, such as bandwidth limitations and signal degradation, greater reliability, and lower installation and maintenance costs [7].

B. TYPES OF MULTIPLEXING

1) Wavelength Division Multiplexing (WDM): Optical wavelength division multiplexing (WDM) was proposed in the 1980s and became commercial in 1990. It is an optical transmission technique that combines multiple carrier signals in a single optical fiber using different wavelengths generated by laser light. WDM takes advantage of this by allowing multiple signals to be transmitted on a single fiber. Therefore, the fiber's capacity is not doubled but rather multiplied by the number of signals that can be transmitted simultaneously over the same fiber. Uses a multiplexer to combine different optical signals from different transponders in a package, but with different wavelengths, and transmit them through a fiber [8] [9].

Figure 2 shows the multiplexing and demultiplexing process that is carried out. At the receiver end, the demultiplexer separates the optical signals with different wavelengths and sends them to the various transponders for further processing and restoration of the original signal. This is how two or more optical signals with different wavelengths are transmitted simultaneously over a single optical link. Each ONT works at different wavelengths. In this approach, the WDM PON architecture is similar to the PON architecture. The main difference is that multiple wavelengths operate on a single fiber, and ONTs operate at different wavelengths, avoiding user interference and better signal quality in each connection. This is because each wavelength can transmit a specific amount of information, the more wavelengths are used, the greater the amount of data that can be transmitted through the network, this is essential in networks that handle large amounts. of information [10] [11].

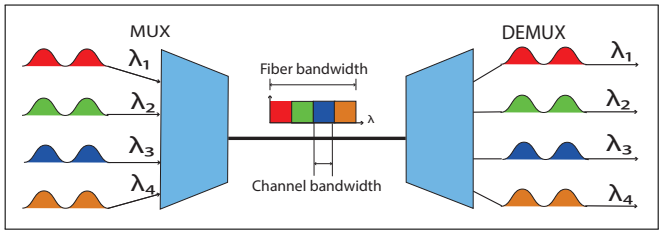

Fig. 2. Multiplexing and demultiplexing in WDM, based on [12].

2) Coarse Wavelength Division Multiplexing (CWDM): Coarse Wavelength Division Multiplexing (CWDM) is a robust and relatively cost-effective method used to increase the bandwidth of an optical cable. This technology is governed by the regulations of the International Telecommunication Union (ITU) ITU-T G.694.2 [13], establishing a separation of 20 nm. CWDM is limited in the number of channels, which typically has a maximum of 18 channels and can reach distances of up to 80 km [14].

Figure 3 shows that a CWDM system is composed of a multiplexer and a demultiplexer, which is used to combine multiple wavelength channels into a single fiber. This solution is effective in improving the capacity of an end-to-end deployed fiber. Optical signals are converted into signals of different frequencies with different wavelengths of optical carriers, where the received signals are combined during transmission, while, on the receiving side, the inverse transformation takes place [10].

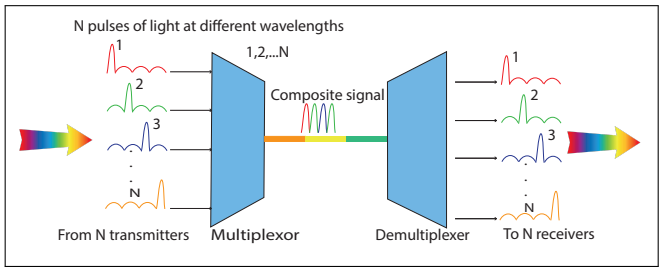

Fig. 3. Multiplexing and demultiplexing in CWDM, based on [14].

A commonly used option in enterprise and telecommunications access networks is CWDM solutions, which primarily employ passive hardware components in a point-to-point topology to the backbone network, allowing the most efficient use of fiber capabilities over very long distances [15].

3) Dense Wavelength Division Multiplexing (DWDM): The primary characteristic of Dense Wavelength Division Multiplexing (DWDM) is that multiple information channels on different wavelengths are transmitted through a single optical fiber. This technology increases the bandwidth of a backbone network, allowing for more efficient use of fiber capabilities over very long distances [16].

Figure 4 illustrates a DWDM system that leverages the optical fiber's ability to transmit light simultaneously at different wavelengths without mutual interference. Each wavelength represents a separate optical channel [17]. This technology

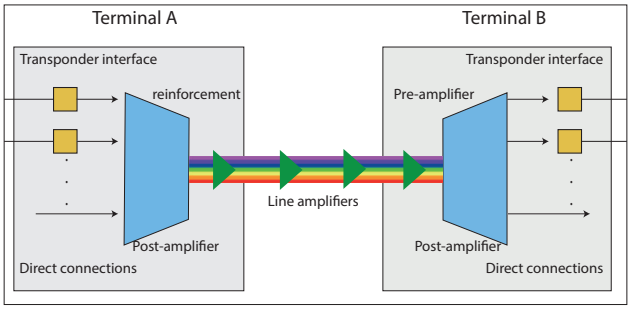

Fig. 4. Multiplexación y demultiplexación en DWDM, basado en [18].

enhances the performance of an optical system by achieving lower attenuation, as its main advantage is high-speed transmission over ultra-long distances, which can reach up to 4000 km without regeneration. However, the maximum transmission distance depends on various factors, such as the quality of the fiber, the quality of the DWDM system components, and the number of optical amplifiers used in the network. To improve the bandwidth of optical lines based on DWDM, it is possible to progressively add new optical channels to the existing equipment as the network develops [16].

An important device in DWDM is the optical transponder, an essential component to convert signals from customer equipment to signals compatible with DWDM technology for transmission over the main fiber. Additionally, transponders are used for signal regeneration, which involves restoring the signal's amplitude, shape, and timing. In most cases, the optical-electrical-optical procedure is used to perform this task, which includes conversion of an optical signal to electrical, 2R or 3R regeneration (reamplification, reshaping and retiming), and then reverse conversion of the regenerated signal back to an optical signal [9].

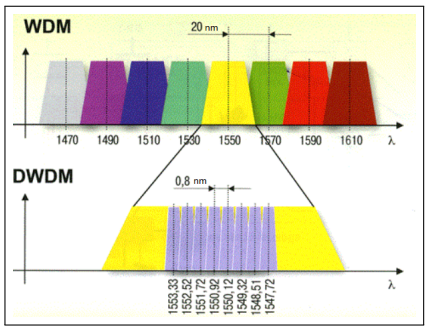

Fig. 5. WDM Channels vs. DWDM [19].

In Fig. 5, the channel spacing comparison between WDM and DWDM is illustrated, a key factor distinguishing the two technologies. WDM technology typically employs a wider channel spacing, usually around 20 nm, whereas DWDM technology utilizes a significantly smaller spacing, typically around 0.8 nm. This discrepancy implies that DWDM can accommodate a significantly larger number of channels than WDM within the same optical fiber.

DWDM can be compared with WDM and CWDM, with several key differences. Fig. 6 demonstrates the channel spacing between CWDM and DWDM. The primary characteristic is the 20 nm channel separation for CWDM, allowing for multiplexing up to 18 different channels on a single pair of optical fibers. It serves as a suitable option for shorter distances and low-capacity applications. Conversely, DWDM employs a much denser separation, typically 0.8 nm, making it a preferred choice for high-capacity applications and longer distances [15].

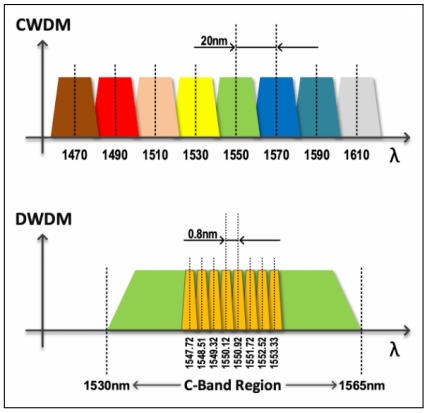

Fig. 6. CWDM Channels vs. DWDM channels [15].

C. Ultra Dense Wavelength Division Multiplexing (UDWDM)

Ultra-Dense Wavelength Division Multiplexing (UDWDM) is one of the most current technologies for access networks and is based on WDM PON. The spacing between channels is much narrower than DWDM; it is characterized by allowing for greater bandwidth compared to the other technologies mentioned above. It allows up to 1022 wavelengths to be sent through the same medium. It takes better advantage of a single optical fiber channel, achieves cost savings, and improves spectral efficiency in a communication system [11] [20].

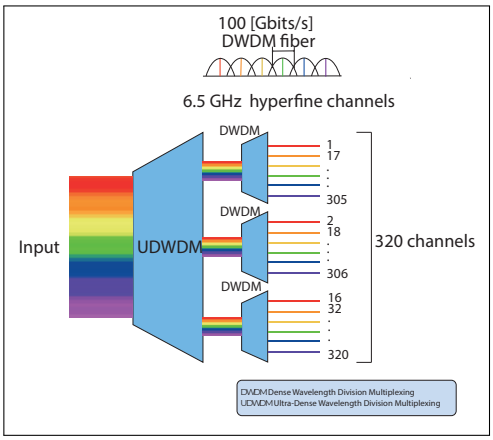

Fig. 7. 320 channels UDWDM transmission, based on [18].

If UDWDM is compared with WDM, it is observed that UDWDM uses a power divider which consists of an important

TABLE I
COMPARISON OF WDM TECHNOLOGIES.

Technology	**WDM**	CWDM	**DWDM**	**UDWDM**
Standard	UIT-T. G.692.	ITU G.694.2	ITU G 694.1	In progress
Wavelengths per fiber	4	18	64-160	1022
Distance [km]	<80	80	Thousands of km	Thousands of km
Spectrum	O, C	O, E, S, C, L	C, L, S	C, L
Channel spacing [GHz]	200	2500	50-100	1.25,1.5,2.5,2.8,3.12.5, 5,6.25,10,15,25
Capacity [Gbps]	2.5	Up to 2.5	10 - 40	> 40
Cost	Low	Low	Medium	High

component in the distribution network, it is important to note that thanks to this, each ONT would have the possibility of access to all the wavelengths [20].

In UDWDM, coherent detection can be inserted to obtain better sensitivity and high selectivity in the receivers of the OLTs and ONTs. Regarding the receiver's sensitivity, it should be noted that this important aspect allows for a high division factor in the power divider, which means that several ONTs can share the same distribution network. Likewise, high selectivity allows for greater spectral efficiency compared to other architectures, such as WDM, whose usability may be limited by factors such as the available bandwidth of the optical fiber and the quality of the light sources. used to generate optical signals [20]. Fig. 7 shows the separation of 320 channels transmitted by an optical fiber. Initially, a device is observed with 16 UDWDM channels separated at 6.25 GHz, where each group has a capacity of 100 GBits/s. From channel 1 to channel 16 there are different outputs, while channel 17 is routed to the same output of channel 1, this is done consecutively. Each set of 16 channels has a capacity of 100 Gbps. Following this, conventional DWDM systems separate multiple channels, entering each of the 16 ultra-dense outputs, resulting in 20 separate outputs on their channels at 100 GHz [21].

Table I summarizes the WDM, CWDM, DWDM, and UDWDM technologies. The most notable differences include channel spacing, wavelengths per fiber, transmission capacity, and distance

D. Raised cosine filter

A raised cosine filter is used to modify a signal's waveform before its transmission. This tool is commonly applied in digital modulation systems, where its main function is to prevent the effect of Inter Symbol Interference (ISI) by limiting the bandwidth of the transmitted signal. The frequency response and impulse response of the raised cosine filter are important characteristics of this type of filter. Therefore, it is necessary to understand how it behaves at different frequencies and how it affects the amplitude and phase of the processed signal. Fig. 8 shows the impulse response (left) and the frequency response (right) of a raised cosine filter. The filter's frequency response is wider than that of the ideal low-pass filter due to the transition band present in the filter. This excess bandwidth is controlled by a parameter known as the roll-off factor. The frequency response can be graphically visualized for different values of the roll-off factor: 0.3, 0.5, and 1. The impulse response exhibits similar characteristics to the impulse response of the sinc function, where zero crossings occur at intervals of time T, so that the signal with smaller amplitude lobes has a larger excess bandwidth or a broader spectrum [22].

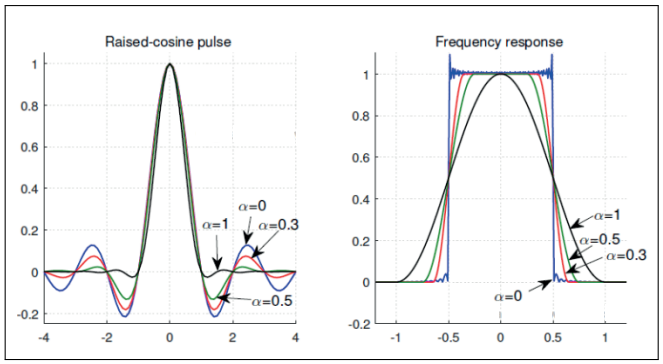

Fig. 8. Impulse response (left) and frequency response (right) of the raised cosine filter [23].

E. Gaussian Filter

Gaussian filter is used in signal processing, information theory, and signal encoding. Gaussian function is an optimal solution to maximize the information transmitted through a communication channel with additive Gaussian noise. Fig. 9 shows the impulse response (left) and frequency response (right) of the Gaussian filter. The impulse response of the Gaussian filter closely approximates a Gaussian function. These filters possess the property of reducing the overflow effect. Simultaneously, they minimize the rise and fall times. This behavior is largely attributed to the Gaussian filter having the minimum possible group delay. Group delay is the time it takes for a wave of a certain frequency to propagate through the filter. On the other hand, the frequency response refers to the filter's behavior when a sinusoidal input signal is applied in the frequency domain. One of the characteristics of the Gaussian filter is its standard deviation, represented by the symbol sigma (σ), which determines the shape of the filter's impulse response and frequency response. A larger standard

deviation results in a wider impulse response and a smoother frequency response, while a smaller standard deviation leads to a narrower impulse response and a higher attenuation of higher frequencies in the frequency response [24].

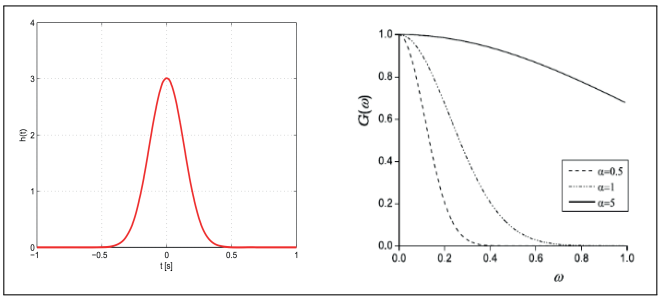

Fig. 9. Impulse response (left) and frequency response (right) of the Gaussian filter [25].

These filters reduce the overflow effect or overflow on a step function input while minimizing the rise and fall time. This behavior is largely because the Gauss filter has the minimum possible group delay. The group delay is the time it takes for a wave of a certain frequency to propagate through the filter. On the other hand, the frequency response is the filter's response when a sinusoidal input signal is applied to it in the frequency domain. Frequency response is measured in terms of the amplitude and phase of the output signal as a function of the input frequency [24].

One of the characteristics of the Gauss filter is its standard deviation, represented by the sigma symbol σ, which allows for determining the shape of the filter's impulse response and its frequency response. A larger standard deviation produces a wider impulse response and a smoother frequency response. A smaller standard deviation produces a narrower impulse response and a frequency response with greater attenuation of higher frequencies [24].

F. Electrical bessel filter

It is a frequency-selective device that passes signals in a desired frequency band, called the pass band, and blocks signals of other frequencies related to the stop band, which is the area where the input signal is completely suppressed. It allows the linearity of the phase-frequency characteristic within the bandwidth. Among the main advantages is the flat and frequency-proportional shape of the phase response in the transmission region, as it lowers distortion of signals with components at different frequencies [26]. The methodology used to design and simulate the UDWDM PON network is presented below.

III. METHODOLOGY

This section presents the design and simulation of a UDWDM-based PON implemented using Optsim software. UDWDM is a technology still under research and does not yet have a standard from the ITU or any other organization. Therefore, we have considered the ITU G.694.1 recommendation for this work, which standardizes DWDM. This recommendation establishes all the requirements for the interoperability of DWDM networks, including transmission power parameters, wavelength ranges, signal spectrum, attenuation, and optical noise levels. Additionally, it provides guidelines for the design of DWDM networks, encompassing parameters for optical fiber links, safety requirements, and nominal central frequencies.

The first step in designing the PON is to calculate the budget of the optical link, which includes analyzing factors such as transmission distance, fiber type and attenuation, transmitter power, and losses from connectors and splitters. This calculation is essential to determine the amount of optical power reaching the receiver and to ensure it is sufficient for high-quality transmission. The system requirements are also described, considering the transmitter, receiver, and communication channel. Subsequently, network simulations are conducted under different scenarios. In the first scenario, the PON network is simulated without signal filtering at the optical level. In scenarios two and three, a raised cosine filter and a Gaussian filter are used to optimize the results of the first scenario, both applied at the optical level. The channels in this study are separated by 25 GHz, 20 GHz, and 15 GHz, and for each separation, transmission rates from 10 Gbps to 17 Gbps are configured at various distances ranging from 10 km to 20 km.

A. Calculation of Optical Link Budget

The optical budget is the maximum allowable link attenuation from the OLT to the furthest ONT. This is a crucial indicator in PON network design because it helps determine the maximum possible length of the optical line in the transmitter-receiver section during the design phase. The optical power budget consists of the difference between the power from the transmitter and the receiver's sensitivity at the ONT [27]. The optical budget calculation is performed for a case where the distance is 10 km. The number of splices should be considered for greater distances, each contributing an additional attenuation value ranging from 0.1 dB to 0.5 dB, with 0.3 dB being an acceptable average value. This means that if there are more splices in the transmission, an additional value must be added to the optical budget calculation to account for the increased attenuation. Fig. 10 presents a diagram indicating the losses of each network component, such as connectors, splitters, and modulators, which contribute to signal attenuation. Table II provides the values for the optical budget calculation obtained from the manufacturer's datasheet [28] [29].

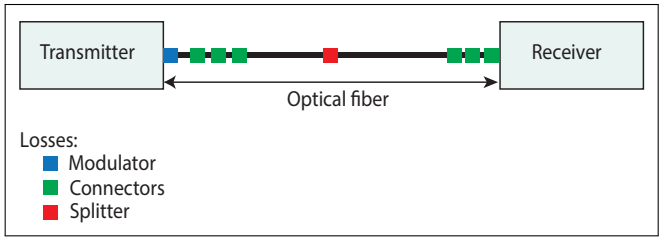

Fig. 10. Loss diagram of the optical link.

Equation 1 corresponds to the formula used to calculate the link budget, in which we sum all the predefined losses.

TABLE II
LINK LOSSES TO ONTS.

Element	Attenuation	Total quantity	Total Attenuation [dB]
G.652D Fiber	0.25 dB/km	10 km	2.5
Modulator	6 dB	1	6
Splitter	3.5 dB	2	7
SC connector	0.25 dB	14	3.5

To obtain the losses from the fiber, we calculate the product of attenuation by the length of the optical fiber [30]. Additionally, we consider the losses introduced by elements such as the modulator, splitters, and connectors. The operational margin is an increment that we budget in advance, anticipating possible additional losses due to fiber degradation, connector deterioration, cable accidents, etc.

$$P_{Tx} - L_t + G = M + S \tag{1}$$

where:
P_{Tx} = Transmitter Power
L_t = Total Link Loss
G = Gain
M = Margin
S = Receiver Sensitivity

By replacing the values into Equation 1, the sensitivity S of the receiver is:

$$\begin{aligned} S &= P_{Tx} - L_t + G - M \\ S &= 0dBm - 19dB + 0dB - 3dB \\ S &= -22dBm \end{aligned} \tag{2}$$

According to ITU G.984.2 recommendation, the standard sensitivity in PON is -30 dBm or 0.001 mW for OLT and -26 dBm or 0.0025 mW for ONT, respectively [31]. The calculated receiver sensitivity of -22 dBm falls within the standardization limits.

After calculating the optical link budget, the next step is to utilize simulation tools to analyze and optimize the network design further. The following section details the tools and methodologies employed in this study.

B. Simulation Tools

OptSim, developed by RSoft, is used for the simulation. It is a leading tool in the simulation of optical communications and is widely used. This software offers an intuitive graphical interface and an extensive library of optical, electrical, and digital components, facilitating precise parameter configuration and efficient simulation of complex systems. The simulated data were then processed and represented in MATLAB. Combining these tools allowed for a detailed analysis and precise graphical representation of the results obtained. The optical communication system simulation comprises a transmitter, a receiver, and a communication channel, as depicted in Fig. 11.

Once the tools to be treated were known, various simulation techniques were employed to explore different scenarios and optimize the network design. The following sections detail

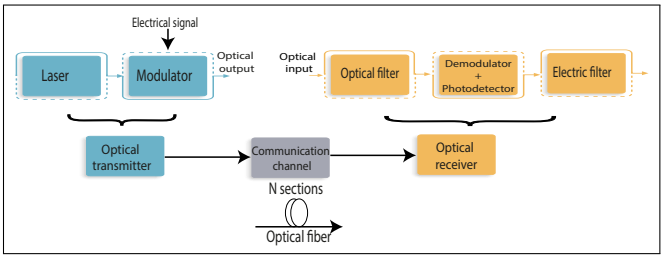

Fig. 11. Diagram of an optical communications system, based on [32].

the different simulated scenarios, each with its respective configurations and analysis of results. These scenarios provide a comprehensive view of the system's feasibility and performance under various operational conditions.

C. First scenario: Simulation without using a filter on transmission side

The first scenario is represented in Fig. 13 through a block diagram and in Fig. 12 in the simulator. In the transmitter, a CW laser is incorporated with a different central frequency depending on the channel spacing, and the configuration parameters are specified in Table IV. The signal is modulated using a Mach-Zehnder modulator. The configuration parameters of the modulator are provided in Table III. Excessive losses and reduction in average power due to modulation must be considered when calculating the optical budget, as they cause attenuation in the link. These values are obtained from the manufacturer's data sheets [33].

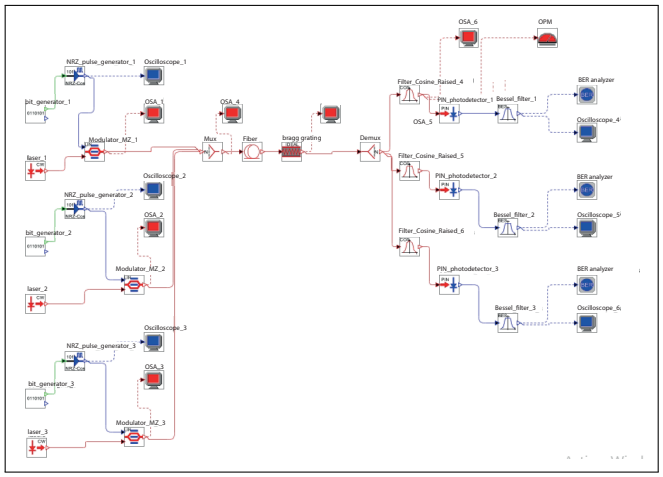

Fig. 12. Simulation without using a filter.

A pseudo-random bit sequence (PRBS) generator is also used at a data rate of 10 Gbps, depending on the bit rate (between 10 Gbps and 17 Gbps), and NRZ pulse generation for the encoding technique. The multiplexing process is carried out with an insertion loss of 3.5 dB, where the signal is transmitted through the communication channel composed of optical fiber and a Bragg grating, with a length of 10 km, as appropriate (between 10 km and 17 km).

Table V presents the most important configuration parameters of single-mode optical fiber that comply with the ITU-T

G.652D recommendation. This type of fiber allows improved performance in high bandwidth and long-distance applications in addition to transmission in an extended wavelength range of 1310-1550 nm [34].

Currently, the Bragg grating is used in multiplexing channels along the wavelength. It allows compensation for chromatic dispersion in the communication channel, obtaining greater efficiency, resource savings, better measurement precision, etc.

TABLE III
MODULATOR CONFIGURATION PARAMETERS.

Parameter	Value [dB]
Excessive losses	3
Average power reduction by modulation	3

TABLE IV
LASER CONFIGURATION PARAMETERS FOR 25 GHZ SEPARATION.

Parameter	Ch 1	Ch 2	Ch 3	Unit
Center frequency	193.100	193.125	193.150	THz
Wavelength	1552.52	1552.32	1552.12	nm
Power	0			dBm

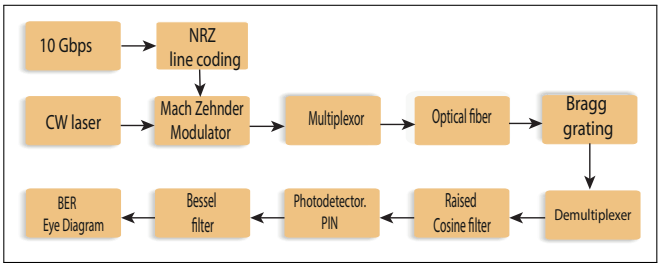

Fig. 13. Schematic view of UDWDM in the PON network.

TABLE V
FIBER CONFIGURATION PARAMETERS.

Parameter	Value	Unit
Fiber length	10-20	km
Attenuation	0.25	dB/km
Dispersion	17	ps/nm/km

The optical receiver's main function is to transform the optical signal received at the fiber output into the original electrical signal. It comprises a raised cosine optical filter, a PIN photodetector, a demodulator, and a Bessel electrical filter (transmitter).

Here, the signal is filtered through a raised cosine filter and detected by a PIN photodetector to obtain the optical signal. The resulting signal is then filtered again with a Bessel low-pass filter connected to the BER analyzer to verify the signal quality through the BER value and the eye diagram shape [35]. The configuration parameters for the Bessel filter are specified in Table VI. Among the configuration parameters of the PIN photodetector shown in Table VII is the dark current, which is the current that flows through the load in the absence of optical radiation. This current causes shot noise and limits the sensitivity of the optical receiver. Quantum efficiency, on the other hand, is a factor that accounts for the fact that, generally, not all absorbed light quanta lead to the generation of current pulses [36].

TABLE VI
ELECTRICAL BESSEL FILTER PARAMETERS.

Parameter	Value	Unit
Type	low pass	THz
Bandwidth	0.75*Bit rate	GHz

TABLE VII
PIN PHOTODETECTOR CONFIGURATION PARAMETERS.

Parameter	Value	Unit
Reference frequency	193.150	THz
Bandwidth	20	GHz
Dark current	0.1	nA
Quantum efficiency	0.7	-

In Table VIII, separations of 25 GHz, 20 GHz, and 15 GHz are considered, with three channels where different wavelengths are transmitted for the 3 scenarios. For example, for a spacing of 25 GHz, the center emission frequency of each CW laser is set as follows: λ_1 = 193.100 THz, λ_2 = 193.125 THz, and λ_3 = 193.150 THz; where λ_1, λ_2, and λ_3 are the terahertz wavelengths for channel 1, channel 2, and channel 3, respectively. The same process is carried out for frequency distances of 20 and 15 GHz.

TABLE VIII
WAVELENGTHS AT DIFFERENT CHANNEL SPACINGS FOR THE THREE SCENARIOS ARE AS FOLLOWS.

Separation	λ_1 [THz]	λ_2 [THz]	λ_3 [THz]
25[GHz]	193.100	193.125	193.150
20[GHz]	193.100	193.120	193.140
15[GHz]	193.100	193.115	193.130

After completing the initial scenario, it has been decided to present two additional scenarios in the design of the PON network using UDWDM technology in conjunction with optical filters. This analysis with filters is crucial for evaluating and selecting the optimal solution. Critical factors will be considered, such as improving transmission quality, reducing data errors, expanding network coverage, and enhancing system reliability. The filter selection process will be conducted to ensure that the chosen solution meets the specific requirements of high efficiency and connection quality, which are essential in advanced optical communication environments.

D. Second scenario: Simulation using a Raised Cosine Filter

Similar to the previous case, this scenario is depicted in Fig.15. To improve the results of the previous case, a raised cosine filter is applied at the optical level before the multiplexing process. This filter models the pulses in digital modulation due to its ability to minimize ISI. The lift constant is adjusted as a function of the signal's symbol rate and amplitude ratio. No changes are made to the communication channel section. At the same time, at the receiver, a second raised cosine filter is set upstream of the PIN photodetector with the same center

frequency for each channel. If the second filter has the same characteristic, the signal at its input will repeat its impulse response, which means the filter will adapt to the given signal.

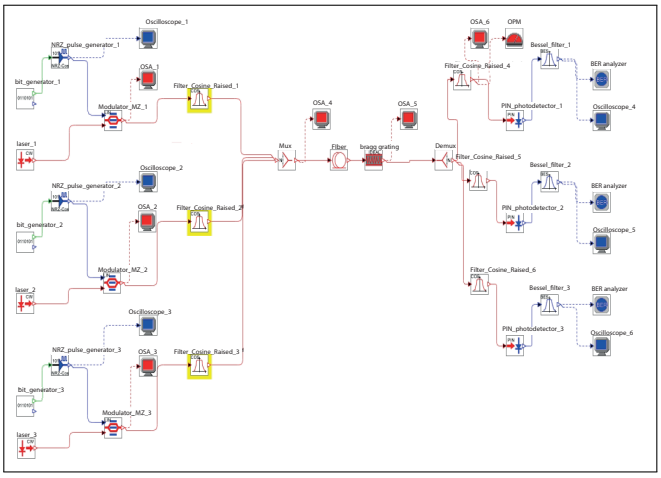

Fig. 14. Simulation using a Raised Cosine Filter.

Table IX displays the configuration parameters of the filter, with a roll-off factor of 0.5. This value allows controlling the degree of smoothing relative to the frequency response of an ideal filter, which corresponds to the level of the side lobes of the impulse response. The suitability of the filter's usage is verified by using the BER analyzer to assess signal quality through BER and the eye diagram. The same procedure as in the first scenario should be followed to configure the channel spacing.

TABLE IX
PARAMETERS OF THE RAISED COSINE FILTER.

Parameter	Value	Unit
Central Frequency	193.100	THz
Roll-off	0.5	-
Bandwidth	2*Bit rate	GHz

E. Third Scenario: Simulation using a Gaussian Filter

In this scenario, a Gaussian filter is used, an electrical filter whose transient pulse function is Gaussian. It is designed to have no overshoot in the transient response and to maximize the time constant. In other words, there will be no temporal increase in the filter response that exceeds the input signal level, ensuring higher signal quality in the output [37]. The filter is configured with the parameters from Table X and with the same central frequency as appropriate for each channel (Table VIII). In the communication channel and at the receiver, the configuration is the same as in scenarios one and two. Finally, the BER analyzer is also used, automatically calculates its value and displays the eye diagram.

The following section presents the results obtained from the methodology section.

IV. RESULTS

We present and analyze the results by simulating the three scenarios. Each scenario is described in detail, and the

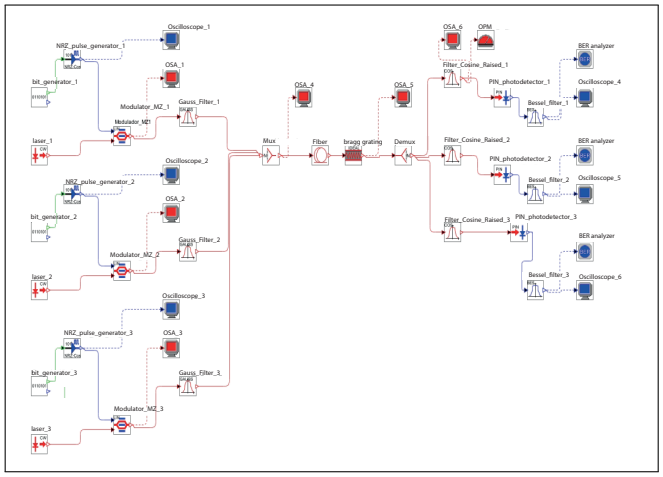

Fig. 15. Simulation using a Gaussian Filter.

TABLE X
PARAMETERS OF THE GAUSSIAN FILTER FOR CHANNEL 1.

Parameter	Value	Unit
Central Frequency	193.100	THz
Bandwidth	2*Bit rate	GHz
Orden Super Gaussiano	1	-

results are illustrated with graphs showing BER vs. distance diagrams. These graphs provide a clear understanding of how the bit error rate (BER) varies with distance in each of the simulated scenarios.

- **Channel Spacing of 25 GHz:** Fig. 16 shows the performance of the three channels in terms of BER, where the lower BER curve indicates better signal quality and higher transmission capacity. It's important to clarify that for this study, BER values of 10^{-9} have been considered, as recommended by the ITU, when no forward error correction is used. Below are the results obtained for the first scenario for each channel.

  1) Results of the first scenario: Simulation without a filter on the transmission side:

  - **Channel 1:** For a distance of 10 km to 12 km at a transmission rate of 10 Gbps to 12 Gbps, a constant BER of 10^{-40} is obtained. However, for distances ranging from 14 km to 20 km at a transmission rate of 13 Gbps, the BER increases from 10^{-40} to 10^{-32}. From a transmission rate of 14 Gbps to 17 Gbps, the error rate grows as it increases. Nevertheless, transmission is still possible up to 18 km, considering that 10^{-9} is an acceptable BER value, meaning that transmission limits are being approached. Beyond 20 km and transmission speeds exceeding 17 Gbps, attenuation and noise in the transmission medium significantly affect signal quality, increasing BER.
  - **Channel 2:** In the case of the second channel, it can be observed that channel 2 is the most affected by phenomena like attenuation, which increases with

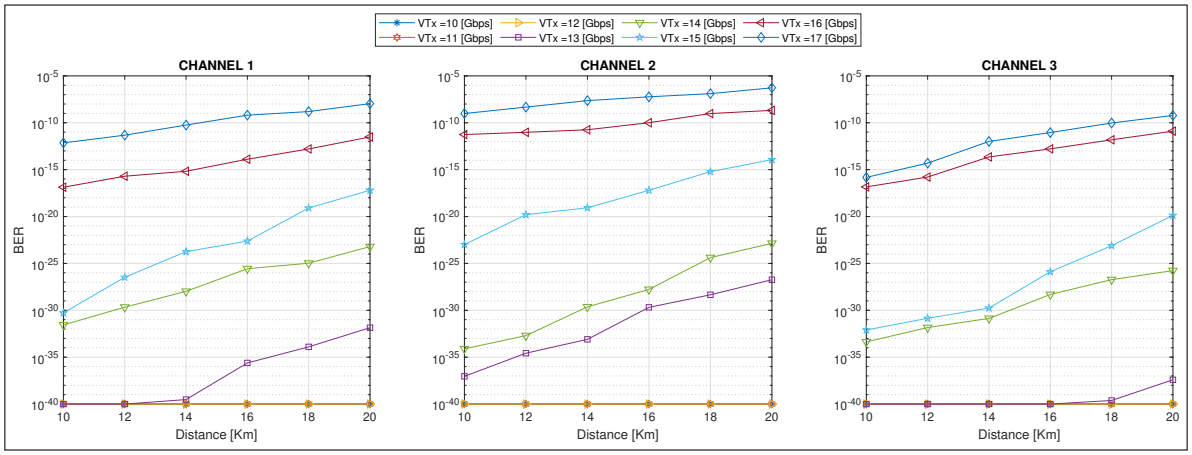

Fig. 16. BER vs. distance for a channel spacing of 25 GHz.

fiber length and distance, affecting transmission. This means that signal intensity decreases as it propagates through the optical fiber, causing the signal to weaken. For example, at 16 Gbps and a distance of 10 km to 12 km, a BER of 10^{-23} is obtained, progressively increasing to 10^{-20}. At a longer distance of 20 km, the BER increases to 10^{-14}.

- **Channel 3:** For this channel, at transmission speeds ranging from 10 Gbps to 13 Gbps and distances from 10 km to 18 km, the BER is 10^{-40} with a variation from 10^{-40} to 10^{-37} when the distance increases to 20 km, due to emerging optical phenomena in the channel. However, at 14 Gbps and 15 Gbps, despite increasing to 10^{-33} and 10^{-20}, respectively, the BER remains within an acceptable range, meaning it is less than 10^{-9}. The BER values in channel 3 indicate that it performs better than channels 1 and 2. In optical communication systems, a high BER of 10^{-8} indicates transmission errors, meaning that the received signal differs from the transmitted signal. This can result in decoding errors, transmission delays, and data loss.

- **Channel Spacing of 20 GHz:** To verify the behavior of the channels, their spacing is reduced from 25 GHz to 20 GHz. Fig. 17 shows the results of BER vs. distance for the three channels, and the following descriptions are provided for each channel:

  - **Channel 1:** When comparing the values in Fig. 17 with those in Fig. 16, it can be observed that the BER remains constant at 10^{-40} for transmission speeds of 10 Gbps and 11 Gbps. Similarly, the error rate progressively increases with distance and transmission speed at a 20GHz spacing, from 12 Gbps to 17 Gbps. The greater the distance between the transmitter and receiver, the more noise there will be in the signal. This affects signal quality, meaning that the BER increases from 10^{-33} to 10^{-3}, where 10^{-3} is no longer considered an acceptable BER. These values allowed the BER figures to be drawn up, where it is observed that as the transmission speed increases, the chromatic dispersion of the signal becomes more pronounced. This means that the effect of chromatic dispersion on the signal becomes stronger as the transmission rate increases, resulting in a higher BER.
  - **Channel 2:** As mentioned earlier, Channel 2 is the most affected by attenuation and chromatic dispersion phenomena. While previously, at a 25GHz channel spacing, the BER remained constant at 10^{-40} for transmission speeds of 10 Gbps and 11 Gbps, this is no longer the case at 20GHz due to signal degradation as it propagates through the transmission channel, contributing to the increase in BER. For 12 Gbps and 13 Gbps transmission speeds, the BER is acceptable in the 10^{-27} to 10^{-10} at distances from 10 km to 20 km. However, from 14 Gbps to 17 Gbps, even at short distances like 10 km, the error rate is significantly high, ranging from 10^{-8} to 10^{-3}. The transmission does not meet the maximum BER limit of 10^{-9}.
  - **Channel 3:** Regarding Channel 3, for a bit rate ranging from 10 Gbps to 15 Gbps at distances from 10 km to 20 km, the UDWDM system is reliable because the BER is in the range of 10^{-40} to 10^{-9}, allowing for stable transmission. This indicates that the channel can maintain signal quality without being affected by disturbances or noise. However, there is poor transmission performance for a bit rate of 16 Gbps and 17 Gbps because the BER is high, ranging from 10^{-6} to 10^{-4} at distances from 10 km to 20 km.

- **Channel Spacing of 15 GHz:** Fig. 18 demonstrates that the BER values are worse than for the other channels' spacing. There are some exceptions for each channel described below.

  - **Channel 1:** It can be observed that effective transmission is only achievable at a rate of 10 Gbps in a distance range between 10 km and 20 km, with an approximate BER value of 10^{-15}. However, transmission is compromised for higher bit rates ranging

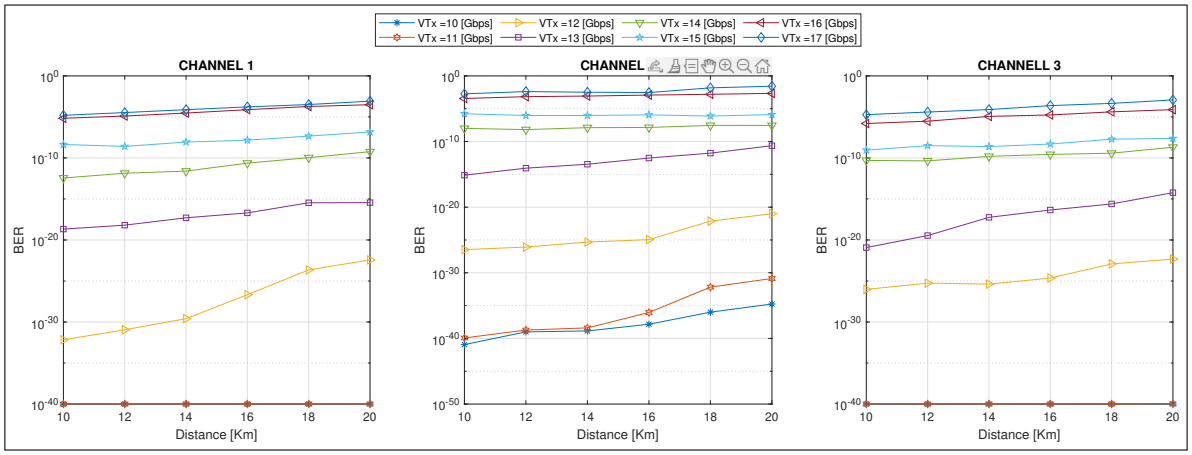

Fig. 17. BER vs. distance for a channel spacing of 20 GHz.

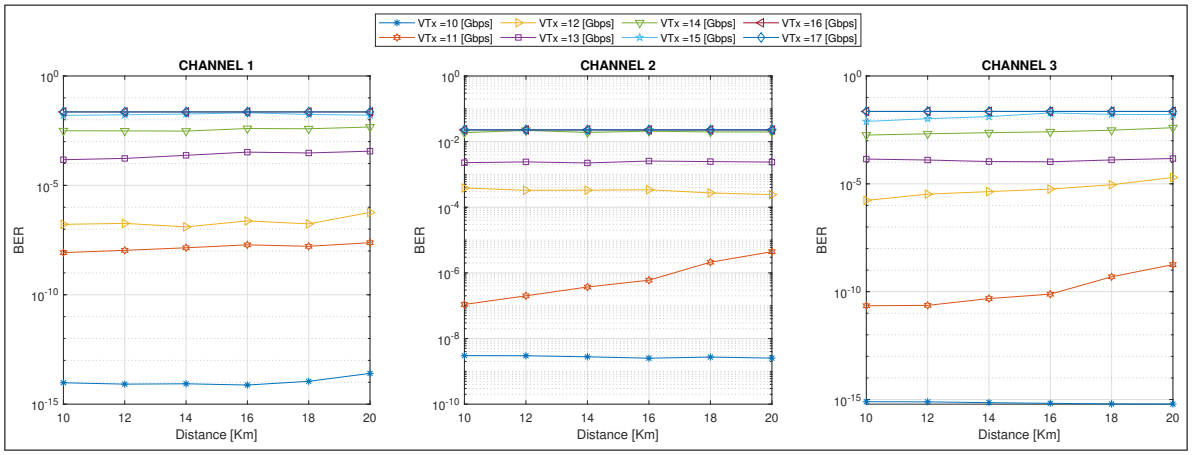

Fig. 18. BER vs. distance for a channel spacing of 15 GHz.

from 11 Gbps to 17 Gbps because the signal quality deteriorates due to optical phenomena affecting the channel, reflected in the BER values increasing to 10^{-8}. This 15GHz channel spacing impacts all three channels because the wavelength of each channel is slightly different and can cause distortion in the transmitted signal because the channels are relatively close to each other in frequency. This 15GHz spacing demonstrates that channel spacing significantly impacts transmission quality, meaning that distortion or interference in one signal can extend to adjacent channels and affect the signal's quality.

– **Channel 2:** After conducting the simulation for this channel, it can be observed that efficient transmission is not achieved for any of the transmission speeds (10 Gbps to 17 Gbps) because the signal is attenuated. The BER is 10^{-8}, which is a high value. These results are due to interference from adjacent channels, attenuation, and chromatic dispersion, among other factors. In the case of adjacent channels in a multiplexing system like UDWDM, the spacing between them is critical to minimize interference and ensure transmission. Therefore, it is recommended that research efforts be continued to improve transmission, especially at high speeds.

– **Channel 3:** After analyzing the channel, the best BER value obtained for this case is 10^{-15} at 10 Gbps, progressively increasing from 10^{-11} to 10^{-9} when reaching 11 Gbps. For the remaining transmission speeds (12 Gbps to 17 Gbps), there is no reliable data transmission, meaning the BER is high (10^{-8} to 10^{-2}). This means that a significant number of the transmitted bits are not received correctly at the receiver. Due to these values, the channel is not valid for these speeds.

2) Results for the second scenario: Simulation using a raised cosine filter: Using the raised cosine filter allows us to verify if the performance is adequate to optimize the results of the first scenario. The configuration is done for channel spacings of 25 GHz, 20 GHz, and 15 GHz. Fig. 19 presents the BER vs. distance values with a raised cosine filter and a channel spacing of 25 GHz. When comparing the BER results from Fig. 16 with the same channel spacing, it can be observed that the channel's performance improved for all bit rates. In **Channel 1**, a BER of 10^{-40} is achieved for a transmission rate from 10 Gbps to 14 Gbps over distances ranging from 10 km to 20 km. It then gradually increases, and finally, a

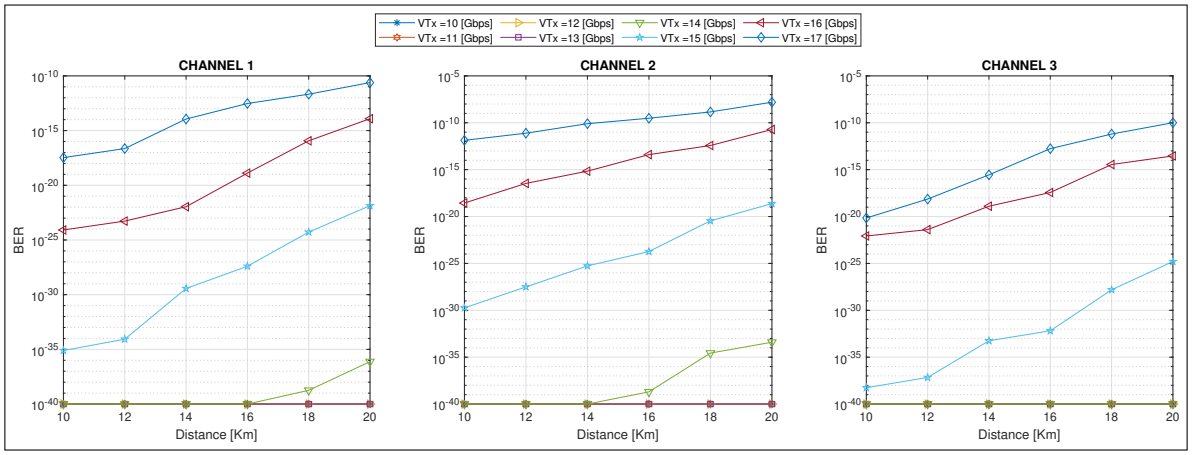

Fig. 19. BER vs. distance with a raised cosine filter and a channel spacing of 25 GHz.

permissible BER of 10^{-10} is reached at 17 Gbps.

Similarly, for transmission rates from 10 Gbps to 15 Gbps, in channel 2, the BER value is improved in the range from 10^{-40} to 10^{-18} compared to the results in the BER vs. distance without a filter (Fig. 16), where the BER values range from 10^{-40} to 10^{-14}. Meanwhile, within the range of 10 km to 18 km, at 17 Gbps using the filter, the BER values range from 10^{-12} to 10^{-9}, in contrast to the results without a filter where the BER values are greater than 10^{-8} starting from 12 km. At 20 km, the signal quality is lost due to propagation over longer distances through the optical fiber, which experiences attenuation and distortion.

For channel 3, it exhibits proper functionality, significantly better than channels 1 and 2, as it achieves lower BER values for all transmission rates (10 Gbps to 17 Gbps) ranging from 10^{-40} to 10^{-10}. These lower BER values indicate fewer erroneous bits in channel 3.

Fig. 20 shows the BER vs. distance values using the raised cosine filter and a 20GHz channel spacing. When comparing the BER values in Fig. 17 with those in Fig. 20, we can see that for channels 1 and 2, the data transmission rates for which the filter is more effective range from 10 Gbps to 14 Gbps, achieving BER values between 10^{-40} and 10^{-10}. However, for channel 3, the filter is effective up to 15 Gbps, achieving BER values as low as 10^{-9} compared to the simulation without a filter. For the remaining transmission rates (16 Gbps and 17 Gbps), the BER is similar to not using the filter, with values ranging from 10^{-6} to 10^{-3}. Therefore, the closer the channels are in wavelength, the more unwanted optical phenomena appear. Undesirable effects such as attenuation and chromatic dispersion impact the quality of the transmitted signal.

Comparing the results from Fig. 18 with the results from Fig. 21, it can be observed that, when using the raised cosine filter with a 15GHz channel spacing, all three channels improve the BER values at 10 Gbps. In the case of **Channel 1**, good performance is also achieved at 11 Gbps, with a range of BER values from 10^{-22} to 10^{-9}. On the other hand, in **Channel 2**, when the filter is not used, there is no transmission for any bit rate, but with the filter at distances of 10 km to 20 km, transmission is achieved only at 10 Gbps, with a BER ranging from 10^{-14} to 10^{-12}. Finally, at a transmission rate of 11 Gbps, **Channel 3** shows improved BER values, decreasing from 10^{-15} without the raised cosine filter to 10^{-22} when using the filter.

From the simulation results with different channel spacings (25 GHz, 20 GHz, and 15 GHz) and for specific transmission rates, it is evident that the raised cosine filter yields better BER values than the first scenario. This filter optimizes the performance of the optical channel in terms of system efficiency and the quality of the transmitted signal. This is demonstrated when the BER values fall within 10^{-40} to 10^{-9}. However, using the filter is not always beneficial, as observed in cases with transmission rates exceeding 15 Gbps and channel spacings narrower than 15 GHz, which result in increased BER.

There are several reasons why the raised cosine filter may be insufficient. First, signal dispersion in the optical medium can affect the filter's frequency response, especially at high transmission rates exceeding 17 Gbps. Another reason is the long fiber span; if the signal travels a long distance through an optical fiber (more than 20 km), the raised cosine filter may not compensate for chromatic dispersion. Additionally, the high-speed optical signal and noise in the optical medium can affect the efficacy of the raised cosine filter. As the signal speed increases, the duration of each bit of the signal decreases. This can lead to bit overlap or ISI, distorting the signal waveform. Under these conditions, the signal may experience significant attenuation, and the BER would also increase, ultimately impacting transmission quality.

3) Results of the third scenario: Simulation using a Gaussian filter: In this section, we compare the results using the Gaussian filter (Fig. 22) and without a filter (Fig. 16). The objective is to analyze the efficiency within the optical channel compared to the first scenario. When analyzing the quality of transmission in the **channels 1, 2, and 3** separated by 25 GHz, it is observed that the use of the Gaussian filter results in an increase in BER compared to when it is not used, especially for transmission speeds between 10 Gbps and 15 Gbps. This is because the Gaussian filter has a wider bandwidth than the raised cosine filter, which could cause

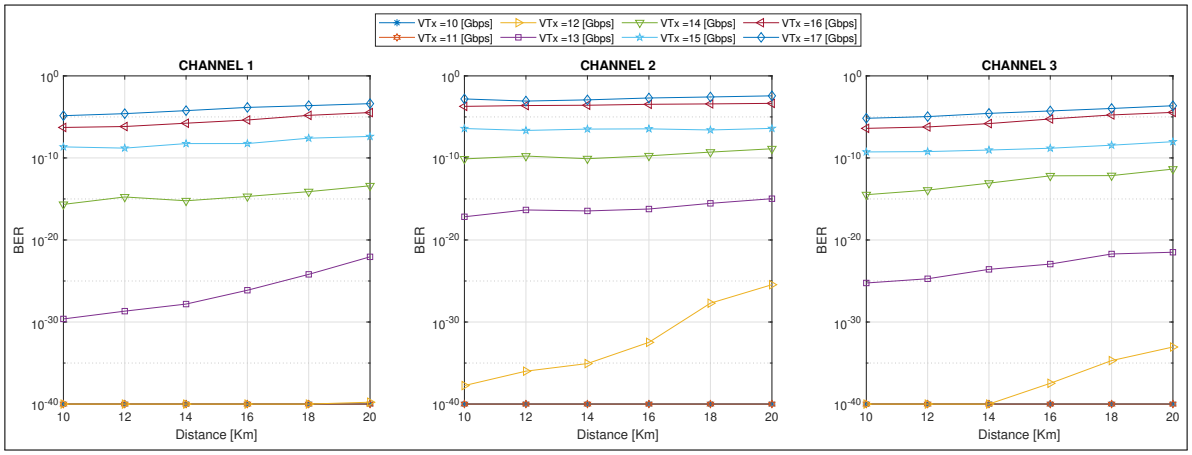

Fig. 20. BER vs. distance with raised cosine filter and 20 GHz channel spacing.

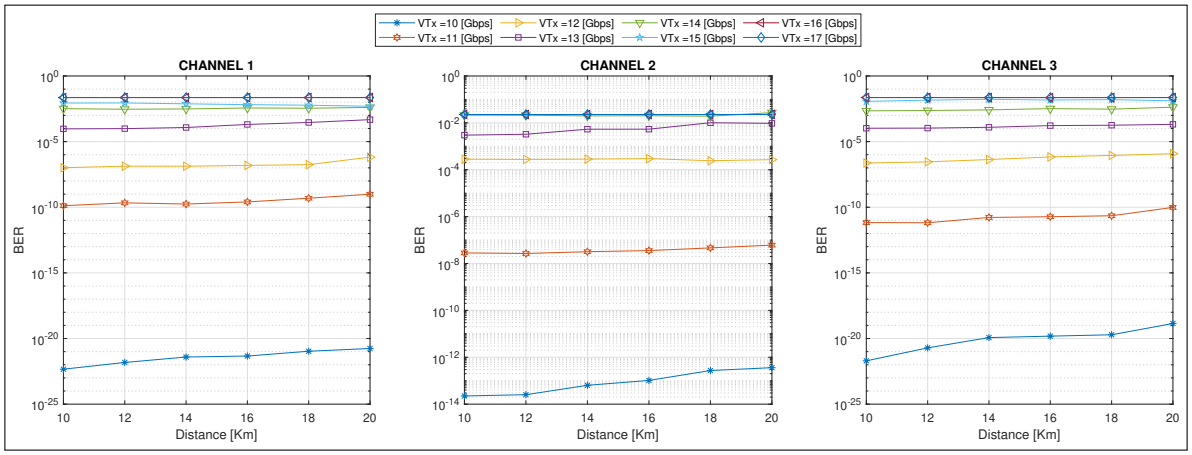

Fig. 21. BER vs. distance with raised cosine filter and 15 GHz channel spacing.

more ISI between nearby channels and reduce signal quality. However, the BER slightly improves when using the filter for 16 Gbps and 17 Gbps transmission speeds. In conclusion, the filter is not always very efficient under these conditions, and its use will depend on the specific characteristics of the application and the optical transmission system.

Fig. 23 shows the BER values vs. distance with a Gaussian filter and 20 GHz channel spacing. The BER values for channels 1 and 2 increase compared to the BER values from Fig. 17 without using a filter. For example, in Fig. 23, for channel 1, at a transmission rate of 12 Gbps and a distance of 10 km, the BER value is 10^{-30}, whereas for the same transmission rate and distance without using the filter (Fig. 17), the BER value is 10^{-32}. Comparing these two values, it is observed that the BER increases when the filter is used. The same applies to channel 2 and the other transmission rates.

In channel 3, at a transmission rate of 11 Gbps without using the filter, as the distance varies from 10 km to 14 km, the BER values increased from 10^{-40} without a filter to 10^{-35} with a filter. The analysis for other distances and transmission rates is similar. Therefore, using the filter, instead of reducing bit errors, increases them, while at transmission rates of 15 Gbps to 17 Gbps, the BER values are similar.

In the last test with the filter, a 15GHz channel spacing was used (Fig. 24). In **channel 1**, when comparing the BER values from Fig. 18 where no filter is used with the BER values from Fig. 24 using the Gaussian filter, it can be observed that at a transmission rate of 10 Gbps and a distance of 10 km, the BER values decrease from 10^{-16} to 10^{-14} compared to when the filter is not used. In **channel 2**, although the BER value decreases slightly when transmitting at 11 Gbps, it does not reach the threshold recommended by the ITU of 10^{-9}; the same happens for the rest of the transmission rates.

Regarding **channel 3** in Fig. 24, for transmission rates of 10 Gbps and 11 Gbps, they achieve the best BER, meaning that this value is less than 10^{-9}, while for the rest of the transmission rates, the BER value is greater than 10^{-9}, indicating more errors in data transmission and, consequently, a decrease in the quality of the transmitted signal.

A. Filter Comparison

The performance of the Gaussian filter raised cosine filter, and no filter is evaluated below by estimating the BER to determine which is more suitable for this specific application in a UDWDM system. Table XI shows the obtained BER results at a distance of 10 km, a transmission speed of 10 Gbps, and a channel separation of 25 GHz. The green color highlights that the BER values for all three channels in all three

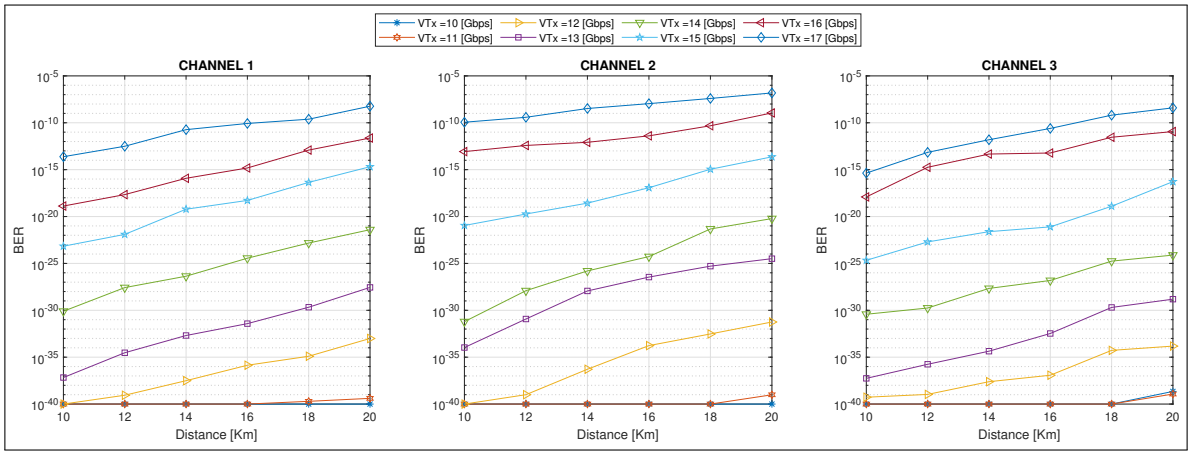

Fig. 22. BER vs. distance with Gaussian filter and 25 GHz channel spacing.

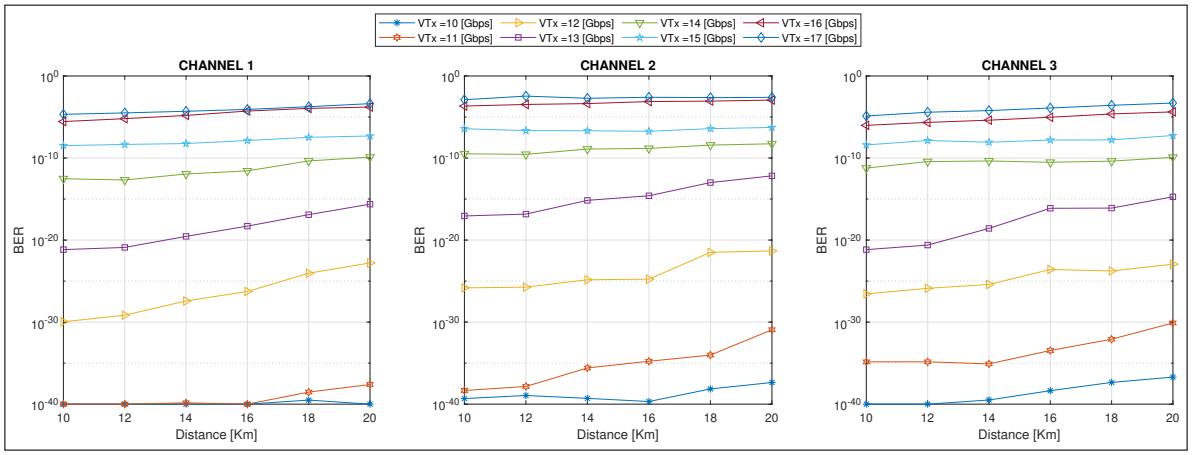

Fig. 23. BER vs. distance with Gaussian filter and 20 GHz channel spacing

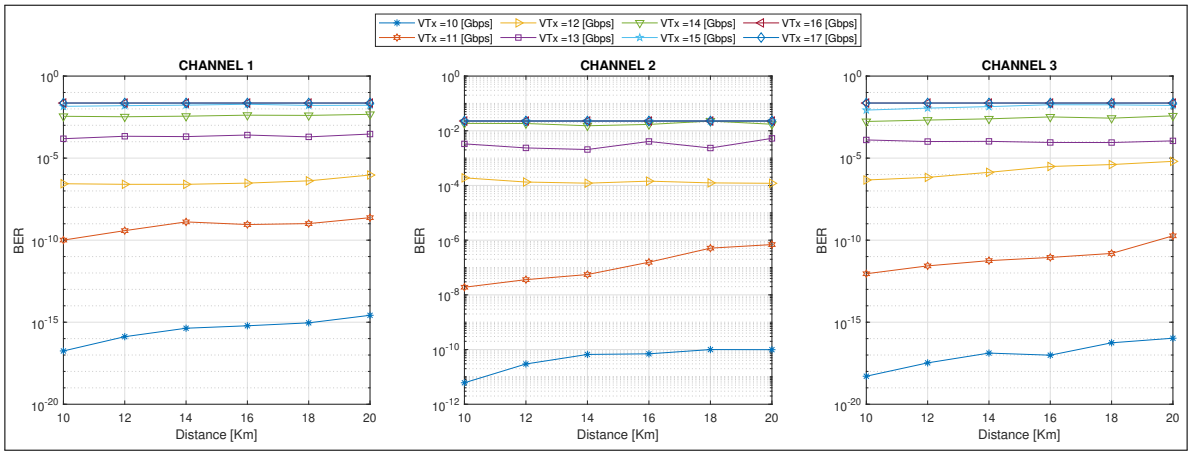

Fig. 24. BER vs. Distance with Gaussian Filter and 15 GHz Channel Spacing.

scenarios are acceptable, meaning they are less than 10^{-9}. When looking at the BER values in the scenario with a raised cosine filter, it is observed that the number of erroneous bits is lower compared to the values in the scenario without a filter and the scenario with a Gaussian filter. However, when using the Gaussian filter, the BER values increase compared to the scenario without a filter and the scenario with the raised cosine filter. Although the BER values for all three channels fall within an acceptable range, for Channel 1, achieving a BER of 10^{-36} is preferable to a BER of 10^{-31} or 10^{-24}, as it means fewer erroneous bits are received. Meanwhile, a BER of 10^{-24} implies that the number of erroneous bits increases compared to the other two BER values.

The possible causes of the previous results are interfer-

ence between adjacent channels due to the narrow channel spacing and signal attenuation due to transmission distance. It's also important to consider that the Gaussian filter has a smoother and wider frequency response, allowing more energy at higher frequencies. Still, it can also cause more interference with nearby channels. In comparison, the raised cosine filter has a tighter frequency response and higher attenuation outside the channel's bandwidth, reducing interference with adjacent channels but potentially causing more signal distortion. Therefore, the choice of the appropriate filter will depend on the specific needs of the communication system in terms of bandwidth, channel spacing, transmission rate, receiver sensitivity, and other factors. Conducting tests and evaluations to determine the most suitable filter for a particular communication system is essential.

TABLE XI
VALUES OF BER FOR FILTER COMPARISON AT A TRANSMISSION SPEED OF 15 GBPS, WITH A CHANNEL SPACING OF 25 GHZ.

BER			
Types of scenarios	**Ch 1**	**Ch 2**	**Ch 3**
No filter	5^{-31}	1^{-23}	8^{-33}
Gaussian filter	7^{-24}	1^{-21}	2^{-25}
Raised cosine filter	8^{-36}	2^{-30}	6^{-39}

TABLE XII
VALUES OF BER FOR FILTER COMPARISON AT A TRANSMISSION SPEED OF 15 GBPS WITH A CHANNEL SPACING OF 20 GHZ.

BER			
Types of scenarios	**Ch 1**	**Ch 2**	**Ch 3**
No filter	4^{-9}	2^{-6}	9^{-10}
Gaussian filter	3^{-9}	4^{-5}	4^{-9}
Raised cosine filter	2^{-9}	4^{-7}	5^{-10}

1) User simulation: After analyzing the obtained results, the raised cosine filter was observed to perform better. To characterize the network's performance, a variable optical attenuator is used as users connected to the network in channel 1, configured at 1 dB. It's important to note that this value doesn't directly represent a real user, as the attenuator value doesn't correlate with the number of users connected to the network. Instead, it adjusts the network's load to evaluate its performance. User simulation is a tool used to assess network performance. By simulating different levels of connected traffic, one can determine how the network behaves under various conditions and how efficient it is in terms of capacity and quality of service.

To simulate a heavier load on the network, the attenuator is configured to the necessary value, and the received power and BER are checked. It's important to mention that when the attenuator was set between 1 and 14 dB, there was no variation in the BER. Therefore, the results shown in Fig. 25 simulate user presence starting from 15 dB, which is gradually increased in 2 dB increments up to 47 dB to simulate the presence of more users.

Fig. 25 shows the BER vs. received power changes. The goal is to determine the received power level that minimizes the BER in channel 1 of the UDWDM system. Upon examining the simulation results, when the received power is -17 dBm, a high-quality eye diagram and a low BER of 10^{-37} are observed. This value indicates a minimal error rate in transmission. Consequently, it can be stated that the UDWDM network configuration with the raised cosine filter and the received power effectively ensures reliable data transmission through the channel. On the other hand, for a BER value of 10^{-19} and received power of -29 dBm, the eye diagram already shows some interference, which is why there are more transmission errors. The eye is not completely open, suggesting that the signal has a larger margin of error and is more susceptible to noise and other interferences. Generally, a BER of 10^{-19} is still acceptable for many communication systems but is considered less robust than the 10^{-37} BER mentioned earlier. Finally, for a BER of 10^{-3} and a received power of -43 dBm, the eye diagram is nearly closed, indicating significant errors in transmission and poor signal quality. This is undesirable for high-speed digital communication systems like UDWDM. As more users are added, the signal level available to each one decreases, reducing received signal quality and decreasing received power. This can affect the system's ability to transmit information effectively.

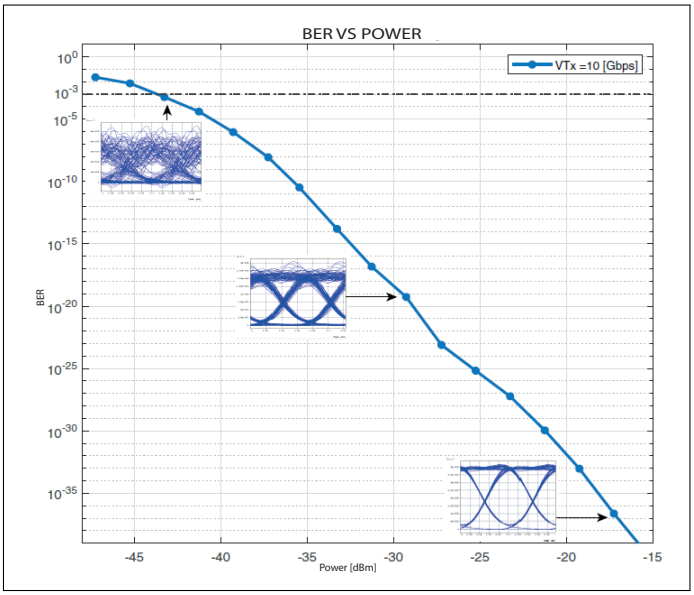

Fig. 25. BER vs. RECEIVED POWER and 25GHz channel spacing.

V. CONCLUSIONS

- This paper analyzes the performance of UDWDM technology in a PON network for which OptSim software has been used and considers three evaluation scenarios. For each scenario, transmission distance varied from 10 km to 20 km, users were connected to the network, transmission speed was 10 Gbps to 17 Gbps, and channel spacing was 25 GHz, 20 GHz, and 15 GHz. Simulation results indicate that UDWDM technology can significantly enhance the capacity and efficiency of the PON network, enabling a greater number of users and higher data rates, provided that proper channel spacing is considered
- Analyzing the simulation results reveals that certain transmission parameters significantly influence the per-

formance of UDWDM systems. As the distance between channels increases, several phenomena can affect the performance of the optical communication system, such as i) optical interference between channels, leading to increased error rates and affected by the optical power level of the channels, ii) wavelength, iii) signal-to-noise ratio, iv) modal dispersion, and v) chromatic dispersion.

- The three simulation scenarios provide valuable insights into how distance, transmission speed, and channel spacing can alter the BER, particularly impacting channel 2, which is most affected by attenuation and chromatic dispersion from adjacent channels. Using raised cosine and Gaussian filters helps mitigate these effects to some extent and improves signal quality. However, for transmission rates exceeding 15 Gbps and distances greater than 16 km, the effectiveness of filters diminishes as the BER value becomes equal to or lower than when no filters are used.
- The channel approach in UDWDM can offer benefits such as increased data transmission capacity and the potential to boost transmission speed by utilizing more bandwidth. However, considering that this approach can also lead to undesired optical phenomena, such as interference between channels and increased optical noise, is essential. Therefore, careful system configuration and design are crucial to ensure optimal performance. Referring to the above, a channel spacing of 25 GHz and distances between 10 km and 20 km results in the most suitable channel performance in all scenarios, while at 20 GHz and especially at 15 GHz, the BER increases to a greater extent.
- Simulation results showed that the choice of the filter is an important factor affecting the performance of a UDWDM system. In particular, it was found that the raised cosine filter provides better overall results compared to the Gaussian filter and no filter. The number of users used on a specific channel also significantly impacts signal quality and, consequently, the BER. As more users are added, the reception power varies, and the eye diagram exhibits interference, indicating that the signal is more susceptible to noise and other interferences. This can be explicitly observed when the BER value is 10^{-3}, and the reception power is -43 dBm.
- It is recommended that future research on UDWDM employ machine learning techniques, such as neural networks, to develop predictive models that anticipate system performance under various conditions. The goal is to provide advanced tools that allow systems to be optimally configured without the need to perform exhaustive simulations for each new configuration, thus optimizing the design process and improving the operational efficiency of networks.
- Energy models could also be developed to evaluate the energy consumption of the UDWDM system in a PON network under different configurations. The goal is to optimize signal quality transmission parameters and improve active components' power efficiency, such as the OLT and ONT, core network equipment, and end-user devices. This will allow a more sustainable and efficient configuration of UDWDM systems, contributing to the reduction of total energy consumption in optical communications, which is especially relevant in long-distance networks.

REFERENCES

[1] A. Paradisi, R. C. Figueirdo, A. Chiuchiarelli, and E. de Sousa Rosa, *Optical Communications*. Brazil: Springer, 2019. [Online]. Available: https://doi.org/10.1007/978-3-319-97187-2

[2] P. R. Y. Pulles, "Análisis de una red pon bajo la influencia de los efectos no lineales," Trabajo de titulación, Quito, 2017. [Online]. Available: https://dspace.ups.edu.ec/bitstream/123456789/14030/1/UPS%20-%20ST003002.pdf

[3] J. Segarra, V. Sales, V. Polo, and J. Prat, "Half-duplex transmission avoiding rayleigh backscattering crosstalk in udwdm-pon with coherent receivers," in *2014 16th International Conference on Transparent Optical Networks (ICTON)*, 2014, pp. 1–5.

[4] V. Solutions, "Red óptica pasiva (PON)." [Online]. Available: https://www.viavisolutions.com/es-es/red-optica-pasiva-pon

[5] V. Khosia, "A Comprehensive Review of Recent Advancement in Optical Communication Networks," *International Journal of Computer Sciences and Engineering*, vol. 6, pp. 617–626, Sep. 2018.

[6] R. Kaur and G. Singh, "A review of pon: Splitters and olt," *International Journal of Scientific & Engineering Research*, vol. 5, pp. 372–376, 2014. [Online]. Available: https://www.ijser.org/researchpaper/A-Review-of-PON-Splitters-and-OLT.pdf

[7] K. Yuksel, V. Moeyaert, M. Wuilpart, and P. Megret, "Optical layer monitoring in passive optical networks (pons): A review," in *2008 10th Anniversary International Conference on Transparent Optical Networks*, vol. 1, 2008, pp. 92–98.

[8] L. Chen and Y. Liu, "Research on wdm technology applied in optical fiber communication," *IOP Conference Series: Materials Science and Engineering*, vol. 365, no. 1, p. 012104, 2018. [Online]. Available: https://iopscience.iop.org/article/10.1088/1757-899X/1094/1/012114

[9] G. Agrawal, *Fiber Optic Communication Systems*, fourth edition ed. The Institute of Optics University of Rochester Rochester, New York: A JOHN WILEY & SONS. [Online]. Available: https://sv.20file.org/up1/169_1.pdf

[10] Y. Hernández, "Diseño de una red de fibra metropolitana para servicios avanzados s-Health en Smart Cities," Ph.D. dissertation, Universitat Oberta de Catalunya, Barcelona. [Online]. Available: https://openaccess.uoc.edu/bitstream/10609/90445/7/yolihernandezTFM0119memoria.pdf

[11] S. Delgado, "Simulation of FTTH Architecture in a Passive Optical Network on the OptiSystem Platform," Ph.D. dissertation, Catholic University of Santiago de Guayaquil, Guayaquil, 2015. [Online]. Available: http://repositorio.ucsg.edu.ec/bitstream/3317/4465/1/T-UCSG-PRE-TEC-ITEL-120.pdf

[12] S. Networks, "Wavelength Division Multiplexing: Taking Dark Fibre Capacity to the Next Level," Jun. 2016.

[13] International Telecommunication Union, "ITU-T Recommendation G.694.2: Spectral grids for wdm applications: Dwdm frequency grid," ITU-T, Tech. Rep. G.694.2, 2012. [Online]. Available: https://www.itu.int/rec/T-REC-G.694.2/en

[14] "CWDM,Cost Effective Alternative to Expand Network Capacity." [Online]. Available: https://www.3coptics.com/News/14.html

[15] W. W. Technology, "Cwdm or dwdm." [Online]. Available: https://www.wwt.com/article/cwdm-or-dwdm-which-should-you-use-and-when

[16] J. Astudillo and E. Ramirez, "Manual para la caracterización de la fibra óptica en DWDM," Ph.D. dissertation, Universidad Politécnica Salesiana Sede Cuenca, Cuenca, Apr. 2014. [Online]. Available: https://dspace.ups.edu.ec/bitstream/123456789/7119/1/UPS-CT003888.pdf

[17] K. Song, "Long-distance transmission of dwdm signals," *Optical Fiber Technology*, vol. 8, no. 3, pp. 163–174, 2002.

[18] D. Montero Hidalgo, "Advantages of the new UDWDM communications technology," Ph.D. dissertation, University of Costa Rica, Dec. 2004.

[19] M. Ali, A. M. Almufti, and S. Saber, "Experimental investigation between wdm-pon and dwdm-pon using different channel spacing experimental investigation between wdm-pon and dwdm-pon using different channel spacing," vol. 745, 03 2020. [Online]. Available: https://iopscience.iop.org/article/10.1088/1757-899X/745/1/012037

[20] V. Sales Zaragozá, "Access networks operated with limited tuning random lasers," Ph.D. dissertation, Polytechnic University of Catalonia, Barcelona, Spain, 2017. [Online]. Available: https://upcommons.upc.edu/bitstream/handle/2117/114015/TVSZ1de1.pdf;jsessionid=3D1C654042DE29C02C255D8A8A421AE9?sequence=1

[21] D. Montero, *Advantages of the New UDWDM Communications Technology*. University of Costa Rica. Faculty of Engineering. School of Electrical Engineering, 2004. [Online]. Available: https://catalogosiidca.csuca.org/Record/UCR.000196700

[22] M. Parker and S. Dhanani, *Digital video processing for engineers: A foundation for embedded systems design*. Newnes, 2012.

[23] Mathuranathan, "Raised cosine pulse shaping," Oct. 2018. [Online]. Available: https://www.gaussianwaves.com/2018/10/raised-cosine-pulse-shaping/

[24] E. Onieva, I. Santos, E. Osaba, H. Quintián, and E. Corchado, *Hybrid Artificial Intelligent Systems: 10th International Conference, HAIS 2015, Bilbao, Spain, June 22-24, 2015, Proceedings*. Springer, 2015, vol. 9121.

[25] G. Li, H. Liu, and S. Yang, "Gaussian filter to process tracer breakthrough curves," *Acta Carsologica*, vol. 48, no. 2, 2019.

[26] N. Pashtoon, "IIR digital filters," 1987. [Online]. Available: https://www-sciencedirect-com.translate.goog/topics/engineering/bessel-filter?_x_tr_sl=en&_x_tr_tl=es&_x_tr_hl=es&_x_tr_pto=sc

[27] FOA, "Presupuesto de potencia y de pérdida óptica." [Online]. Available: https://www.thefoa.org/ESP-Design/Ch9.htm

[28] "Conectores de fibra óptica sc/apc," Excel Networking. [Online]. Available: https://documents.excel-networking.com/datasheets/200-564

[29] C. Comunicaciones, "Fibra óptica g652d," 2019. [Online]. Available: https://www.c3comunicaciones.es/Documentacion/Alcance%20fo.pdf

[30] CISCO, "Atenuación máxima para enlaces de fibra óptica - Cisco." [Online]. Available: https://www.cisco.com/c/es_mx/support/docs/optical-networking/ons-15454-sonet-multiservice-provisioning-platform-mspp/27042-max-att-27042.html

[31] ITU-T, "Gigabit-capable passive optical networks," Aug. 2019. [Online]. Available: https://www.itu.int/rec/T-REC-G.984.2/es

[32] H. Elgamal, A. Haggag, M. Eltokhy, and A. E. A. Mohamed, "Bit rate maximizing by optimizing repeater spacing product for optical communication systems," *Automatic Control and System Engineering Journal*, vol. 21, no. 2, pp. 1–10, 2021.

[33] Thorlabs, "Thorlabs Modulator Mach-Zehnder." [Online]. Available: https://www.thorlabs.com/drawings/76fd6c473f930042-95C911E7-D2FB-2849-C916630FD9B3CF37/LNP4216-SpecSheet.pdf

[34] M. C. España, *Comunicaciones ópticas: conceptos esenciales y resolución de ejercicios*. Madrid: Ediciones Diaz de Santos, 2005. [Online]. Available: https://www.academia.edu/33300228/MAR%C3%8DA_CARMEN_ESPA%C3%91A_BOQUERA_COMUNICACIONES_%C3%93PTICAS_Conceptos_esenciales_y_resoluci%C3%B3n_de_ejercicios

[35] A. Bateman, *Digital Communications*, 1st ed. Madrid: Pearson Education, 2005.

[36] D. Martinez De La Cruz, "Diseño de un Sistema de Adquisición de datos para un Fotodiodo deAvalancha APD con aplicaciones en Experimentos de Óptica," Ph.D. dissertation, Benemérita Universidad Autónoma de Puebla, Puebla, México, Nov. 2018. [Online]. Available: https://repositorioinstitucional.buap.mx/handle/20.500.12371/7947

[37] H. Zumbahlen, *Linear Circuit Design Handbook*, 1st ed., USA, 2008. [Online]. Available: https://www.sciencedirect.com/topics/engineering/gaussian-filter

Thiamethoxam Residuality in Papaya Plant and Fruit (*Carica papaya* Linnaeus) Cultivated in Rotation with Watermelon (*Citrullus lanatus*)

Megchun-García Juan Valente[1, 2*], Castañeda-Chávez María del Refugio[3], Rodríguez-Lagunes Daniel Arturo[4], Lango-Reynoso Fabiola[5], and Amaro-Espejo Isabel Araceli[6]

***Abstract*—There is evidence of the high use of the neonicotinoid insecticide thiamethoxam, in tropical crops, for its effectiveness in the control of soil and plant pests. The objective of this study was to know the residuality and concentration of thiamethoxam in the papaya agroecosystem, in the main papaya fruit producing zone in the central area of the Gulf of Mexico. It was carried out during a papaya growing cycle with watermelon rotation; the taking of samples was according to the technique established by the NOM -AA-103-1988 for leaves and for fruit the NMX -FF-041-1996 by the method of quartering in papaya and watermelon, the samples were analyzed with a HPLC-UV, the data obtained were statistically analyzed by parametric and non-parametric Kruskal-Wallis tests. The presence of thiamethoxam was found in papaya and watermelon cultivation plants, the concentrations in papaya leaves reported a maximum value of 0.29 mg/kg, while for the leaves of the watermelon rotation fruit it was 0.15 mg/kg. In papaya fruit, thiamethoxam concentrations are within a range of 0.24 to 0.32 mg/kg. The concentrations and residuality of thiamethoxam mainly exceed the maximum tolerance and residuality limits of the EFSA and FAO.**

Keywords: **Agroecosystems, neonicotinoids, tropical fruit trees.**

***Resumen* — Existe evidencia del alto uso del insecticida neonicotinoide thiamethoxam en los cultivos tropicales por su efectividad en el control de plagas del suelo y la planta. El objetivo de este estudio fue conocer la residualidad y concentración del thiamethoxam en el agroecosistema de papaya en la principal zona productora de este fruto de la zona centro del Golfo de México. Este estudio se realizó durante un ciclo de cultivo de papaya con rotación de sandía; la toma de muestras se hizo según la técnica establecida por la NOM-AA-103-1988 para hojas y para fruta la NMX-FF-041-1996 mediante el método de cuarteo en papaya y sandia. Las muestras se analizaron con un equipo HPLC-UV, y los datos obtenidos se analizaron estadísticamente mediante pruebas paramétricas y no paramétricas de Kruskal- Wallis. Se encontró la presencia de thiamethoxam en la planta del cultivo de papaya y sandía. Las concentraciones en hojas de papaya reportaron como valores más altos 0.29 mg/kg, mientras que para las hojas del fruto de rotación de la sandía fue de 0.15 mg/kg. En el fruto de papaya, las concentraciones de thiamethoxam estuvieron dentro de un rango de 0.24 a 0.32 mg/kg. Las concentraciones y residualidad del thiamethoxam superan principalmente los límites máximos de tolerancia y residualidad de la EFSA y la FAO.**

Palabras Clave: **Agroecosistemas, neonicotinoides, árboles frutales tropicales.**

I. INTRODUCTION

ECOSYSTEMS are made up of biotic systems within a single physical system, in it there is a coexistence of organisms with the inorganic environment, and processes of exchange of matter, energy and organisms occur [1]. Modified ecosystems are used for the production of food and thus satisfy the needs of society; The management of pesticides is essential to obtain high levels of production performance, the use of these technologies generates contamination of water, soil and the environment. In Colombia, methamidophos pesticide residues of 5.1µg/L in cabbage plants [2]. A metabolite of neonicotinoids produces secondary metabolites in the water and some may have a toxicity equal to or greater than the original, thiamethoxam has a molecular weight of 291.71 g/mol, and was found in Wisconsin EE. UU, in water soluble in ranges of 1-9µg/L, and the average concentrations of several sampled places is 1.59 µg/L in periods of 5 years [3].

In the United States, they found thiamethoxam in concentrations of 3.6 µg/L in water samples from the plains. [4]. Thiamethoxam residues of less than 0.02 to 0.17 mg/kg were reported in coffee leaves and in leaves collected in the middle of the treetops, values between a range of 0.02 to 0.09 mg/kg; while in upper leaves the concentrations of thiamethoxam were

* **Corresponding author:** Juan Valente Megchun-García, Email: megchun.juan@inifap.gob.mx, megchj@gmail.com
1. Instituto Nacional de Investigaciones Forestales, Agrícolas y Pecuarias/ Campo Experimental Ixtacuaco. Veracruz, México. C.P. 93600. Email: megchun.juan@inifap.gob.mx, ORCID: https://orcid.org/0000-0002-2902-8088
2. Tecnológico Nacional de México/Instituto Tecnológico de Boca del Río. CP. 03330. Boca del Río, Veracruz. Email: megchj@gmail.com, ORCID: https://orcid.org/0000-0002-2902-8088.
3. Tecnológico Nacional de México/Instituto Tecnológico de Boca del Río. CP. 03330. Boca del Río, Veracruz. Email: mariacastaneda@bdelrio.tecnm.mx, ORCID: https://orcid.org/0000-0002-9209-0431
4. Universidad Veracruzana/Facultad de Ciencias Biológicas y Agropecuarias. CP. 94500. Córdoba, Veracruz. Email: darodriguez@uv.mx, ORCID: https://orcid.org/0000-0003-2987-3342
5. Tecnológico Nacional de México/Instituto Tecnológico de Boca del Río. CP. 03330. Boca del Río, Veracruz. Email: fabiolalango@bdelrio.tecnm.mx, ORCID: https://orcid.org/0000-0001-8359-434X
6. Tecnológico Nacional de México/Instituto Tecnológico de Boca del Río. CP. 03330. Boca del Río, Veracruz. Email: isabelamaro@bdelrio.tecnm.mx, ORCID: https://orcid.org/0000-0002-7115-5486
Manuscript Received: 01/03/2024
Revised: 21/05/2024
Accepted: 03/06/2024
DOI: https://doi.org/10.29019/enfoqueute.1037

between 0.02 to 0.17 mg/kg during handling and application of the dose of 2.25 g i.a. of thiamethoxam for the control of *Leucoptera coffera* (Guérin-Meneville). In lower coffee leaves the residuality of thiamethoxam was registered between a range of 0.04 to 0.12 mg/kg; in leaves collected in the middle of the tree canopy it was 0.04 to 0.18 mg/kg and in upper leaves it was 0.05 to 0.23 mg/kg managed with doses of thiamethoxam sprayed with 0.30 g i. a. [5].

As a consequence of global warming, the presence of new pests and resistance to different insecticides has increased. Low yields have been generated in fruit production; this implies the formulation of new, more effective and toxic chemicals; neonicotinoid pesticides worldwide as of 2008 are highly used in tropical fruit and vegetable crops. In foods such as honey, it was found that 70 % of the total samples analyzed contain neocotinoid residues, mainly in the regions of the continent of Africa, 80 % in Asia and Europe, in North America 90 %, 58 % in South America and 70 % in Oceania; This new generation of insecticides is made up of Imidacloprid, Nitenpyram, Acetamiprid, Thiamethoxam, Thiacloprid, Clothianidim and Dinotefuran. In the European Union there is evidence of the death of honey bees due to the use of neonicotinoids [4, 6 and 7]. Neonicotinoids are used in 120 countries to control insects, in Japan it has been applied to crops since 1995 [7]. This generated negative impacts on public health, the World Health Organization (WHO) estimates that each year around 500 000 to a million people are poisoned and between 5 000 and 20 000 die [8]. There is little information on neonicotinoid poisoning but in Antioquia and Salgar (Colombia), there are reports of people who were poisoned with thiamethoxam and Imidacloprid, individuals presented abundant diarrheal stools, nausea, vomiting, autonomic and neurological alterations, it is important to mention that neonicotinoids have a higher affinity with the nicotinic receptors of vertebrates and less with the receptors of invertebrates, and due to their high water solubility they do not cross the blood-brain barrier in humans, they are considered to interfere with the transmission of impulses in the central nervous system [9].

The European Union through EFSA, (European Food Safety Authority, 2012), established the maximum permissible limits for Imidacloprid at 0.05 mg/kg, thiamethoxam at 0.05 mg/kg, and for insecticides such as clothianidin at 0.02 mg/kg. The United States through the EPA (Environmental Protection Agency, 2012) established the maximum permissible limits for Imidacloprid of 1.0 mg/kg, thiamethoxam with the concentration of 0.4 mg/kg and for clothianidin there are no regulations. In Mexico there are no standards that regulate the use of neonicotinoids [10]. Neonicotinoid insecticides can act acropetally and basipetally in the plant, and can be retained by organic matter and clays, these particles are assimilated, transported and accumulated in the organs of plants such as flowers, fruits and leaves. In Venezuela, was found an Imidacloprid particle retention of 2.96 ± 1.56 in soil and thiamethoxam of 2.81 ± 1.4 mg/kg, in guava orchards [11]. Thiamethoxam is efficient in the control of *Paracocus marginatus*, *Bemisia tabaci*, *Leptinotarsa decemlineata* and *Myzus persicae* [12, 13 and 9]. This is due to the ability to translocate from the xylem and be transported to the phloem, it also has characteristics of translocation to flower pollen, there is a probability of being present in the nectar and participating in the guttation processes of plants [4, 14]. The presence of thiamethoxam in the fruits could be a reason for contamination and impact on public health, studies in the papaya culture in Veracruz, Mexico demonstrate the efficacy of the insecticide thiamethoxam in insects associated with the crop, with 15-day intervals applied to the tree canopy [14]. The use of pesticides applied to the foliage could generate residuality in fruits for human consumption, in addition to thiamethoxam due to its toxic effectiveness in pest control, in developed countries it is decreasing, with strict environmental legislation and with new active groups that exercise pressure for controlled use [15].

In Mexico, the group of neonicotinoids is widely used in tropical crops such as papaya, due to its economic importance and as the main product and export. To avoid phytosanitary problems in papaya cultivation, the rational use of pesticides and herbicides is recommended [16, 17]. The main producers in the center of the Gulf of Mexico, Veracruz, irrationally handle pesticides in the agroecosystem with papaya, intended to control nematodes, red spider mites, whiteflies and aphids, 35 % of producers use organophosphates in a higher proportion, and currently new molecules are being used to face the problems of resistance to pesticides and decrease in the effectiveness of control, such is the case of the chemical group of neonicotinoids, 6 % of the producers, use thiamethoxam, without a control in large volumes during crop cycles [18]. The objective of this research was to know the concentration and residuality of thiamethoxam in plant and fruit in the papaya agroecosystem in the main tropical fruit producing area in the center of the Gulf of Mexico, during papaya cultivation with watermelon rotation.

II. MATERIALS AND METHODS

The experiment was developed in the agroecosystem with papaya, the main crop in the central area of the Gulf of Mexico. An experimental plot was established with the Maradol papaya crop and with the watermelon rotating crop (Figure 1), located at the coordinates 18° 53´51´´ north latitude and 96° 22´37´´ west latitude, the papaya orchard has a population density of 2778 plants/ha.

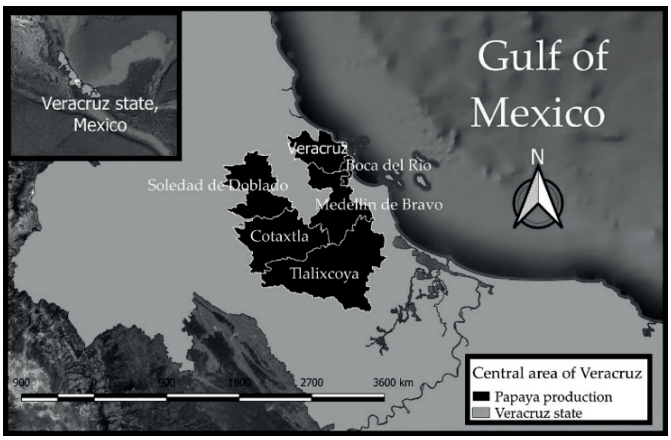

Fig. 1. Papaya producing area of the central gulf of Veracruz, Mexico.

The characteristics of the experimental plot.

In the central area of the Gulf of Mexico is the main Maradol papaya producing zone, where producers use thiamethoxam during the crop cycle, with a volume of around 500 ml ha^{-1}, to control whiteflies, thrips and aphids.

The soils of the agroecosystem with papaya in the study area are characterized by having 45 % constituted by the sowing of watermelon and papaya, on different dates and with crop rotation. The soil type is vertisol, and the insecticide thiamethoxam has a period of 5 consecutive years that is used in the papaya agroecosystem. For the study of thiamethoxam in watermelon leaf, papaya and thiamethoxam in papaya fruit; the study treatments were in phenological stages in the papaya agroecosystem; and three treatments were carried out; T1: the watermelon crop (*Citrullus lanatus*); T2: After the papaya transplant; T3: Papaya fruit production. In the production of papaya fruit, thiamethoxam was analyzed in three dates of papaya fruit harvests, named: T1 = Cut of fruit at 475 days, T2 = Cut of fruit at 495 days and T3 = Cut of fruit at 555 days.

The sampling technique was in accordance with the provisions of the Official Mexican Standard NOM-AA-103-1988 and the Mexican Standard NMX-FF-041-1996, The technique of the quartering method was used to analyze the papaya fruit. The samples were collected and transferred to the Laboratory of Agricultural Resources Research (LIRA) of the Technological Institute of Boca del Río.

For the determination of thiamethoxam concentrations in plant and fruit, the HPLC-UV equipment, Thermo scientific-model Finnigan surveyor, was used. It is made up of a quaternary pump, a 200 vial autosampler, a 250 µL syringe, a UV visible and fluorescence detector, contains four solvents and a separation column of 10 cm by 4.6 in diameter of 5 µ and a 20 µL loop of sample with a capture system. The instrumental conditions of the chromatographic column is C18 RP 5 µm, with a temperature of 25 ° C, a mobile phase of 45/55 (AC/AG), with a flow of 1mL min^{-1} and λ = 254 nm, a working range of 10 to 100 µg of thiamethoxam L^{-1}, the linearity of R≥0.9 and a recovery of ≥90 %. For the determination of thiamethoxam, the samples were kept in refrigeration, later 5 g of the sample was added with 10 ml of Acetonitrile (CH_3CN), it was left for 5 minutes; vortexed one minute, 3 ml of HPLC water was added with 6 ml of hexane (C_6H_{14}), 4 g of Magnesium Sulfate (MgSO4), 1 g of N-acetylcysteine (NAC), 500 mg of sodium citrate ($Na_3C_6H_5O_7$); subsequently, manual shaking was carried out for 20 seconds plus vortexing for one minute; then it was continued with 10 minutes of centrifugation; 6 ml of excess was taken and 90 mg of magnesium sulfate, 150 mg of Primary Secondary Amine (PSA), 150 mg of Octadecyl Carbon Chain (C18) were placed in tube II; stirring was carried out for 1 minute in vortex, and it was centrifuged at 5000 rpm for 10 minutes; 3 ml of supernatant was taken and brought to dryness at 40 ° C and with N2; 200 µl of methanol (CH_3OH) was added to the mobile phase, and 100 µl + 900 µl was measured, and then 0.22 µl was filtered with discs, later they were recovered in vials. All the reagents used are of chromatography quality (Mr), in addition, thiamethoxam 37924-100MG-R was used as standard, with a confidence interval = 95 % / n = 6, its function point is 139.2-139.6 ° C, and its analytical test (HPLC) is 99.6 %, in water (Karl Fischer) 0.01 %. The eluted peaks for thiamethoxam, present were greater than 0.1 mg / kg. The statistical design for the analysis of plant leaves in watermelon-papaya and papaya fruit was complete random blocks with 6 repetitions. The statistical software was with the Statistica version 2007 program, with parametric (ANOVA) and non-parametric Kruskal-Wallis statistical analyzes, and categorization of graphs with pie charts.

III. RESULTS

In plant it was found that thiamethoxam in the transplant stage (T2) registered the highest values with respect to the concentrations of thiamethoxam in *Citrullus lanatus* (T1), this could be due to the sowing date between both crops, since It is carried out at different periods during the year, for example for papaya, the sowing date is located in the period from May to August in the central area of Veracruz., and then it begins with the sowing of watermelon in the months of December until February. In the papaya fruit production stage (T3), lower concentrations of thiamethoxam were observed in the photosynthetically active leaf, but higher than the concentrations of thiamethoxam in *Citrullus lanatus* leaves corresponding to T1 (Fig. 2). This phenomenon responds to the fact that papaya producers are not only producers of one species, some produce two or even three crops in the central zone of Veracruz.

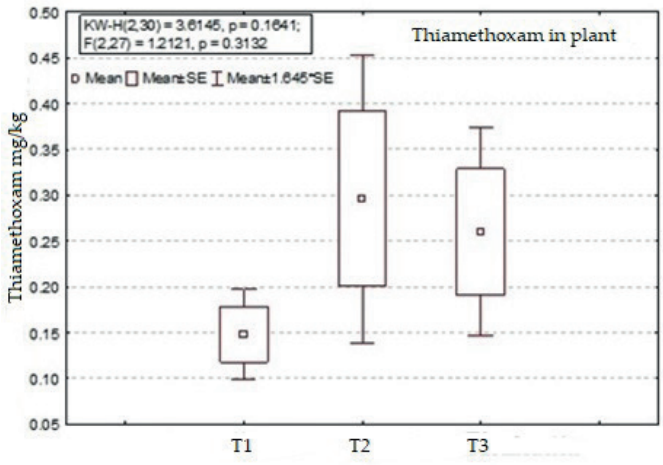

Fig. 2. Thiamethoxam concentrations in papaya plant (*Carica papaya* L.) in rotation with watermelon (*Citrullus lanatus*). T1 = Watermelon cultivation, T2 = After papaya transplant, T3 = Papaya fruit production.

80 % of the leaves sampled in papaya presented concentrations of thiamethoxam in the fruiting stage, higher than the samplings carried out in the other stages corresponding to the papaya agroecosystem; It is deduced that there is greater migration of thiamethoxam in the fruiting stage of the *Carica papaya L.* crop, that is, considering the osmosis processes that intervene in the plant, in high rainfall periods (Fig. 3).

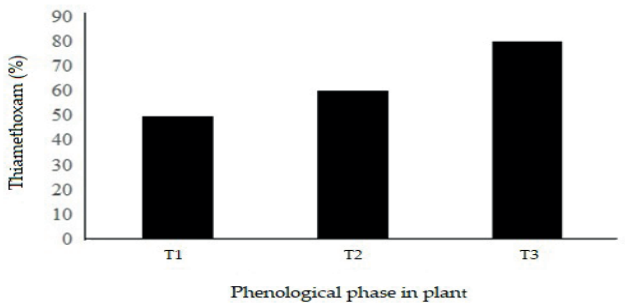

Fig. 3. Presence of thiamethoxam in papaya plant in rotation with watermelon. T1 = Watermelon cultivation, T2 = After transplanting, T3 = Papaya fruit production.

Regarding the concentrations of thiamethoxam in papaya fruits, collected in the physiological maturity stage and whole fruit, they did not present significant differences in the three main harvest cuts. At 470 days after transplantation-express values higher than 0.3 mg / kg, followed by the fruits harvested 556 days after cutting (Fig. 4). 80 % of the fruits sampled at 556 days, presented concentrations of thiamethoxam higher than the other cuttings of papaya fruits. This implies that the transpiration processes are the mechanisms by which the thiamethoxam molecule uses as a route to bioconcentrate in the fruit (Fig. 5).

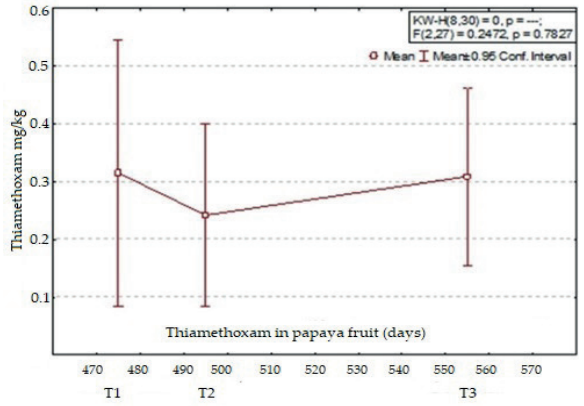

Fig. 4. Thiamethoxam concentration in whole papaya fruit (*Carica papaya* L.). In papaya fruit it was, T1 = Cut of fruit at 475 days, T2 = Cut of fruit at 495 days and T3 = Cut of fruit at 555 days.

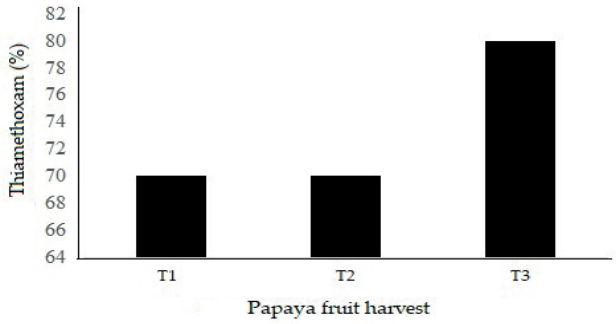

Fig. 5. Presence of thiamethoxam in papaya fruit between cut dates. In papaya fruit it was, T1 = Cut of fruit at 475 days, T2 = Cut of fruit at 495 days and T3 = Cut of fruit at 555 days.

The papaya fruits in physiological maturity, presented concentrations without statistically significant differences of thiamethoxam with respect to the concentrations registered in the photosynthetically active leaves, otherwise with the leaves of *Citrullus lanatus* (relay culture), whose values are lower than those found in growing papaya. The cause of this behavior may be in response to the doses of thiamethoxam per hectare, applied to the association and replacement of watermelon and papaya crops, or the ability of thiamethoxam to bioaccumulate in soil and be transported via apoplast and sympathetic aerial organs of plants (leaves, flowers and fruits). Considering that the input mechanisms of thiamethoxam are mainly where the processes of photosynthesis and cellular respiration take place (Fig. 6). There are other entry and exit mechanisms for thiamethoxam in the plant called porous spaces (ostioli) such as lenticels in the stems, stomata in the leaves, hydathodes in the leaves and nectaries, which play an important role in the transport of thiamethoxam. The thiamethoxam is characterized by being mobile and participating in the transpiration processes, which is why it can be in the root zone of the plants, when the thiamethoxam is applied in the irrigation system or remain in the root zone for the control of pests, this indicates their participation in the soil transport processes, such as the phenomena of water erosion, infiltration and percolation, which go directly to the aquifer. The water cycle explains the mobility process of thiamethoxam in water in the atmosphere and soil, due to the fact that thiamethoxam molecules tend to evaporate easily through the stomata of plants during the day and from the surface of the floor. The mobility of thiamethoxam in water could allow its presence in water for domestic use and for irrigation of crops (Fig. 7).

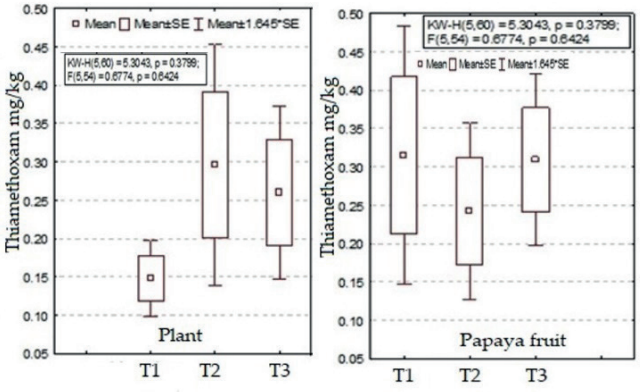

Fig. 6. Plant thiamethoxam concentrations in watermelon and papaya, concentrations in papaya fruit. In plant T1: The watermelon crop; T2: After the papaya transplant; T3: Production of papaya fruit. In papaya fruit it was, T1 = Cut of fruit at 475 days, T2 = Cut of fruit at 495 days and T3 = Cut of fruit at 555 days.

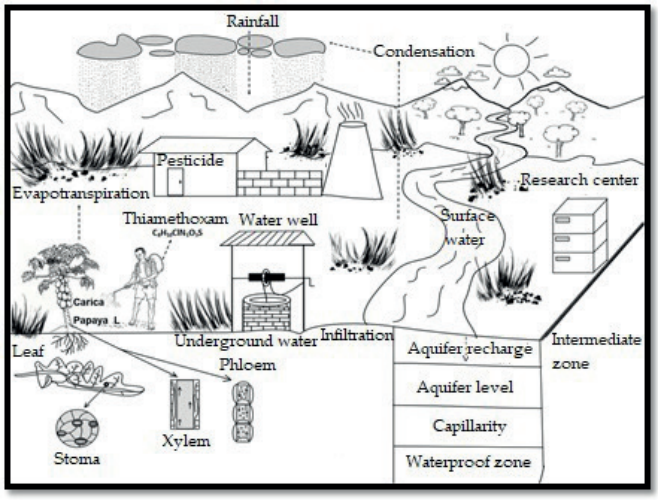

Fig. 7. Mobility of thiamethoxam in the papaya agroecosystem (by Eulises Megchún-García and Juan Valente Megchún-García).

IV. DISCUSSION

The presence of thiamethoxam was found in the nectar and pollen of the plants with values of 4 µg/kg, such is the case of *Cucurbita pepo*, the concentrations corresponded to 12 ± 9 µg/kg in pollen and 11 ± 6 µg/kg in nectar; 13 ± 3 µg/kg of thiamethoxam were found in irrigation drops established with plants with female flowers, and in soil particles managed with plants with female flowers, a concentration of thiamethoxam of 26 ± 12 µg/kg was found [19]. The *Citrullus lanatus* leaves analyzed presented higher thiamethoxam residuality than Cucurbita pepo, in this sense the thiamethoxam particles in *Carica papaya* L. are higher than those reported for *Citrullus lanatus* in leaves and fruits, this phenomenon is a consequence of the crop cycle of each species. During the papaya experiment, 556 days elapsed from the transplant to the third cut in the fruit production stage, it was observed that in this period there is the presence of thiamethoxam.

This phenomenon can be attributed to the residuality of thiamethoxam, since it has a tendency to decrease over time to more than 50 %, making periodic applications of thiamethoxam every 90 days; In sandy loam and clay loam soils, residuality of linuron + thiamethoxam + mancozeb was found in concentrations of 1 380 to 1 439 mg/kg [20]. In Hungary in different types of soil thiamethoxam was found, the values were 0.20 µg/ml of thiamethoxam in clay soils, and in loamy soils 0.40 µg/ml, with respect to sandy soils it was 0.70 µg/ml, This phenomenon could be due to the structure of each soil sample, due to the influence on the concentrations of thiamethoxam in the soil atmosphere, since some types of soils have greater porosity and different texture [21]. Thiamethoxam exerts an inhibitory effect on the soil on phosphatases and dehydrogenase activities [22]. Faced with this situation, the microbial processes and the release processes of C, N and P in the soil are affected when they are interrupted with the presence of thiamethoxam, this is the result of the agronomic management of the soil such as tillage, weed control and pest control [23].

Thiamethoxam, due to its physical-chemical characteristics, is absorbed by plants and distributed throughout the structure until they become toxic for variable periods in time; Although it has a similar structure to nicotine, neonicotinoids have in their structure a nitro or cyano radical that makes them electronegative and makes them more related to nicotinic receptors in insects, in addition, they have a physiological pH that allows them to be water soluble and the volume of distribution is variable in the plant [9]. The mobility of neonicotinoids in the phloem of the plant can occur to a certain extent, but it is possible to find it in drops of guttation water from treated seeds, with the risk of causing toxicity to bees, there are arguments that mention that the drops of water of this physiological process in the plant, it does not have much relevance for the colonies of honey bees (*Apis mellifera*), The concentration of neonicotinoid residues in flowers, nectar and pollen, less than 20 µg/kg, has been demonstrated, these concentrations are not toxic to bees [24]. The European community, as of 2004, prohibited the use of neonicotinoids in crops, due to the mortality that occurred in honey bees, however, the review processes were continued, in addition to that residuality in pollen and nectar has been found in a range from 1 to 10 µg/kg in the case of Imidacloprid, it is estimated that acute toxicity in bees occurs from 60 µg/kg, although chronic effects have been reported in lower concentrations, In 2005, the French Community for Food Standards published a study to refute that there is no toxic influence of Imidacloprid (Neonicotinoids) on bee hives fed with syrup contaminated with Imidacloprid [15]. With respect to what was found in this study of thiamethoxam in watermelon and papaya, the concentrations exceed those established by the international standards of EPA (Environmental Protection Agency) and EFSA (European Food Safety Authority) in 2002, of 0.4 and 0.05 mg/kg, thiamethoxam at high concentrations could translocate to nectars and pollen in the flowering and fruiting stage of papaya, considering that the residuality of thiamethoxam is a function of the amount bioaccumulated in the main organs of the plant, There is a risk of consuming contaminated agricultural food, in addition, thiamethoxam could be involved in the biogeochemical processes of the papaya agroecosystem, in turn generating ecological damage to surface and underground water, which leads to negative impacts on the consumption of fish food and in the consumption of water for domestic use [18].

Previously, the damage of neonicotinoids in bees was briefly discussed. There are studies that affirm that in bees, the use of thiamethoxam in doses of 0.2, 1 and 2 ng/bee affect thermoregulation, decreases foraging activity and deteriorates the strength of the bees, colonies, reduces the density of colonies and nesting, is highly toxic to bees including bumblebees [25]. Therefore, thiamethoxam is one of the agents responsible for the drainage of bees and the contamination of surface and ground water, its characteristics of toxic bioaccumulation of difficult mineralization and highly resistant to biological treatment, represents a risk for ecosystems and the human health [26]. The environmental profile of neonicotinoids such as thiamethoxam indicate that they are persistent with high potential for leaching and runoff, highly toxic to a wide range of invertebrates, generating a significant risk for aquatic and terrestrial fauna of ecosystems [27]. In Croatian studies in the cultivation of sugar beet (*Beta vulgaris vulgaris* var. altissima), residual neo-

nicotinoids were found in beneficial soil organisms, such as earthworms and ground beetles; in beetles, Imidacloprid was found at a concentration of 0.027 mg/kg, in earthworms it was 0.2141 mg/kg, while for Thiamethoxam it does not exceed 0.0008 mg/kg in these organisms [28]. In Sri Lanka, 56 patients poisoned with Imidacloprid presented to the emergency department were reported, demonstrating that neonicotinoids reach high concentrations in the blood of humans once administered orally and can remain for 10 to 15 hours [9]. The risk of harm from thiamethoxam to the population of adolescents, adults and schoolchildren in the state of Veracruz, Mexico has been estimated, fetoxicity and skeletal anomalies (malformations) have been demonstrated [29].

V. CONCLUSIONS

Thiamethoxam was found in watermelon leaves with values of 0.15 mg/kg, and in papaya leaves the highest values were 0.29 mg/kg, when papaya plants were transplanted in the field. The residuality in whole papaya fruit in the three cuts in physiological maturity had a similar behavior, but they exceeded the concentrations of thiamethoxam in leaves, this indicates that thiamethoxam migrates to bioconcentrate in papaya fruits. The thiamethoxam values in papaya fruit correspond to 0.24 to 0.32 mg/kg.

The concentrations of thiamethoxam exceed the residuality and tolerance values of EFSA (European Food Safety Authority) and FAO (Food and Agriculture Organization of the United Nations). But some concentrations are below the limits of tolerance and residuality of the EPA (United States Environmental Protection Agency).

ACKNOWLEDGMENTS

To CONAHCYT, for the financial support to carry out this research.

REFERENCES

[1] D. Armenteras, T. M. González, L. K. Vergara, F. J. Luque, N. Rodríguez and M. A. Bonilla., "Revisión del concepto de ecosistema como unidad de la naturaleza 80 años después de su formulación," *Ecosistema,* vol. 25, no.1, pp. 83-89, 2016. https://doi.org/10.7818/ECOS.2016.25-1.12

[2] D. H. Ramírez, A. M. Zuluaga and E. de J. Gómez "Evaluación del riesgo de contaminación por metamidofos en la microcuenca el salto del municipio de El Santuario, Antioquia," *Revista EIA*, vol. 8, pp. 165-180, 2007.

[3] C. J. M. Bonmatin, V. C. Giorio, V. Girolami, D. Goulson, D. P. Kreutzweiser, C. K. Krupke, M. Liess, E. Long, M. Marzaro, A. D. Mitchell, D. A. Noome, N. Simon-Delso and A. Tapparo, "Enviromental fate and exposure; neonicotinoids and fipronil," *Environ Sci Pollut Res*., vol. 22, pp. 35-67, 2015. https://dx.doi.org/10.1007/s11356-014-3332-7

[4] J. P. Van der Sluijs, N. Simón-Delso, D. Goulson, L. Jean-Mar Bonmatin and L. P. Belzunces, "Noenicotinoids, bee disorders and the sustainability of pollinator services. *Current opinión in Environmental Sustainability*, vol. 5, pp. 293-305, 2013. http://dx.doi.org/10.1016/j.cosust.2013.05.007

[5] R. G. I. Diez, G. C. De Baptista, L. R. P. Trevizan, M. L. Haddad and E. D. Nava, "Residuos de tiametoxam, aldicarbe e de seus metabólitos em folhas de cafeeiro e efeito no controle de *Leucoptera coffeella* (Guerin-Meneville) (Lepidoptera: Lyonetiidae). Crop protection," *Neotropical Entomology,* vol. 35, no. 2, pp. 257-263, 2006. https://doi.org/10.1590/S1519-566X2006000200016

[6] G. J. V. Megchún, C. Ma. del R. Castañeda, L. D. A. Rodríguez, G. J. Murguía, R. F. Lango and O. O. R. Leyva, "Thiamethoxam in tropical Agroecosystems," *Global Journal of Biology, Agriculture & Health Sciences*. vol. 5, no. 3, pp. 75-81. 2016.

[7] M. Renaud, T. Akeju, T. Natal-da-luz, S. Lestón, J. Rosa, F. Ramos, J. P. Sousa and H. M. V. S. Azevedo-Pereira, "Effects of the noenicotinoids acetamiprid and thiacloprid in their commercial formulations on soil fauna," *Chemosphere*, vol. 194, pp. 85-93, 2018. https://doi.org/10.1016/j.chemosphere.2017.11.102

[8] S. B. Valdez, D. E. L. García, R. J. M. Cobo and B. G. López, "Impacto de los plaguicidas en la salud de los habitantes del valle de Mexicali, México," *Rev. Ecologica Latino Americana*, vol. 6, no. 3, pp. 15-21, 2000.

[9] A. F. Estrada, M. C. Berrouet M. and J. A. Giraldo, "Toxicidad por neonicotinoides: revisión de tema y reporte de dos casos," *Medicina U.P.B.* vol. 35, no. 1, pp. 41-46, 2016. https://doi.org/10.18566/medupb.v35n1.a06

[10] B. M. A. Sánchez, B. F. Santamaría, L M. J. Zavala and N. C. López, "Plaguicidas organosintéticos autorizados en México y el mercado internacional para su uso en papaya". Instituto Nacional de Investigaciones Forestales, Agrícolas y Pecuarias. Campo Exprimental Mocochá. Centro de Investigaciones Regional Sureste. Mérida, Yucatán, México. 2012. 36 p.

[11] G. Ettiene, R. Bauza, L. Sandoval, D. Medina, J. Raga, M. Quiros, Y. Petit, N. Poleo and I. Dorado, "Estudio de la sorción de los insecticidas imidacloprid y tiamethoxam en muestras de suelo," *Revistas Facultad de Agronomía,* vol. 33, pp. 458-481, 2016. https://produccioncientificaluz.org/index.php/agronomia/article/view/27210

[12] University the Hertfordshire. PPDB: Pesticide Properties database. 2015.

[13] A. Seni and A. K. Sahoo, "Efficacy of certain insecticides on papaya mealybug, *Paracoccus marginatus* Williams y Granara de Willink (Hemiptera: Pseudococcidae)," *Journal of Entomology and Zoology Studies*, vol. 3, no. 4, pp. 14-17, 2015.

[14] G. J. V. Megchún, C. Ma. R. Castañeda, L. D. A. Rodríguez, G. J. Adame, G. J. Murguía, R. F. Lango and O. O. R. Leyva, "Use of thiamethoxam, associated with insect populations in papaya (*Carica papaya* Linnaeus) cultivation," *International Journal of Research Granthaalayah*, vol. 6, no. 1, 2018. https://doi.org/10.5281/zenodo.1168978

[15] G. J. Devine, D. Eza, E. Ogusuku and M. J. Furlong Uso de insecticidas: contexto y consecuencias ecológicas. *Rev. Perú Med. Salud Pública*, vol. 25, no.1, pp. 74-100, 2008.

[16] A. Bogantes A., M. Hernández C. and E. Mora N., "Herbicidas para el control de *Spermacoce tenuior* L. En papaya (*Carica papaya* L.)," *Agronomía Mesoamericana*, vol. 21, no. 1, pp. 185-192, 2010.

[17] A. Vásquez L., E. Hernández C., A. Mora A., C. Nava D. and F. Sánchez G., "Etiología y epidemiología de la necrosis de flores y frutos juveniles del papayo (*Carica papaya* L.) en Guerrero, México," *Agrociencia,* vol. 46, pp. 757-767, 2012.

[18] G. J. V Megchún, L. D. A. Rodríguez, C. Ma. del R., Castañeda, G. J. Murguía, R. F. Lango and O. O. R. Leyva, "Thiamethoxam in papaya (*Carica papaya* Linnaeus) Agroecosystems," *International Journal of Environment, Agriculture and Biotechnology,* vol. 2, no. 2, pp. 874-880, 2017. http://dx.doi.org/10.22161/ijeab/2.2.40

[19] K. A. Stoner and B. D. Eitzer, "Movement of soil-applied Imidacloprid and Thiamethoxam into néctar and pollen of squash (*Cucurbita pepo*)," *Plos one,* vol. 7, no. 6, e39114, 2012. http://dx.doi.org/10.1371/journal.pone.0039114

[20] M. Swarcewicz, A. Gregorczyk and J. Sobczak, "Comparison of linuron degradation in the presence of pesticide mixtures in soil under laboratory conditions," *Environ monit assess.,* vol. 185, pp. 8109-8119, 2013. http://dx.doi.org/10.1007/s10661-013-3158-7

[21] M. Mortl, O. Kereki, B. Darvas, S. Klatyik, A. Vehoszky, J. Gyori and A. Szekacs, "Study on soil mobility of two neonicotinoid insecticides," *Journal of Chemistry,* p. 6, 2016. http://dx.doi.org/10.1155/2016/4546584

[22] G. Jyot, K. Mandal and B. Singh, "Effect of dehydrogenase, phosphatase and urease activity in cotton soil after applying thiamethoxam as seed treatment," *Environ Monit Asses,* vol. 187, no. 298, 2015. https://doi.org/10.1007/s10661-015-4432-7

[23] C. Henríquez, L. Uribe, A. Valenciano and R. Nogales, "Actividad enzimática del suelo-deshidrogenasa, β-glucosidasa, fosfatasa y ureasa-

bajo diferentes cultivos," *Agronomía Costarricense,*vol. 38, no. 1, pp. 43-54, 2014.

[24] C. van Breukelen and y C. Maus, "Seguridad de los insecticidas neonicotinoides para las abejas," *Bee Care Center. Beeinformed*, 3, 2017. https://www.bayer.com/sites/default/files/BEEINFOrmed_3_Bee_Safety_of_Neonicotinoids__Spanishj4qsl75i_0.pdf

[25] N. Y. Martin and N. E. Suárez, "Daño colateral en abejas por la exposición a pesticidas de uso agrícola," *Entramado,* vol. 14, no. 1, pp. 232-240, 2018. https://doi.org/10.18041/entramado.2018v14n1.27113

[26] J. C. Forti, P. E. M. Robles, Y. S. Tadayozzi, M. A. F. Demori, F. A. Santos, F. F. Putti and E. F. Vicente, "Electrochemical processes used to degrade thiamethoxam in water and toxicity analyses in non-target organisms," *Processes*, vol. 12, no. 5, p. 887, 2024. https://doi.org/10.3390/pr12050887

[27] K. Y. García, M. Salazar and J. E. García, "Efecto del neonicotinoide-tiametoxam en el desarrollo embrionario del pez cebra (Dania rerio)," *Rev. Toxico,* vol. 35, pp. 22-27, 2018.

[28] G. H. Viric, D. Lemic and R. Bazok, "Neonicotinoid residues in earthworms and ground beetles under intensive sugar beet production preliminary study in Croatia," *Agronomy,* vol. 12, no. 9, 2022. https://doi.org/10.3390/agronomy12092102

[29] J. Díaz, A. Barraza, L. Yánez and L. Hernández, "Plaguicidas en alimentos: riesgo a la salud y marco regulatorio en Veracruz, México," *Salud pública Mex.*, vol. 63, pp. 486-497, 2021. https://doi.org/10.21149/12297

Ecological Motorcycle Taxi, incorporation of an electrolyzer as an alternative for the suppression of pollutants and noise reduction

Manuel Antonio Rodríguez-Perez[1], Agustín Pio Estrada-Ramírez[2]

***Abstract* — Environmental pollution from transportation has been a fundamental challenge for humanity throughout history, with conventional fuels contributing significantly to environmental degradation. This project seeks to suppress pollution and reduce noise generated by motorcycle taxis, whether for personal and/or private use. The main objective of the research work was to implement an electrolyzer in the combustion system of a motorcycle taxi to suppress environmental pollution and reduce noise. Methods included vehicle preparation, electrolyzer installation, battery adjustment, hydrogen generation, emissions measurement, safety, and data collection. As a result, the electrolyzer was implemented in the single-cylinder motorcycle taxi; The noise limit allowed at work in Peru is 85 dB, which is equivalent to 100 % noise at most; When using gasoline, a value of 76.4 dB was obtained, equivalent to 89.88 % noise, and when using hydrogen, a value of 71.7 dB was obtained, equivalent to 84.35 % noise, therefore, the total noise reduction was 4.70 dB (5.53 %) than established. The discussion highlighted that hydrogen is a clean fuel, with zero emissions and only emitting water vapor instead of polluting gases [5]. The conclusion highlights the critical importance of the research, supported by the total reduction of 5.53 % of noise with this new technology and in turn external sources support that using hydrogen produced a smoother and quieter combustion; Regarding the useful life of the engine, due to the cleaner and more efficient combustion, the accumulation of waste was reduced, which benefits reducing the wear of internal components and the need for costly maintenance.**

***Keywords* - electrolysis of water; electrolyzer; electrolyte; green hydrogen; technology; renewable resource.**

***Resumen* — La contaminación ambiental derivada del transporte ha sido un desafío fundamental para la humanidad a lo largo de la historia, con los combustibles convencionales contribuyendo significativamente a la degradación ambiental. Este proyecto busca suprimir la contaminación y reducir el ruido generada por mototaxis, ya sean de uso personal y/o privado. El trabajo de investigación tuvo como objetivo principal implementar un electrolizador en el sistema de combustión de un mototaxi para suprimir la contaminación ambiental y reducir el ruido. Los métodos incluyeron la preparación del vehículo, instalación del electrolizador, ajuste de la batería, generación de hidrógeno, medición de emisiones, seguridad y recolección de datos. Como resultado, se logró implementar el electrolizador en el mototaxi monocilíndrico; el límite de ruido permitido en el trabajo en el Perú es de 85 dB, que equivalen el 100 % de ruido como máximo; al utilizar gasolina se obtuvo un valor de 76.4 dB equivalentes a 89.88 % de ruido y al usar hidrógeno se obtuvo un valor de 71.7 dB siendo el 84.35 % de ruido, por lo tanto, la reducción total de ruido fue de 4.70 dB (5.53%) de lo establecido. La discusión destacó que el hidrógeno es un combustible limpio, con nulas emisiones y solo emitiendo vapor de agua en vez de gases contaminantes [5]. La conclusión subraya la importancia crítica de la investigación, respaldada por la reducción total del 5.53 % de ruido con esta nueva tecnología y a su vez fuentes externas apoyan, que el utilizar hidrógeno produjo una combustión más suave y silenciosa. En cuanto a la vida útil del motor, la combustión más limpia y eficiente reduce la acumulación de residuos, lo que disminuye el desgaste de los componentes internos y la necesidad de mantenimientos costosos.**

***Palabras Clave* – Electrólisis del agua; electrolizador; electrolito; hidrógeno verde; tecnología; recurso renovable.**

I. INTRODUCTION

IN the past, one of the greatest challenges facing humanity has been the reduction of environmental pollution generated by transportation [14].

As an argument for the problem, the use of gasoline in internal combustion engines had several environmental and efficiency problems [21]. First, gasoline was a fossil fuel extracted from petroleum, which meant that its production and consumption contributed significantly to climate change. In addition, the burning of gasoline in internal combustion engines emitted a large amount of greenhouse gases, such as carbon dioxide and nitrogen oxide, which contributed to global warming and air pollution [4].

Air pollution had a negative impact on lung development and had been linked to the development of various respiratory conditions such as emphysema, asthma and chronic obstructive pulmonary disease [24]. The presence of particulate matter and nitrogen oxide was associated with the development of chronic bronchitis.

In this context, motorcycle cabs, as a means of transport widely used in some regions of the world, had been identified as a major source of toxic emissions. The combustion of gasoline

1. Manuel Antonio Rodríguez-Perez is an undergraduate student at the Professional School of Mechanical and Electrical Engineering at the César Vallejo University of Trujillo, Peru. Email: roperezma@ucvvirtual.edu.pe, ORCID: https://orcid.org/0009-0003-8786-6009

2. Agustín Pio Estrada-Ramírez has a bachelor's degree in education from the Professional School of Education of the Catholic University of Trujillo Benedicto XVI, Peru. Email: pioape.5@gmail.com, ORCID: https://orcid.org/0009-0002-6193-9751

Manuscript Received: 09/01/2024
Revised: 14/02/2024
Accepted: 15/05/2024
DOI: https://doi.org/10.29019/enfoqueute.1021

in the internal combustion engines of these vehicles produced a large amount of carbon dioxide, carbon monoxide and nitrogen oxides, among other gases. This problem not only had negative consequences for the environment, but also represented a risk to public health. Lead particles were detected in the air, especially in vehicles that lacked catalytic converters. These lead particles tended to rise to a maximum height of two meters, which meant that we inhaled them directly.

Therefore, it was important to formulate this problem: What effect would the implementation of an electrolyzer in the combustion system of a motorcycle cab have on reducing environmental pollution?

Meanwhile, the reasons why such a project was carried out have been justified. What concerned society and the world at that time was the fight against vehicular pollution caused by internal combustion vehicles. In recent decades, concern about environmental protection had been increasing due to the negative effects that human activity had on the planet. For this reason, it was considered important to look for alternatives to suppress the emission of pollutants in transportation.

One of these alternatives was the implementation of hydrogen as a fuel. The usefulness of this technology would not only contribute to improving air quality, but also to reducing engine noise, which would also help combat climate change and preserve a healthier planet, thus increasing knowledge about how the electrolyzer works.

The impact on engine noise when using hydrogen in a motorcycle taxi can be significant. Hydrogen, when burned in the engine, produces a smoother and quieter combustion compared to traditional fossil fuels. This can result in a reduction in engine noise, contributing to a quieter and more comfortable driving experience for both the driver and passengers. Additionally, noise abatement may have additional benefits for quality of life in urban areas by reducing noise pollution and its potential negative effects on hearing health and general community well-being.

The noise reduction in this research is not only a relevant finding, but also constitutes a significant benefit with important implications. In addition to improving quality of life in urban environments by reducing noise pollution, this noise reduction can contribute to public health by mitigating health problems associated with prolonged exposure to noise, such as stress, fatigue, and sleep disorders. dream. Additionally, it can improve the productivity and general well-being of people living in urban areas by reducing noise interference in daily activities. This noise reduction can also have economic benefits by decreasing costs associated with healthcare and increasing property values in quieter urban areas. In summary, noise reduction not only improves the sound environment, but also has positive impacts on health, well-being and the economy, supporting the importance of this finding in the research project.

The useful life of the engine when using hydrogen in a motorcycle taxi is based on several factors. Hydrogen fuel produces cleaner, more efficient combustion compared to fossil fuels, which can reduce engine wear and debris buildup. This could result in less degradation of engine components, thus extending their life. Additionally, by preventing the combustion of hydrocarbons, corrosive effects and associated wear are reduced, which could further contribute to increased engine durability. However, factors such as engine design, proper maintenance and operating conditions can also influence the life extension when using hydrogen as fuel in a motorcycle taxi.

In addition, this research would benefit workers and users of public and private transportation by reducing transportation costs and improving the quality of the air they breathe. The benefits of this research were significant, as it would considerably reduce environmental pollution and extend the useful life of the engines, increasing the conservation of the exhaust pipe and its component parts.

This research was vital for the automotive and environmental sector, as it would contribute to reducing the amount of pollution produced daily on the planet. Emissions of polluting gases were the main reasons for the decomposition of the protective ozone layer and the increase in greenhouse gases, which affected both human health and the environment in general. Reducing pollution was therefore essential to preserve the planet.

The overall objective was to implement an electrolyzer in the combustion system of a motorcycle cab to reduce environmental pollution. This technology was considered to contribute significantly to the country's development, improve health and the environment, and benefit all those who use minor vehicles as a means of transportation, whether public and/or private. The specific objectives included the identification of the pollution factors associated with the exhaust gases of a motorcycle cab using 90 octane gasoline, the selection of the electrolyzer as a green hydrogen generator for a 124 CC motorcycle cab, the determination of the exhaust gases generated by the electrolyzer associated with a motorcycle cab, and finally, the comparison of the pollution factors using gasoline and hydrogen in a 124 CC motorcycle cab.

Favorable results were expected that would be of great help to society, the users of minor vehicles as a means of transportation, the vehicle fleet, the environmental sector and the World Health Organization (WHO). The hypothesis put forward in this topic stated that the implementation of an electrolyzer in the combustion system of a motorcycle cab would drastically reduce the environmental pollution generated by carbon monoxide (CO) and carbon dioxide (CO2) [6].

Therefore, it was considered important to promote research and development of this technology for large-scale implementation.

II. MATERIALS AND METHODS

Within the framework of this study, various materials and resources were used in order to facilitate data collection and carry out a comprehensive analysis. The elements that will be used in the development of the research are detailed below. The total cost of implementation, materials and supplies was S/.743.90 (Table 1).

TABLE I
MATERIAL AND IMPLEMENTATION COSTS

Materials	Unit	Quantity	Price
AISI 302 Stainless Steel Plate - 0.12mm	m^2	1.20	S/.150.00
PVC and glass tank	ud.	1	S/.20.00
Acrylic plastic 30cm x 20cm x 7mm	ud.	1	S/.15.00
Cable 10-AWG	m	3	S/.24.00
Stainless steel ¼" threaded rod	m	2	S/.14.00
Clamps	ud.	12	S/.6.00
¼" stainless elbow	ud.	3	S/.18.00
5/16" to ¼" bronze flaked nipple	ud.	4	S/.20.00
5/8" to 5/16" bronze flaked nipple	ud.	2	S/.12.00
¼" x 1" stainless nipple	ud.	3	S/.12.00
5/16" bronze flake tee	ud.	1	S/.8.00
5/16" clear hose	m	5	S/.10.00
Assembly and implementation on motorcycle taxi	ud.	2	S/.100.00
¼" metal nuts	ud.	26	S/.5.20
¼" metal rings	ud.	26	S/.5.20
¼" Chrome-plated steel female quick-connector	ud.	1	S/.9.00
¼" and 7/16" steel drill bits	ud.	2	S/.24.00
5/8" stainless threaded union	ud.	1	S/.7.00
½" Teflon tape	ud.	4	S/.6.00
3M duct tape	ud.	1	S/.5.00
Cold glue (SoldiMix)	ud.	1	S/.8.50
5/16" to ¼" pneumatic connector	ud.	2	S/.16.00
DC 12V battery	ud.	1	S/.220.00
Fuse holder	ud.	1	S/.4.00
35A 12VDC 2 pole circuit breaker	ud.	1	S/.7.00
10-AWG 5/16" non-insulated ring terminals 10-AWG 5/16	ud.	4	S/.2.00
Insulated female ¼" spigot terminal	ud.	2	S/.1.00
Caustic Soda	kg	1	S/.15.00
TOTAL PRICE			S/.743.90

The nature of the research was applied, since the project focused on the technological field and sought to acquire in-depth knowledge about the operation of the electrolyzer for its implementation in smaller vehicles. Regarding the suppression of polluting agents, it is merely informative, since this approach allowed the development of practical and concrete solutions that addressed the challenge of reducing noise and combating environmental pollution generated by internal combustion vehicles, which at that time at the time it was considered the main source of polluting gases that affected our health and the planet.

The proposed research approach was field experimental, which involved conducting a real-world study to analyze, determine and collect detailed information on the results obtained from real data. This approach allowed a deeper understanding of the phenomena involved in obtaining hydrogen and provided the opportunity to evaluate its feasibility and efficiency under real conditions.

The technique used was both observation and measurement to collect relevant data. Observation involved systematically visualizing and recording the different aspects related to the implementation of the electrolyzer in the motorcycle cab's combustion system. On the other hand, measurement involved quantifying specific aspects, such as the percentage of exhaust gases allowed in the technical reviews established by the Ministry of Transportation and Telecommunications. The data required for the study included information on the type of fuel used, as this could affect the emissions and the results obtained with the implementation of the electrolyzer. In addition, the performance of the combustion system was analyzed both with and without the electrolyzer installed to evaluate the effects of its implementation on the reduction of environmental pollution.

As a data collection instrument, a guide or data sheet was used, which served as a structured tool to collect relevant information. This guide contained fields for recording data such as the name of the observer, the specific engine being observed, the exhaust gases that polluted the environment, and other specific characteristics.

As procedures, the operation of the motorcycle cab with conventional fuel (90 octane gasoline) was analyzed, and the registration and measurement card were used to collect information on engine performance, including fuel efficiency, exhaust gases generated, engine vibration force and noise impact. It was observed that one liter of gasoline yielded 26 kilometers and with a 9-liter fuel capacity tank, a total distance of 234 km was covered. Therefore, the electrolyzer was implemented to generate hydrogen as fuel to be injected into the motorcycle cab. The electrolyzer worked with a plastic tank that stored 1 liter of water, which was supplied to the electrolyzer dry. Corresponding notes were taken to improve the efficiency and prolong the useful life of the motor, with the objective of avoiding pollution from this minor vehicle, producing water vapor instead of polluting gases. Finally, the results obtained were evaluated, comparing the feasibility, performance, efficiency and gases generated before and after implementing the electrolyzer.

A. Calculation of gasoline fuel per kilometer of driving distance

Cubic centimeters or CC indicate the power of the motorcycle engine. It is the capacity to produce energy and speed (125 CC, 250 CC, 600 CC, etc.) define what is known as engine displacement.

As data we have the calorific value of gasoline being 47.7 MJ/kg, displacement of the motorcycle cab of 124 CC, fuel capacity of 9 liters and distance per liter of gasoline of 26 km. We convert 124 CC to liters and milliliters:

$$1\ cm^3 = 0.001\ L\ =\ 1\ ml \tag{1}$$

$$124\ CC = 0.124\ L\ =\ 124\ ml \tag{2}$$

We use the simple rwule of 3 to decompose:

$$\begin{bmatrix} 1\ L & 26\ km \\ x & 1\ km \end{bmatrix} \tag{3}$$

$$26x\ (km) =\ 1\frac{\mathrm{L}}{\mathrm{km}} \tag{4}$$

$$x = \frac{1\ L/km}{26\ km} = 0.03846\ L = 38.5\ ml \tag{5}$$

The motorcycle cab consumes 0.03846 L = 38.5 ml per kilometer of travel.

We convert the values to kilograms of gasoline, considering that:

$$Mass = density*volume \tag{6}$$

$$0.03846\frac{L}{km}*0.750\ kg/L = 0.0288\ kg/km \tag{7}$$

234 km of total travel distance is equivalent to:

$$9\ L*0.750\ kg/L = 6.75\ kg \tag{8}$$

Note: If the calorific value of gasoline and hydrogen are equal, the same fuel flow will be used. But if the hydrogen is lower, a higher flow rate will be used to move the motorcycle cab.

B. Calculation of hydrogen flow rate in one liter of water

To calculate the hydrogen flow rate, consider the following data of water: Molar mass 18 g/mol, Density 997 kg/m^3 equivalent to 1000 kg/m^3, boiling point 100 °C and 1 liter of water is equal to 1000 grams. Moles of water in equation (9):

$$\frac{1000\ g}{18\ g/mol} = 55.56\ mols \tag{9}$$

As a note: "55.55 moles of oxygen atoms, plus 111.11 moles of hydrogen atoms" [3].

Hydrogen data: Molar volume of some common gases at standard temperature and pressure (0°C and 1 atm pressure).

Equation (10) is the flow rate of hydrogen in 1 liter of water.

$$111.11\ mol\ *\ 22.414\frac{L}{mol} =\ 2490.4\ L\ H2 \tag{10}$$

We convert to kilograms of hydrogen. How much hydrogen is needed to move the 124 CC, 10 HP, 7000 revolutions per minute (RPM) motorcycle cab?

Some data on hydrogen: Density 89.9 kg/m^3, 1 liter of H2 equals to $0.0899\ kg\ =\ 0.0899\ kg/L$

$$2490.4\ L*0.0899\ \frac{kg}{L} = 223.89\ kg\ H2 \tag{11}$$

Equation (12) is to obtain 1 kg of H2, in liters H2.

$$\frac{1\ kg\ H2}{0.0899\ kg/L} = 11.123\ L\ H2 \tag{12}$$

C. Hydrogen flow rate and flow per kilometer of run

The electrical conversion efficiency of electrolysis, measured in terms of kilowatt-hours per kilogram of hydrogen (KWh/kg H2), ranges from 60 % to 70 %. This translates into an approximate consumption of 50 to 60 KWh of electrical energy to generate 1 kg of hydrogen. As an additional result, 8 to 10 kg of oxygen is generated for every 1 kg of hydrogen produced [10]. "1 liter of water is equivalent to 500 km of travel" [30].

The calorific value of hydrogen is 120.9 MJ/kg.

The flow rate is calculated per kilometer of travel:

$$\frac{2490.4\ L\ H2}{500\ km} = 4.98\ L\ H2/km \tag{13}$$

In kg H2 would be:

$$4.98\frac{L}{km}*0.0899\frac{kg}{L} = 0.448\ kg\ H2/km \tag{14}$$

Current required per kilometer of travel:
50 to 60 KWh is equivalent to 1 kg of H2.

$$\frac{1\ kg\ H2}{0.448\ kg\ H2/km} = 2.232\ km \tag{15}$$

To consume 1 kg of H2, it is necessary to travel 2.232 km.

$$\frac{50\ KWh}{2.232\ km} = 22.40\ KWh/km \tag{16}$$

We convert to watts and meters:

$$22.40\frac{KWh}{km}*\frac{1000W}{1\ KW}*\frac{1km}{1000m} = 22.40\ Wh/m \tag{17}$$

We convert to current per meter:

$$\frac{22.40\ Wh/m}{12\ V} = 1.87\ A/m \tag{18}$$

D. Carbon dioxide pollution per passenger and kilometer of traveled route

Calculations are detailed, a motorcycle cab carries 3 passengers besides the driver.

$$72\frac{g}{km}*passenger \tag{19}$$

$$72\frac{g}{km}*3\ passenger = 216\ \frac{g\ CO2}{km} \tag{20}$$

In this calculation, a value of 216 g CO_2 per km of travel is given. These values were taken as a reference and can be found in the (Fig. 1).

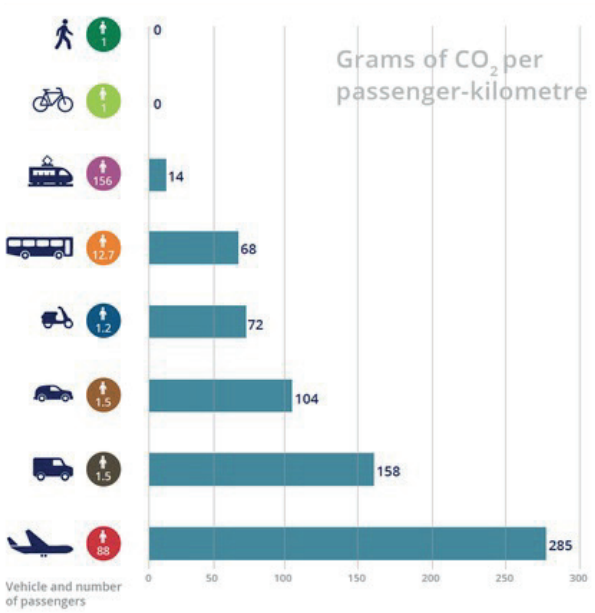

Fig. 1. Pollution footprint, by European Environment Agency (EEA).

III. RESULTS AND DISCUSSION

For the results obtained, a single-cylinder motorcycle cab of the Itálika brand was used as the object of study based on statistical reasons and representativeness; the data was obtained by observing the motorcycle cab in operation and recorded on an observation sheet.

A. Identification of pollution factors associated with the exhaust gases of a motorcycle cab using 90 octane gasoline

OBSERVATION SHEET

"Implementation of an electrolyzer in the combustion system of a motorcycle cab to reduce environmental pollution"

FILE N° 001

Observer's name: Manuel Rodríguez Perez

Observed engine

Brand:	ITALIKA
Model:	FT125
Engine serial number:	LLCLPP206BE105056
Industry:	MEXICO
Plate number:	C2-9318

Date: 2023-12-02

Observation location: SEGUCAR S.A.C. - Av. de La Marina, Núcleo Urb. Buenos Aires Mz. G Lt. 11 – New Chimbote.

Observation start time: 2:45 PM **Observation end time:** 3:25 PM

Fig. 2. Motorcycle cab characteristics

The (Fig. 2), shows the characteristics of the motorcycle cab in an observation sheet, containing parameters such as the title of the project, N° of the sheet, name of the observer, the engine observed which includes the Itálika brand, the FT125 model, the serial N° LLCLPP206BE105056, the industry of manufacture Mexico, N° of plate C2-9318, the date of observation on August 15, 2023, place of observation carried out in the Asentamiento Humano Vista Alegre mz: L. lt: 5 - Nuevo Chimbote and a duration of 40 minutes of observation of the mototaxi.

TABLE II
SPECIFIC CHARACTERISTICS OF THE MOTORCYCLE CAB

Item	Quantity	Type
No. of strokes	4	
No. of cylinders	1	
Displacement	124 CC	
Cooling		Aire
No. of camshafts	2	
No. of wheels	3	

In relation to the emissions of polluting gases, the test with the maximum value of pollution with the variation of gases when using gasoline in the motorcycle cab, the data are presented in (Table 3), where it turns out that the data of CO and CO_2 are the ones that harm public health.

TABLE III
MAXIMUM VALUE OF POLLUTANT GAS EMISSIONS

Item	Quantity (%V)	Quantity (ppm)	Type
Carbon monoxide (CO)	3.739 %	37,390	Gas
Hydrocarbons (HC)	0.0372 %	372	Gas
Carbon Dioxide (CO_2)	1.96 %	19,600	Gas
Oxygen (O_2)	20.24 %	202,400	Gas

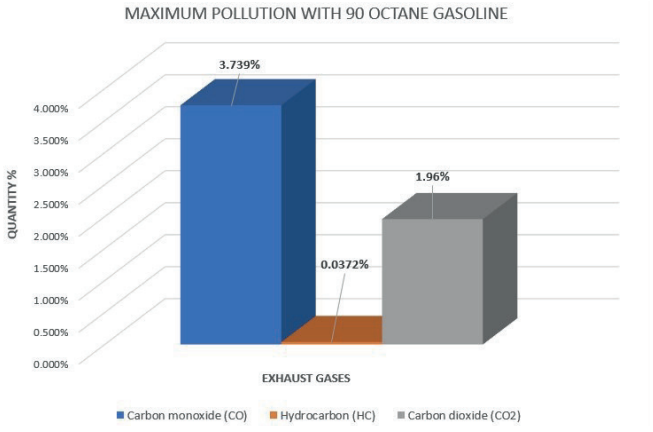

Fig. 3. Statistical graph of maximum gasoline contamination.

Note: (Fig. 3) shows the maximum pollutant emission when using conventional gasoline, being the carbon monoxide (CO) value of 3.739 %.

In relation to the sound emissions using 90 octane gasoline, the test with the maximum variation of the sound pressure level (SPL), as data; the noise level allowed in the work in Peru is 85 dB as maximum [15], being 100 % (Table 4).

TABLE IV
MAXIMUM NOISE EMISSION VALUE USING 90 OCTANE GASOLINE

Item	Quantity (dB)	Quantity (%)	Type
Sound pressure level (SPL)	76.4	89.88 %	Noise

When analyzing the permitted noise emissions in Peru, the maximum noise pollution value is 76.4 dB, which is equivalent to 89.88 of the permitted level in Peru.

As an interpretation of this result, it is due to the fact that conventional fuel is used, which causes noise pollution and generates health problems such as nervousness, ringing in the ears, among other health problems.

B. Selection of an electrolyzer as green hydrogen generator for a 124 DC motorcycle cab

The design of the electrolyzer is a dry cell, it has 13 AISI 302 stainless steel plates of 0. 12 mm thick, measuring 10 cm long by 15 cm high, the electrolyzer has 9 neutral plates, 2 positive plates and 2 negative plates, the cells work stacked together, with an insulator between plates of rubber material so that they do not make contact and do not generate short circuit; the stacked configuration is 1 negative plate plus 3 neutral plates, successively 1 positive plate plus 3 neutral plates, then 1 positive plate plus 3 neutral plates and finally ends with 1 negative plate; so that the water is a good conductor of electricity and breaks the molecules that make up the water, it is necessary to add caustic soda, in 1. 5 liters of water 150g of caustic soda is added. The electrolyzer has a water capacity of ½ liter, and in the tank or reserve tank with a capacity of 1 liter, uses a working voltage of 12 volts which is supplied by the battery of the motorcycle cab, also uses a 30-amp fuse, 1 two-pole switch to allow the operation of the system, and 1 flame arrester filter safety to prevent accidents from the return of the flame produced by combustion. Hydrogen gas enters through the engine air filter to explode in the combustion chamber of the motorcycle cab.

In relation to the electrical energy consumed by the electrolyzer, the test with maximum voltage variation (Table 5).

TABLE V
MAXIMUM VALUE OF ELECTRIC CURRENT CONSUMED BY THE ELECTROLYZER

Item	Quantity	Type
Voltage (V)	14.15	Voltage
Current (A)	7.20	Current
Power (kW)	0.1019	-

In this analysis as a characteristic of the electrolyzer, the maximum value of consumption of higher electric current; the data of the electrolyzer are in order of highest consumption: The voltage with a maximum value of 14.15 volts, the current with a maximum value of 7.20 amperes and the working power with a maximum value of 101.9 Watts (Fig. 4).

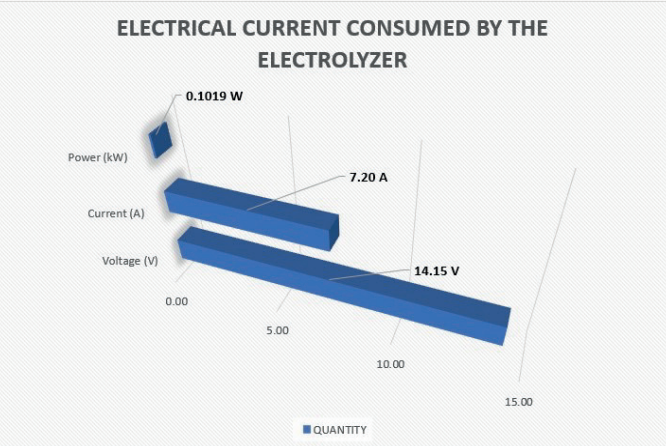

Fig. 4. Statistical graph of the maximum current consumed by the electrolyzer.

(Fig. 4) shows the current with the highest consumption in the electrolyzer, with a maximum value of 7.20 amperes.

In relation to hydrogen generation, the test with maximum hydrogen flow generated is shown (Table 6).

TABLE VI
MAXIMUM ELECTROLYZER HYDRENE FLOW RATE VALUE

Item	Quantity (L/min)	Type
Hydrogen-oxygen flux	0.100	Fluid
Water (L)	1.50	Liquid
Caustic Soda (g)	150	Chemical
AISI 302 plates (0.12mm)	13	Steel
Velocity (km/h)	0	

The analysis of some characteristics and the generation of hydrogen, in this test has in order of higher hydrogen generation with a maximum value of 0.100 liters per minute being 100 ml/min, with a maximum value of caustic soda addition of 150 grams per 1.50 liters of water as maximum value of the electrolyzer, using a speed of 0 km / h (idle).

C. Determination of the exhaust gases generated by the electrolyzer associated with a motorcycle cab

Regarding the emissions of pollutant gases using hydrogen, we have the test with the total reduction of pollutant gases when using hydrogen in the motorcycle cab (Table 7), where the CO and CO_2 gases tend to 0 % pollution values, being these harmful to health.

TABLE VII
MAXIMUM EMISSION VALUE USING HYDROGEN

Item	Quantity (%V)	Quantity (ppm)	Type
Carbon monoxide (CO)	0.0 %	0	Gas
Hydrocarbons (HC)	0.0 %	0	Gas
Carbon Dioxide (CO_2)	0.0 %	0	Gas
Oxygen (O_2)	25.10 %	251,000	Gas

In an analysis of the contamination factors using hydrogen, the maximum values of CO and CO_2 are equal to 0 %; there is only a maximum value of O2 of 25.10 %.

In relation to sound emissions using hydrogen, the maximum value of the sound pressure level test (SPL), as data; the level allowed in the work in Peru is 85 dB being 100 % as maximum (Table 8).

TABLE VIII
MAXIMUM SOUND EMISSION VALUE USING HYDROGEN

Item	Quantity (dB)	Quantity (%)	Type
Sound pressure level (SPL)	71.7	84.35 %	Noise

When analyzing the permitted noise emissions in Peru, the tests showed a maximum value of 71.7 dB, equivalent to 84.35 % of the permitted level.

As an interpretation of this result, the sound pressure level is within the permitted range, this is due to the fact that hydrogen is used as fuel, this causes a great noise reduction, generates less noise and avoids alterations such as noise-related health diseases.

D. Compare pollution factors using gasoline and green hydrogen in a 124 CC motorcycle cab

Table 9 shows the pollution data to be compared, the amounts in percentage values using gasoline and hydrogen.

TABLE IX
COMPARISON OF EMISSIONS OF POLLUTANT GASES USING GASOLINE AND HYDROGEN

Item	Quantity (%V) Gasolina	Quantity (%V) Hidrógeno	Type
Carbon monoxide (CO)	3.739 %	0.00 %	Gas
Hydrocarbons (HC)	0.0301 %	0.00 %	Gas
Carbon Dioxide (CO_2)	1.96 %	0.00 %	Gas
Oxygen (O_2)	20.24 %	20.93 %	Gas

In this analysis of the comparison of pollutant gas emissions generated by gasoline and hydrogen, it is found that gasoline has a maximum CO value of 3.739 %, CO_2 of 1.96 %; on the other hand, when using hydrogen, the maximum values of CO and CO_2 become null or 0.00 %, since there is no pollution at all, and the total pollution of the motorcycle cab is reduced by 100 %.

TABLE X
COMPARISON OF NOISE EMISSIONS AND HYDROGEN

Item	Quantity (dB)	Quantity (%)	Type
Sound pressure level (LPS 1) With gasoline	76.4	89.88 %	Noise
Sound pressure level(LPS 2) With Hydrogen	71.7	84.35 %	Noise

In the analysis of the comparison of noise emissions using gasoline and hydrogen (Table 10), there is a maximum limit of 85 dB allowed in the work in Peru, which is equivalent to 100 %, with gasoline having a maximum value of 76.4 dB equivalent to 89.88% and hydrogen with a lower value than gasoline of 71.7 dB equivalent to 84.35 % of the total allowed.

TABLE XI
REDUCTION OF NOISE EMISSIONS USING GASOLINE AND HYDROGEN

Item	Quantity (dB)	Quantity (%)	Type
Sound pressure level (LPS 1) With gasoline	76.4	89.88 %	Noise
Sound pressure level (LPS 2) With Hydrogen	71.7	84.35 %	Noise
Total reduction (LPS 1 - LPS 2)	4.7	5.53 %	

In this analysis of the reduction of noise emissions using gasoline and hydrogen (Table 11), we have the maximum reduced value of 4.7 dB which is equivalent to 5.53 %, thus making less noise than when using conventional fuel by default.

TABLE XII
COMPARISON OF AUTONOMY OF GASOLINE AND HYDROGEN

Item	Quantity (liters)	Distance (Km)
Regular gasoline	9.0	26
Hydrogen (Water with electrolyte)	1.0	500

According to the autonomy of the mototaxi (Table 12) when using gasoline with a full tank of fuel, its travel range is 26 kilometers in total until the fuel is completely exhausted, since the storage tank is 9 liters.

When using hydrogen, it changes since by using 1 liter of soluble water with electrolyte (caustic soda), the motorcycle taxi is capable of traveling 500 kilometers until all the hydrogen contained in the liter of water is exhausted [30].

As a comparison, the distance that a motorcycle taxi can travel with gasoline is less than what it can travel if it only uses 1 liter of water with electrolyte. Allowing autonomy and being more feasible to refuel with hydrogen than with gasoline (Table 13), since not everywhere is a fuel sales service tap. Saving time and money when it comes to moving from one place to another. The only drawback would be to constantly maintain the battery that supplies the electrolyzer.

TABLE XIII
AUTONOMY COSTS OF GASOLINE AND HYDROGEN

Item	Distance (Km)	Price (S/.)	Observation
Regular gasoline	500	723.00	Constant spending
Hydrogen (Water with electrolyte)	500	743.90	Unique price

To travel 26 kilometers, which is 9 liters of regular gasoline fuel, costs 37.60 soles, since gasoline costs 15.81 per gallon. To travel 500 kilometers with gasoline the cost would be 723 soles, if only conventional fuel were used.

Which would be almost entirely the cost of implementing and assembling the electrolyzer capable of generating hydrogen to be used as fuel in the motorcycle taxi.

The cost of assembly and implementation of the electrolyzer has a value of 743.90 soles. The difference being that conventional fuel has to be purchased at storage taps, on the other hand, hydrogen is generated through the electrolyzer, being the only expense after implementation, of the electrolyte, costing an average of 15 soles per kilogram.

The discussion of the results obtained in this research is fundamental to understand their significance and relevance. In this project, an electrolyzer device was designed that has 13 AISI 302 stainless steel plates of 0.12 mm thick, this prototype covers a size of 10 cm long by 15 cm high; the plates were distributed as follows, 2 negative plates, 2 positive plates and 9 neutral plates stacked together, as plate separator was used rubber sheets of 3 mm thick to avoid a short circuit, the device was rectangular in shape and used a battery of 12 volts and 7. 20 amperes, all the plates were fixed on two 6 mm thick blue acrylic bases, measuring 14.5 cm long by 20 cm high. This system takes advantage of the energy stored in the battery, maintaining an average consumption of 7.20 amps. This operation is possible as long as the motor remains running; otherwise, the device stops due to high energy consumption and runs the risk of completely discharging the battery. set of 12 cells, each with dimensions of 8 cm by 12 cm and a thickness of 1 mm, all made from stainless steel. These cells were solidly fixed to a bakelite base with a thickness of 10 mm. The layout included 9 neutral, 1 positive and 2 negative plates, all meticulously insulated with rubber sheets. It should be noted that most of the materials used in the construction of the electrolytic system were obtained through recycling. In addition, they used a 12V - 6A battery. The system takes advantage of the residual or reserve energy stored in the battery, maintaining a constant average current of 2 amps whenever the engine is running. In the absence of this condition, the device stops due to its high energy consumption and the possibility of completely draining the battery charge. All electrolytic devices have been conceived and constructed following the same fundamental principle. Therefore, the inherent characteristics of electrolysis devices will always share a common factor, which is the use of specific materials and a certain form of assembly. However, the variability lies in the number of plates, which is directly related to the size and hydrogen production capacity of each device. Both devices share similarities in terms of using stainless steel plates and 12V batteries. However, they differ in the number of cells, dimensions, plate thickness, type of separators, and in the consideration of the use of recycled materials. In addition, the latter project highlights energy consumption and the need to keep the motor running for constant operation, while the former project does not specifically address this consideration.

In comparison, Diaz et al. [9], designed an electrolyzer with a cell made up of 7 stainless steel plates, each plate has a length of 4.14 cm and a thickness of 1 mm. In this arrangement, 5 plates acted as neutral, one as positive and one as negative, all of them isolated by means of neoprene spacers with a thickness of 3 mm, with the purpose of avoiding short circuits. These plates had a diameter of 9 cm, since the device adopted a circular configuration. In addition, the system was powered by a 12 V, 3 A battery. Overall, both projects share similarities in terms of the energy source and the general objective of generating hydrogen by electrolysis, but differ in several key aspects, such as the number and type of plates, the thickness of the plates, the materials of the separators and the shape of the device. The choice between the two designs will depend on the specific project objectives and desired performance requirements.

As part of this research project, the device incorporated a capacity of 500 ml of electrolyte water in the main source of the system, while 1000 ml or 1 liter of electrolyte water was stored in the reserve tank. In addition, the system was equipped with a 30-amp fuse and a 35-amp circuit breaker, both 12-volt DC and 2-pole. Similarly, the electrolyzer device used a rectangular configuration with 13 AISI 302 stainless steel plates and a 12V battery. These findings are linked to the design proposed by Baltazar [25], which incorporated stainless steel plates with a thickness of 0.15 mm and a capacity of 140 ml in the device chamber. Also, rubber gaskets with a triangular configuration, a contact plate, a fuse, a 12 V relay and a 12 V battery were used. In addition, he suggested three alternative configurations for the device: hexagonal, square or circular. The decision on the shape to be adopted was made considering an analysis of efficiency and economic feasibility, finally deciding on the square shape. Unlike the project established in this research, this alternative device incorporates graphite electrodes, a glass tank and three conduits for the inlet and outlet of both water and hydrogen. In addition, it has a hydrogen tank made of glass, protected by an electromagnetic relay that is connected to the contact plate. The separation between plates is made by aluminum gaskets, and the power supply is carried out by solid wires. In addition, various shapes and materials were considered, highlighting the use of graphite, glass and a protection system with electromagnetic relay.

The results of the project established in this research, using gasoline registered values of 372 ppm of HC, 3.739 % of CO and 1.96 % of CO_2; and when using the hydrogen generator electrolyzer, they tend to a total reduction of polluting gas emissions, since using only hydrogen as fuel proves that gases such as carbon monoxide (CO), carbon dioxide (CO_2) and Hydrocarbons (HC) tend to values of 0. 0 %, this represents a total decrease of 100 %, being the pollution values null, only giving as a by-product the oxygen coming from the combustion. In comparison, Flórez et al. [29], who used pure gasoline as a fuel source and also combined with hydrogen as an energy source. The researchers recorded concentrations of 344 ppm hydrocarbons (HC), 4.59 % carbon monoxide (CO) and 2.82 % carbon dioxide (CO_2) without the application of the electrolyzer system. In contrast, with the introduction of hydrogen as a power source, values of 40 ppm HC, 0.00 % CO and 0.21 % CO_2 were obtained. These results represent an 88.37 % reduction in HC, a total elimination of CO and a 92.55 % decrease in CO_2, which is highly beneficial for the environment.

As results of the main research, the pollutant gas reduction values are 100 % for the motorcycle cab, while the results ob-

tained by Diaz et al. [9] show that the use of conventional fuel combined with hydrogen led to a reduction in emissions of CO in the range of 13 % to 18 %. In terms of CO_2, a reduction ranging from 5 % to 9 % was observed thanks to the electrolyzer device, which is attributed to more efficient combustion. A significant 20 % reduction in O2 emissions was also recorded, as a result of optimized combustion that allowed for better oxygen utilization. Finally, a notable reduction in unburned hydrocarbons was documented, reaching a range of 30 % to 50 %, as a consequence of an improvement and enrichment of the mixture, which contributed to a more effective burning of hydrocarbons through the use of the electrolyzer device.

These findings underscore the diversity of approaches available for hydrogen production, reinforcing the idea that this resource can be obtained in diverse and effective ways.

The conduct of this applied and experimental research study, with the objective of addressing environmental pollution by incorporating an electrolyzer in a single-cylinder motorcycle cab, poses a number of strengths and weaknesses that are essential to understand and evaluate the validity and implications of the results obtained. Among the strengths of this research approach, the high controllability over the study variables stood out. In addition, the reproducibility of the experiments was a significant advantage, demonstrating that the observed effects are consistent and not random. The methodology that was used lends itself particularly well to establishing cause and effect relationships, which facilitated the identification of whether the introduction of the electrolyzer had a direct impact on the reduction of pollutant emissions. In addition, the experiment allowed for accurate and quantifiable data measurements, which were essential when evaluating emissions and other critical parameters. However, it was recognized that this experimental methodology also presented weaknesses that must be considered when interpreting the results. One of the weaknesses was that, despite providing a high degree of control, experiments can sometimes oversimplify reality and not fully reflect real-world conditions. This lack of correspondence with real situations may limit the practical applicability of the results. In addition, the experiment can be costly and consume significant resources, including time and specialized equipment, which may restrict its scope and replicability on a large scale.

This research makes significant contributions compared to other studies of hydrogen implementation in motorcycle cabs, as it addresses multiple key issues related to the feasibility and benefits of using hydrogen as a fuel in this specific context. One of the main contributions of this study is the evidence of a significant elimination of polluting gas emissions by using hydrogen instead of gasoline.

Research has an outstanding relevance both in the scientific field and in the social context in which it is developed. It addresses a current and pressing problem, contributes to sustainability, can influence public policy, and can promote awareness of the importance of reducing environmental pollution. The application of clean technologies, such as the use of hydrogen as a fuel in motorcycle cabs, is essential to address environmental challenges and improve the quality of life in urban environments and beyond.

IV. CONCLUSION

From the results obtained, the following conclusions were reached:

It was possible to implement the electrolyzer in the combustion system of the motorcycle cab, eliminating the environmental pollution produced by the motorcycle cab when using gasoline (conventional fuel), the total removal was 100 % of carbon monoxide and carbon dioxide; and instead of polluting with greenhouse gases, it only produces water vapor through the exhaust pipe, combustion is smoother and quieter; Regarding the useful life of the engine, due to the cleaner and more efficient combustion, the accumulation of waste was reduced, which benefits reducing the wear of internal components and the need for costly maintenance.

Pollution factors associated with exhaust gases were identified using 90 octane gasoline; such as carbon monoxide emissions at a maximum value of 3.739 % and carbon dioxide value of 1.96 %. There were also noise pollution values of 76.4 dB being 89.88 % with respect to 85 dB which are the maximum level allowed at work in Peru

To select the electrolyzer as green hydrogen generator for the 124 DC mototaxi, it was based on the dry cell design, it has 13 plates of which 9 are neutral, 2 positive and 2 negatives; the plates work together with a rubber separator to avoid short circuit in the electrolyzer system, the material of the plates was stainless steel AISI 302 of 0. 12 mm thick, measuring 10 cm long by 15 cm high and using an electrolyte such as caustic soda, which allows better current conductivity in the water.

When implementing the electrolyzer in the motorcycle cab system, it was determined that the polluting gases that cause health problems were suppressed in their totality, since CO and CO_2 showed values of 0.0 % contamination and only emitting 25.10 % of oxygen as a maximum value instead of polluting gases.

As a comparison of the contamination factors using gasoline and green hydrogen in a 124 CC motorcycle cab, maximum contamination values with gasoline were 3.739 % of CO, in comparison with hydrogen it was 0.00 % in CO with no contamination at all. Regarding noise emissions, the total reduction using hydrogen was 4.70 dB being 5.53 % less noise than with gasoline.

Unlike previous research that focuses solely on reducing pollutants or improving engine performance independently, this project proposes a comprehensive solution by integrating an electrolyzer into the combustion system. This integration allows multiple problems to be addressed simultaneously, such as reducing polluting emissions and noise, and extending engine life.

This project focuses on motorcycle taxis, although there is research on alternative fuel technologies in larger vehicles, such as cars and buses, this study focuses specifically on motorcycle taxis. This represents a novelty, as this type of vehicle is common in many regions, especially in urban and rural areas of developing countries, where air pollution and noise can be significant, but often overlooked, problems.

It also provides multidimensional benefits; In addition to reducing pollution and noise, the implementation of the electrolyzer aims to extend the useful life of the engine and improve the health of users and local residents. This holistic approach to sustainability and human well-being is innovative and marks a sig-

nificant difference from previous research that may have focused primarily on one specific aspect, such as emissions reduction.

Finally, in practical application, unlike theoretical or laboratory studies, this project focuses on the practical implementation of the technology in a real operating motorcycle taxi environment. This allows for a more accurate assessment of the feasibility and effectiveness of the proposed solution under real-world conditions of use, representing a significant step forward towards commercial application and widespread adoption of the technology.

REFERENCES

[1] A. Lois, "¿Qué medio de transporte contamina más? Coche, autobús, avión, barco…", August 02, 2019. [Online]. Available: https://www.autopista.es/noticias-motor/que-medio-de-transporte-contamina-mas-coche-autobus-avion-barco_155360_102.html.

[2] A. Marin Muñoz and L. F. Jiménez Cárdenas, "Diseño e implementación de una celda generadora de hidrógeno en un motor de combustión interna en la Ciudad de Bogotá", Universidad Distrital Francisco José de Caldas, Bogotá, 2021. [Online]. Available: http://hdl.handle.net/11349/28510.

[3] AreaCiencias, "El Mol en Química y Numero de Moles con Ejercicios Resueltos", June 8, 2020. [Online]. Available: https://www.areaciencias.com/quimica/mol/.

[4] Arrieta Veintemilla and J. D. Sánchez Soto, "Reducción de emisiones de CO2 y ahorro de gasolina, mediante electrólisis del agua en un vehículo menor, Tarapoto, 2022", Universidad César Vallejo, Tarapoto, 2022. [Online]. Available: https://hdl.handle.net/20.500.12692/109723.

[5] Asociación Española del Hidrógeno, "¿Cómo funciona el Hidrógeno como fuente de energía?", Jan 12, 2021. [Online]. Available: https://www.aeh2.org/hidrogeno/.

[6] D. A. Duque Franco y F. Torres Ochoa, "Generador de hidrógeno como fuente no convencional de energía renovable –FNCER– para la mitigación de la contaminación generada por motores de combustión interna", Institución Universitaria Pascual Bravo, 2022. [Online]. Available: https://repositorio.pascualbravo.edu.co/handle/pascualbravo/1812.

[7] D. Cavaliere, A. Perrone and A. Silvello, "Water electrolysis for the production of hydrogen to be employed in the ironmaking and steelmaking industry", *Metals (Basel),* vol. 11, no. 11, p. 1816, 2021. https://doi.org/10.3390/met11111816

[8] Durand Vilca, "Oxidación del monóxido de carbono producto de la combustión incompleta a dióxido de carbono por radiación ultravioleta mediante el uso de óxido de zinc como foto-catalizador, Arequipa 2018", Universidad Alas Peruanas, Arequipa, 2019. [Online]. Available: https://hdl.handle.net/20.500.12990/9314.

[9] E. González Gil, Á. O. Díaz Rey and O. A. González-Estrada, "Análisis de un generador de HHO de celda seca para su aplicación en motores de combustión interna", *Rev. UIS Ing.,* vol. 17, no. 1, pp. 143–154, 2018. https://doi.org/10.18273/revuin.v17n1-2018013

[10] E. Zetticci, "Como funciona Un motor De hidrogeno?", Asesor automotriz, December 21, 2022. [Online]. Available: https://www.austral-gomas.com.ar/gasolina/como-funciona-un-motor-de-hidrogeno.html.

[11] F. Ahmad Kamaroddin et al., "Membrane-based electrolysis for hydrogen production: A review", *Membranes (Basel*), vol. 11, no. 11, p. 810, 2021. https://doi.org/10.3390/membranes11110810

[12] F. Ortiz Sánchez and M. C. Pardo Castillo, "Evaluación del rendimiento de un motor de cuatro tiempos, usando hidrógeno como combustible", Escuela Superior Politécnica Agropecuaria de Manabí Manuel Félix López, 2019. [Online]. Available: http://repositorio.espam.edu.ec/handle/42000/1005.

[13] F. Rocha, Q. de Radiguès, G. Thunis and J. Proost, "Pulsed water electrolysis: A review", *Electrochim. Acta,* vol. 377, no. 138052, p. 138052, 2021. https://doi.org/10.1016/j.electacta.2021.138052

[14] G. Bruguera Matute, "Estudio de la reducción de la contaminación atmosférica en el transporte marítimo", Universidad Politécnica de Catalunya, Barcelona, 2021. [Online]. Available: http://hdl.handle.net/2117/347419.

[15] G. P. Toledo, "¡Alerta! Conoce Los Niveles De Ruido Permitidos En El Trabajo Perú. - Diciembre 2023", Aug 11, 2023. [Online]. Available: https://ceficperu.org/alerta-conoce-los-niveles-de-ruido-permitidos-en/.

[16] H. Alvarado Campos, "Implementación del generador de hidrógeno en los vehículos menores para reducir costos de transporte de la empresa MOTARD Chulucanas 2019", Universidad César Vallejo, Piura, 2019. [Online]. Available: https://hdl.handle.net/20.500.12692/41925

[17] H. Kim, H. Park, H. Bang and S.-K. Kim, "Electrodeposition-fabricated catalysts for polymer electrolyte water electrolysis", *Korean J. Chem. Eng*., vol. 37, no. 8, pp. 1275–1294, 2020. https://doi.org/10.1007/s11814-020-0626-y

[18] H. L. Yip et al., "A review of hydrogen direct injection for internal combustion engines: Towards carbon-free combustion", *Appl. Sci. (Basel)*, vol. 9, no. 22, p. 4842, 2019. https://doi.org/10.3390/app9224842

[19] H.-Y. Wang, M.-L. Sun, J.-T. Ren and Z.-Y. Yuan, "Circumventing challenges: Design of anodic electrocatalysts for hybrid water electrolysis systems", *Adv. Energy Mater.,* vol. 13, no. 4, 2023. https://doi.org/10.1002/aenm.202203568

[20] J. Gao, X. Wang, P. Song, G. Tian and C. Ma, "Review of the backfire occurrences and control strategies for port hydrogen injection internal combustion engines", *Fuel (Lond.),* vol. 307, no. 121553, p. 121553, 2022. https://doi.org/10.1016/j.fuel.2021.121553

[21] J. J. Vega Puculpala and E. H. Carrasco Satán, "Análisis de la eficiencia energética con el uso de un aditivo elevador de octanaje en el biocombustible ecopaís y combustible tradicional extra aplicado a un motor de combustión interna", Escuela Superior Politécnica de Chimborazo, Riobamba, 2022. [Online]. Available: http://dspace.espoch.edu.ec/handle/123456789/17989.

[22] J. Santillana and J. S. de Santilana, "Problemática de la Masificación Gas Natural al 2018", Educación en Ingeniería Química, 2018. [Online]. Available: https://ssecoconsulting.com/masificacioacuten-gas-natural-peruacute-iii.html.

[23] J. Wei, G. Dong and Z. Chen, "Model-based fault diagnosis of Lithium-ion battery using strong tracking Extended Kalman Filter", *Energy Procedia,* vol. 158, pp. 2500–2505, 2019. https://doi.org/10.1016/j.egypro.2019.01.391

[24] L. Andrade Vallejos, G. López Muñoz and D. Palma Nahuelcoy, "Nivel de adherencia a los inhaladores en pacientes con Asma o Enfermedad Pulmonar Obstructiva Crónica en CESFAM La Bandera, San Ramón", Universidad Gabriela Mistral, Santiago, 2020. [Online]. Available: https://hdl.handle.net/20.500.12743/1835. [

[25] M. Baltazar Ortega, "Diseño de un generador de hidrógeno para optimizar la combustión de un motor Volkswagen 1.5 L en la ciudad de Huancayo", Universidad Continental, Huancayo, 2020. [Online]. Available: https://hdl.handle.net/20.500.12394/8444.

[26] M. Mandal, "Novel electrocatalyst for alkaline membrane water electrolysis", *ChemElectroChem*, vol. 7, no. 21, pp. 4303–4305, 2020. https://doi.org/10.1002/celc.202001074

[27] M. Rajora et al., "A review on production processes, performance and emissions analysis of hydrogen as a fuel in I.C. engines", *Int. J. Environ. Sustain. Dev.,* vol. 21, no. 1/2, p. 76, 2022. https://doi.org/10.1504/ijesd.2022.119383

[28] Marin Soler, "Pasado, presente y futuro del hidrógeno en automoción", Universidad Politécnica de Catalunya, Barcelona, 2020. [Online]. Available: http://hdl.handle.net/2117/329695. 2023].

[29] Moreno Gamboa, E. G. Flórez Serrano and G. G. Moreno Conteras, "Influencia de productos de la hidrólisis en el desempeño de un vehículo que opera con gasolina y gas natural en la altura", INGE CUC, vol. 15, no. 1, pp. 89–98, 2019. https://doi.org/10.17981/ingecuc.15.1.2019.08

[30] R. Azevedo, "Brazilian inventor builds water-powered motorcycle", August 2, 2016. [Online]. Available: https://newsroom.ap.org/editorial-photos-videos/detail?itemid=5b31ee1422c81188f2085bf95dc14e5d.

CFD simulation of the surface pumping of heavy crude oil in eastern Ecuador

José Cabrera-Escobar[1], Guillermo Machado Sotomayor[2], Diego Cajamarca Carrazco[3], María Magdalena Paredes Godoy[4], Raúl Cabrera-Escobar[5]

Abstract- **The research addresses the study of heat exchange between heavy crude oil and the environment during surface pumping, specifically of a crude oil with an API gravity of 17.5, under the particular atmospheric conditions of Eastern Ecuador. The main objective of the study is to evaluate the temperature loss in a 50-meter segment of SCH-80 pipe, with a diameter of 4 inches, used for the transportation of heavy crude. This aims to understand how heavy crude loses temperature and to determine the convective coefficient, knowing that the heat loss from the fluid to the environment occurs mainly by convection. This is to determine what the temperature losses will be in longer pipe sections. For this purpose, a methodology using computational fluid dynamics (CFD) simulation was employed, a key tool for predicting the thermal behavior of crude in interaction with the environment. It was determined that the convective coefficient is 52 W/m2.K, and there is a temperature loss of 3.2 K in the 50-meter section. With this data, future research could evaluate potential heating technologies that facilitate the transport of heavy crude oil. This approach would allow for exploring innovative solutions to improve efficiency and effectiveness in managing heavy crude, facing one of the main challenges in *its transport: managing its high viscosity***

Keywords: **heavy crude oil, CFD, simulation.**

Resumen **–La investigación aborda el estudio del intercambio de calor del crudo pesado con el ambiente en el bombeo superficial, específicamente de un crudo con gravedad API de 17.5, bajo las condiciones atmosféricas particulares del Oriente ecuatoriano. El principal objetivo del estudio es evaluar la pérdida de temperatura en un segmento de 50 metros de tubería SCH-80, con 4 pulgadas de diámetro, utilizado para el transporte de crudo pesado. Con esto se busca entender cómo el crudo pesado pierde temperatura y determinar el coeficiente convectivo sabiendo que el calor que pierde el fluido con el ambiente se da principalmente por convección. Esto permitirá determinar cuáles van a ser las pérdidas de temperatura en tramos de tubería mayores. Para ello se empleó una metodología que utiliza la simulación por dinámica de fluidos computacional (CFD), una herramienta clave para predecir el comportamiento térmico del crudo en interacción con el ambiente. Se determinó que el coeficiente convectivo es de 52 W/m^2.K, y que existe una pérdida de temperatura de 3.2 K en el tramo de 50 metros. Con esta base de datos se podría en investigaciones futuras evaluar potenciales tecnologías de calefacción que faciliten el transporte del crudo pesado. Este enfoque permitiría explorar soluciones innovadoras para mejorar la eficiencia y efectividad en el manejo del crudo pesado, enfrentando uno de los principales desafíos en su transporte: la gestión de su alta viscosidad.**

Palabras Clave: **Crudo pesado, CFD, simulación.**

I. INTRODUCTION

HEAVY crude is characterized by its high density and viscosity. This type of oil is located at the lower end of the classification spectrum according to the API scale, indicating that it is denser and more viscous compared to other types of crude oil [1]. The exploitation and transportation of heavy crude present significant challenges for the oil industry, especially in areas with unique environmental conditions, such as the Ecuadorian east. Due to its high viscosity, heavy crude requires specialized technologies for efficient handling. One of the main challenges is to prevent temperature loss during transport, as this can significantly increase its viscosity and hinder its flow [2]. The viscosity of crude oil, which is closely related to its temperature, has a significant impact on both the efficiency and cost of pumping through pipelines. Higher viscosity requires more energy to move the crude oil, thus increasing operational costs [3].

Cazorla et al. [4] they investigated the impact on production and recovery factor in ultra-heavy crude reservoirs through the application of electromagnetic waves in horizontal wells. The main objective was to study how electromagnetic heating can contribute to increasing the production of viscous hydrocarbons, specifically in the Orinoco Oil Belt in Venezuela. A numerical simulation was conducted to analyze the behavior of the reservoir and the effectiveness of this technology in reducing crude viscosity, which could lead to significant improvements in the extraction of these resources.

Tolentino et al. [5] they implemented a novel technology for heating oil fields using nuclear reaction capsules. A steady-state thermal simulation of an oil field similar to Cerro Negro was conducted using COMSOL Multiphysics software with the Finite Element Method. A nuclear reaction capsule was designed with

1. José Cabrera-Escobar. Email: omar.cabrera@unach.edu.ec, ORCID: https://orcid.org/0000-0002-0197-5163, Filiation: Universidad Nacional de Chimborazo.

2 Guillermo Machado Sotomayor. Email: gmachado@unach.edu.ec, ORCID: https://orcid.org/0000-0001-5226-468X, Filiation: Universidad Nacional de Chimborazo.

3 Diego Cajamarca Carrazco. Email: diego.cajamarca@espoch.edu.ec, ORCID: https://orcid.org/0000-0003-1157-8900, Filiation: Escuela Superior Politécnica de Chimborazo.

4 María Magdalena Paredes Godoy. Email: maparedes@unach.edu.ec, ORCID: https://orcid.org/0000-0002-8211-0400, Filiation: Universidad Nacional de Chimborazo.

5 Raúl Cabrera-Escobar. Email: rvce0001@red.ujaen.es, ORCID: https://orcid.org/0009-0005-8589-7578, Filiation: Universidad de Jaén.

Manuscript Received: 27/02/2024
Revised: 05/04/2024
Accepted: 20/05/2024
DOI: https://doi.org/10.29019/enfoqueute.1034

specific dimensions to heat the porous medium, and 11 capsules were distributed throughout the reservoir to enhance the extraction of heavy and extra-heavy crude oil, thereby demonstrating the viability and effectiveness of this innovative technology.

Ramírez et al. [3] they carried out the prediction of temperature and viscosity profiles in heavy oil production wells by implementing an induction heater at the bottom of the well. The study focuses on the impact of electric heating on the viscosity of heavy oil, with the goal of improving crude mobility and well efficiency. A CFD model was developed to simulate the thermal and viscosity behavior of heavy oil in the well, demonstrating a significant reduction in the dynamic viscosity of the crude with electric heating. The results validate the effectiveness of induction heating in reducing the viscosity of heavy oil, which could have significant implications for oil production in heavy crude wells.

Pinilla et al. [6] they conducted a Computational Fluid Dynamics study on water production in mature heavy oil fields with horizontal wells. Numerical experiments were performed based on a complete set of 3D Navier-Stokes equations to simulate multiphase flows in porous media in horizontal heavy oil production wells. A sensitivity analysis was conducted on different rock and fluid properties, such as permeability and oil viscosity, assuming homogeneous porous media. The numerical model was verified with field data using two approaches: one assuming homogeneous rock properties and another using heterogeneous rock properties measured from well logs. The validation results showed that the numerical model could reproduce the observed field production trend with a deviation of 20 % compared to actual data. Additionally, critical hydraulic data in the well, such as pressure and velocity profiles, were obtained, which could be used to enhance production efficiency.

Zhang et al. [7] they conducted a three-dimensional numerical simulation to study the heat transfer behavior and flow of waxy crude oil in an inclined pipeline. The main objective was to analyze how the temperature and velocity fields of waxy crude oil vary in pipelines with different inclination angles, providing a theoretical guide for the safe operation of pipelines. Factors such as three-dimensional heat transfer, heat transfer in the surrounding soil, and changes in physical parameters with temperature were considered to develop a more accurate and realistic mathematical model.

Kumar et al. [8] they conducted a study using computational fluid dynamics analysis to investigate the flow behavior in the annular core of heat exchangers composed of nanoparticles, specifically employing a heat exchanger made up of nanoparticles. The study focused on the flow of crude oil and water in the annular pipe system, aiming to analyze the heat transfer efficiency, pressure drop, and overall performance of the system. Additionally, the flow characteristics and variations between the crude oil and water were explored, along with the molecular behaviors induced by the central channels. The research also aimed to enhance the understanding of heat generation and fluid flow within the annular core, in order to predict variations in annular flow and improve the control of fluid density within the annular core.

While research has focused on the analysis through CFD simulation of crude oil heating methods, as well as velocity, pressure, and temperature profiles, the heat loss of heavy crude during surface transport has received less attention. This critical aspect of heavy crude handling still requires detailed studies that could significantly improve efficiency in the transport and management of such hydrocarbons. In this context, the current study focuses on the simulation of surface pumping of heavy crude with an API gravity of 17.5, under the specific atmospheric conditions of eastern Ecuador. Using CFD, this research aims to analyze the temperature loss over a 50-meter pipeline section, in addition to determining the convective coefficient at which the fluid loses heat, knowing that the main mechanism by which heavy crude loses temperature is through convection with the environment.

This introduction to the problem and the methodological approach adopted lays the groundwork for a broader discussion on potential solutions and the practical implications of the findings, ultimately aiming to move towards more efficient and economically viable management of heavy crude.

II. METHODOLOGY

CFD simulation is widely used in the industry due to its multiple advantages, which include lower costs compared to experimental techniques and the ability to simulate complex physical phenomena. However, CFD simulation must be experimentally validated to confirm that the model configurations and parameters are appropriate for the case study [9], CFD has been widely used in the study of processes where there is mass and heat transfer in the air [10],[11]. In Figure 1, the methodology used for the CFD simulation can be observed.

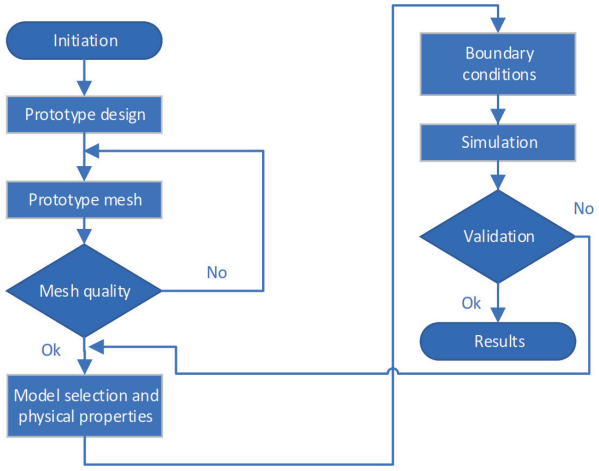

Fig. 1. Methodology used in the CFD simulation [12].

The model used in the CFD simulation has the same dimensions as the actual pipeline. In Figure 2, you can see the model used in the simulation.

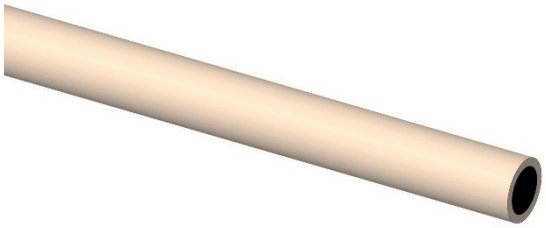

Fig. 2. Model used in the simulation.

For meshing, Tetrahedron elements are used as can be seen in Figure 3. The Orthogonal Quality metric is used to measure the quality of the mesh [13],[14], in the simulation, 501 800 elements were used; this is the optimal number of elements because, beyond this number, the analyzed variable, which is temperature, stabilizes, as can be observed in Figure 4.

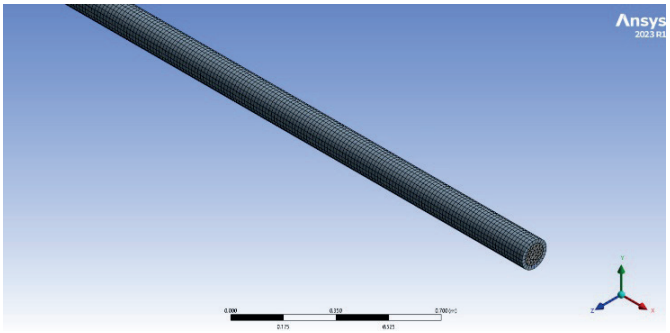

Fig. 3. Meshed Model.

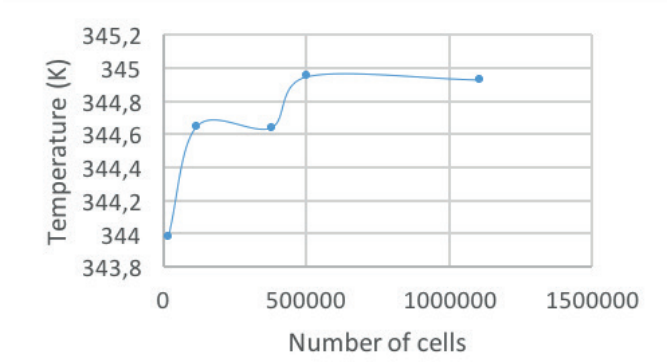

Fig. 4. Optimal Mesh Size.

The properties of the pipeline and heavy crude can be seen in Table 1 and Table 2, respectively.

TABLE I
THERMAL PROPERTIES OF THE PIPE

Material properties	Pipeline SCH-80
Density (kg/m^3)	7850
Thermal Conductivity (W/(m.k))	53
Specific Heat (J/(Kg.k))	0.49

TABLE II
THERMAL PROPERTIES OF HEAVY CRUDE

Fluid properties	Heavy crude
Density (Kg/m^3)	908.92
Specific heat (J/Kg.K)	1880
Thermal conductivity (W/m.K)	0.12
Viscosity (Kg/m.s)	0.0798

The fluid properties are determined from the curves obtained in the laboratory, which are shown in Figure 5, Figure 6, and Figure 7. This is done using an average temperature of 347.04 K.

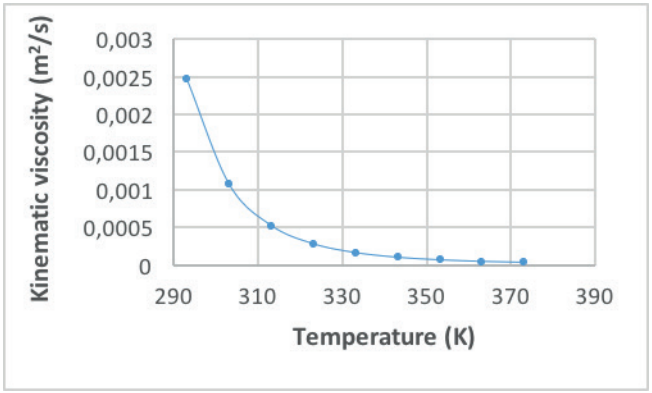

Fig. 5. Kinematic viscosity of heavy crude oil.

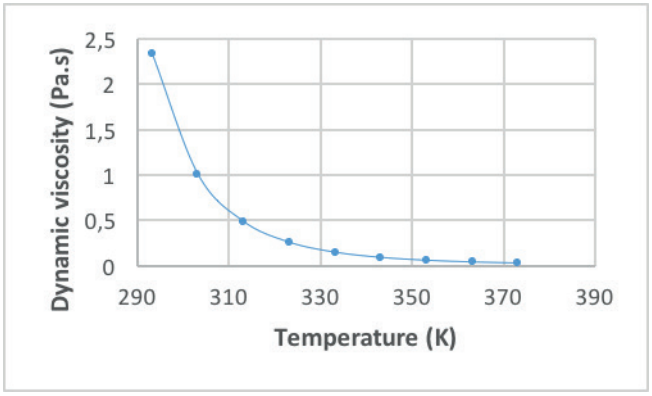

Fig. 6. Dynamic viscosity of heavy crude oil.

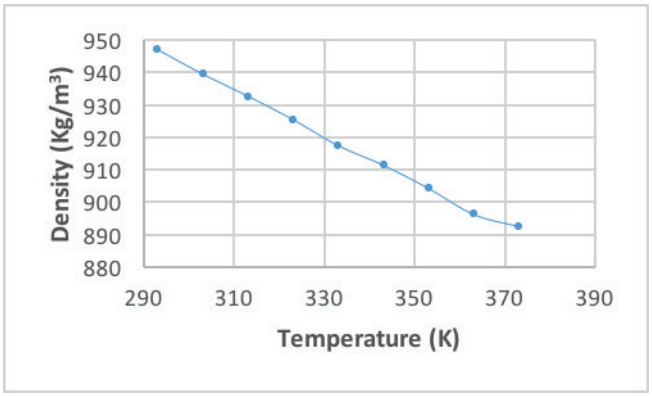

Fig. 7. Density of heavy crude oil.

In computational fluid dynamics simulations, phenomena are modeled using mathematical formulas, which are usually partial differential equations. To analyze the surface pumping of heavy crude, the Navier-Stokes equations are used, which describe the movement of fluids. When considering the fluid as incompressible, two fundamental equations are applied: the

continuity equation (1), which ensures mass conservation, and the momentum equation (2), which describes the conservation of momentum [15], [16].

$$\nabla . \vec{v} = 0 \tag{1}$$

$$\rho\left(\frac{\partial \vec{v}}{\partial t} + \vec{v}.\nabla\vec{v}\right) = -\nabla p + \mu\nabla^2\vec{v} + \vec{f} \tag{2}$$

where ρ is the density of the fluid, $\vec{v}$ is the velocity field, p is the pressure, μ is the dynamic viscosity of the fluid and $\vec{f}$ are external forces.

To model the heat transfer between the fluid flowing inside the pipeline and the external environment, the fluid is considered incompressible and not involved in chemical reactions. In this context, the heat transfer equation (3) is used, which allows for the calculation of the fluid's thermal variation in response to environmental conditions and the characteristics of the pipeline.

$$\rho c_p\left(\frac{\partial T}{\partial t} + \vec{v}.\nabla T\right) = \nabla.(k\nabla T) + \Phi + S_T \tag{3}$$

where c_p is the specific heat at constant pressure, T is the temperature, k is the thermal conductivity, Φ represents heat generation by viscous dissipation and S_T is an additional source term that may include effects such as radiation heat transfer or internal or external heat sources.

The algorithm used for the numerical simulation of the equations is SIMPLE [17], for the spatial discretization of pressure, the method used is PRESTO [18], the flow of heavy crude oil through the pipeline is considered laminar since the Reynolds number is less than 2000. The equation used is equation (4).

$$Re = \frac{\rho V D}{\mu} \tag{4}$$

where V is the velocity and D is the diameter of the pipe.

Given the exposure of the pipe to the environment, it is imperative to determine the convective heat transfer coefficient. For this purpose, the Nusselt number is used, a dimensionless magnitude that quantifies heat transport by convection. The correlation between the Nusselt number and the convective coefficient is established through equation (5):

$$Nu = \frac{hL}{k} \tag{5}$$

where Nu is the Nusselt number, h is the convection heat transfer coefficient, L is the length of the pipe and k is the thermal conductivity of the pipe.

The Nusselt number for a flow like this case, which is developed both hydraulically and thermally, is 4.36 [19][20].

The boundary conditions used are as follows:

Inlet: the fluid enters at a speed of 0.73043 m/s, due to the analyzed well producing 2225 barrels and the internal diameter of the pipeline being 0.0848 m. The entering temperature is 348.15 K, a data point taken in the field.

Outlet: for simplicity in the simulation and considering that the objective is to calculate the temperature of the fluid at the outlet, it is assumed to be exposed to atmospheric pressure.

Outside of the pipeline: the exterior of the pipeline is exposed to an ambient temperature of 292.15 K.

To obtain temperature data in the field, bimetallic thermometers model E from Ashcroft were used, as shown in Figure 8.

Fig. 8. Ashcroft Bimetallic Thermometer.

III. RESULTS

For the validation of the simulation, the experimental outlet temperature of 345.93 K and the CFD simulation result of 344.95 K were used. With these values, a Mean Absolute Percentage Error (MAPE) of 0.28 % was obtained. Additionally, to validate the convective coefficient value obtained from the simulation of 52 W/m².K, it was compared with the analytically derived value of 52.9 W/m².K, resulting in a MAPE of 1.7 %. For a simulation to be considered a good approximation, the MAPE should not exceed 2 % [21], [22].

In Figure 9, the residuals are presented, which are essential for evaluating the convergence of numerical simulations. The residuals represent the difference between the calculated values and the expected values of the flow variables. For this specific case, an absolute convergence criterion of 1e-06 is used, ensuring adequate accuracy in the simulation results.

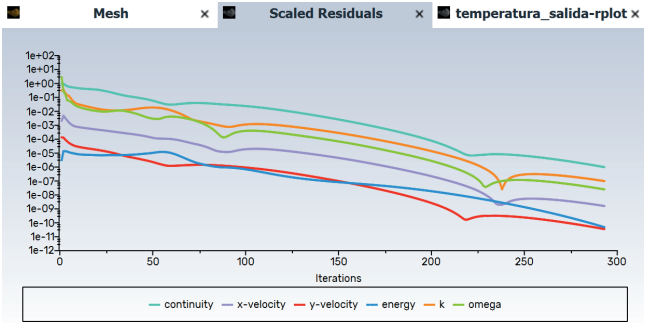

Fig. 9. Simulation Residual Curves.

In Figure 10, the average temperature curve at the pipeline outlet can be observed. The temperature at which the simulation converges is 344.95 K, which is reached at iteration 293.

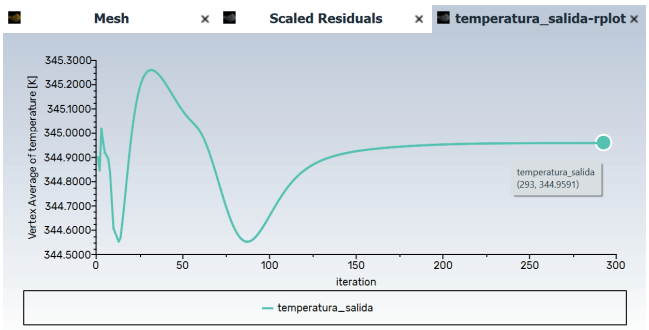

Fig. 10. Temperature at the Pipeline Outlet.

In Figure 11, the temperature profile at the pipeline inlet can be observed, representing the highest temperature recorded in this simulation. Specifically, the crude oil temperature at the inlet of the analyzed section is 348.15 K. It can be seen that the closer the heavy crude is to the surface of the pipeline, the lower the temperature.

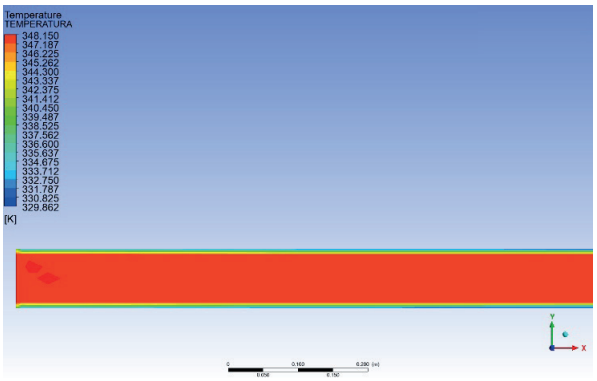

Fig. 11. Temperature Profile at the Pipeline Inlet.

In Figure 12, the temperature profile at the pipeline outlet can be observed. This area has the lowest temperature recorded in this simulation. Specifically, the crude oil temperature at the outlet of the analyzed section is 344.95 K. Similar to the start of the analyzed section, it can be seen that the closer the heavy crude is to the surface of the pipeline, the lower the temperature.

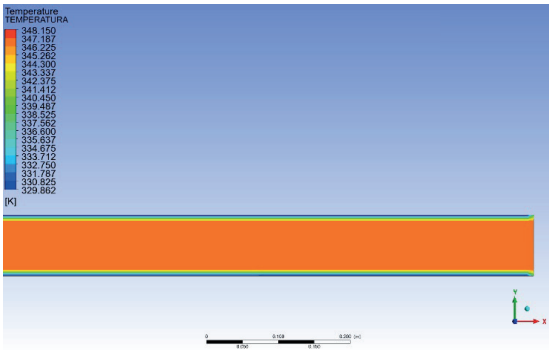

Fig. 12. Temperature Profile at the Pipeline Outlet.

IV. DISCUSSION

From the experimental and simulation results, it can be observed that there is a temperature reduction from 348.15 K at the starting point of the analysis to 344.95 K at the endpoint of the 50 m pipeline section. This temperature decrease is due to the ambient air temperature being 292.15 K. The primary reason for the heat loss is convection with the environment. The convective coefficient determined through the simulation is 52 W/m²·K. This coefficient can be used to evaluate the temperature loss over long pipeline sections, allowing for the determination of the heat that needs to be added to the fluid. Temperature loss in the pipeline during transport significantly affects the viscosity of heavy crude, which in turn influences the efficiency and costs associated with pumping it over long distances.

The simulation identifies that the variables most influencing this heat loss are the ambient temperature, the crude temperature, the convective heat transfer coefficient, and the crude velocity. Other parameters that also influence but cannot be modified include the area exposed to the environment, and the thermal properties of the pipeline and the fluid. Ambient temperature affects heat loss because, according to Newton's law of cooling, the rate of heat loss from the pipeline is proportional to the temperature difference between the pipeline and the environment. Crude temperature is important in heat loss because a higher temperature implies a greater potential for heat loss to a cooler environment. The convective heat transfer coefficient is crucial in heat loss, as the loss occurs primarily through convection. The convective transfer coefficient is directly proportional to the heat loss. The crude flow velocity is critical since a higher velocity implies that the crude remains in contact with the environment for less time, resulting in lower heat losses. Conversely, a lower velocity means that the crude is exposed to the environment for a longer time, increasing the heat losses.

V. CONCLUSIONS AND RECOMMENDATIONS

Through the application of computational fluid dynamics, it was possible to quantify the temperature variation along a 50-meter segment of heavy crude oil transportation pipeline, determining that there is a 3.2 K reduction in the analyzed section. Additionally, the convective coefficient was found to be 52 W/m²·K. This analysis provided a detailed understanding of the temperature profiles and thermal dynamics involved, which is essential for optimizing transportation processes and ensuring the operational integrity of the system. The results obtained offer valuable insights for the design and improvement of thermal maintenance strategies, significantly contributing to the efficiency and safety in the management of heavy crude transportation.

The results obtained serve as a foundation for future studies that introduce heating technologies for heavy crude to maintain its viscosity within optimal ranges for efficient transportation.

ACKNOWLEDGEMENT

The authors would like to thank the Baker Hughes Company for all the facilities they provided for this research.

REFERENCES

[1] J. G. Speight, "Chapter 1-occurrence and formation of crude oil and natural gas," *Subsea and Deepwater Oil and Gas Science and Technology*, pp. 1–43, 2015.

[2] C. Zou, "Heavy oil and bitumen," *Unconventional petroleum geology*, pp. 345–370, 2017.

[3] J. Ramírez, A. Zambrano and N. Ratkovich, "Prediction of Temperature and Viscosity Profiles in Heavy-Oil Producer Wells Implementing a Downhole Induction Heater," *Processes*, vol. 11, no. 2, 2023, https://doi.org/10.3390/pr11020631

[4] Cazorla and J. J., "Evaluación de la producción y el factor de recobro en yacimientos de crudo extra pesado a través de la aplicación de ondas electromagnéticas en pozos horizontales," Sep. 2013, http://saber.ucv.ve/handle/10872/4261

[5] S. L. Tolentino, S. Caraballo, Á. Duarte and J. Mendoza, "Calentamiento de yacimientos petrolíferos mediante cápsulas de reacción nuclear," *Universidad, Ciencia y Tecnología*, vol. 20, no. 79, pp. 58–68, 2016, Online]. Available https://bit.ly/3WT8qgS

[6] A. Pinilla, M. Asuaje, C. Pantoja, L. Ramirez, J. Gomez and N. Ratkovich, "CFD study of the water production in mature heavy oil fields with horizontal wells," *PLoS One*, vol. 16, no. 10, pp. 1–24, Apr. 2021, https://doi.org/10.1371/journal.pone.0258870

[7] L. Zhang, C. Du, H. Wang and J. Zhao, "Three-dimensional numerical simulation of heat transfer and flow of waxy crude oil in inclined pipe," *Case Studies in Thermal Engineering*, vol. 37, p. 102237, 2022, https://doi.org/10.1016/j.csite.2022.102237

[8] R. Kumar R *et al.*, "Investigation of nano composite heat exchanger annular pipeline flow using CFD analysis for crude oil and water characteristics," *Case Studies in Thermal Engineering*, vol. 49, p. 103297, 2023, https://doi.org/10.1016/j.csite.2023.103297

[9] Q. Tu, Z. Ma and H. Wang, "Investigation of wet particle drying process in a fluidized bed dryer by CFD simulation and experimental measurement," *Chemical Engineering Journal*, vol. 452, p. 139200, 2023, https://doi.org/10.1016/j.cej.2022.139200.

[10] E. Getahun, M. A. Delele, N. Gabbiye, S. W. Fanta, P. Demissie and M. Vanierschot, "Importance of integrated CFD and product quality modeling of solar dryers for fruits and vegetables: A review," *Solar Energy*, vol. 220, pp. 88–110, 2021, https://doi.org/10.1016/j.solener.2021.03.049

[11] P. D. Tegenaw, M. G. Gebrehiwot and M. Vanierschot, "On the comparison between computational fluid dynamics (CFD) and lumped capacitance modeling for the simulation of transient heat transfer in solar dryers," *Solar Energy*, vol. 184, pp. 417–425, 2019, https://doi.org/10.1016/j.solener.2019.04.024.

[12] José Cabrera-Escobar, David Vera Francisco Jurado, Manolo Córdova-Suárez, Gonzalo Santillán-Valdiviezo, Antonio Rodríguez-Orta and R. Cabrera-Escobar, "Optimization of olive pomace dehydration process through the integration of computational fluid dynamics and deep learning," *Energy Sources, Part A: Recovery, Utilization, and Environmental Effects*, vol. 46, no. 1, pp. 4756–4776, 2024, https://doi.org/10.1080/15567036.2024.2331563

[13] ANSYS Inc, *Ansys Fluent Tutorial Guide*, 2023 R1. Canonsburg, 2023.

[14] ANSYS Inc, "ANSYS Meshing User's Guide," 2024. [Online]. Available: http://www.ansys.com

[15] K. Garg, S. Singh, M. Rokade and S. Singh, "Experimental and computational fluid dynamic (CFD) simulation of leak shapes and sizes for gas pipeline," *J Loss Prev Process Ind*, vol. 84, p. 105112, 2023, https://doi.org/10.1016/j.jlp.2023.105112

[16] Y. Xiao *et al.*, "Bionic pipeline transport characteristics with transverse protuberances in slurry shield circulation system based on CFD-DEM," *Powder Technol*, vol. 432, p. 119133, 2024, https://doi.org/10.1016/j.powtec.2023.119133.

[17] A. Benhamza, A. Boubekri, A. Atia, T. Hadibi and M. Arıcı, "Drying uniformity analysis of an indirect solar dryer based on computational fluid dynamics and image processing," *Sustainable Energy Technologies and Assessments*, vol. 47, p. 101466, 2021, https://doi.org/10.1016/j.seta.2021.101466.

[18] ANSYS Inc, *Ansys Fluent Theory Guide*, 2023 R1. Canonsburg, 2023.

[19] T. L. Bergman, A. S. Lavine, F. P. Incropera and D. P. DeWitt, *Introduction to Heat Transfer*. Wiley, 2011. [Online]. Available: https://books.google.com.ec/books?id=YBaNaLurTD4C

[20] A. J. Ghajar, D. Yunus. and A. Cengel, *Heat and Mass Transfer: Fundamentals and Applications*. McGraw-Hill Education, 2014. [Online]. Available: https://books.google.com.ec/books?id=B89MnwEACAAJ

[21] F. Hussain, M. Jaskulski, M. Piatkowski and E. Tsotsas, "CFD simulation of agglomeration and coalescence in spray dryer," *Chem Eng Sci*, vol. 247, p. 117064, 2022, https://doi.org/10.1016/j.ces.2021.117064

[22] J. Cabrera-Escobar, D. Vera, F. Jurado and R. Cabrera-Escobar, "CFD investigation of the behavior of a solar dryer for the dehydration of olive pomace," *Energy Sources, Part A: Recovery, Utilization, and Environmental Effects*, vol. 46, no. 1, pp. 902–917, Dec. 2024, https://doi.org/10.1080/15567036.2023.2292242

Reduction of Setup Times in a Metal Fabrication Company Using a Lean-Sigma Approach

Omar Celis-Gracia[1], Jorge Luis García-Alcaraz[2], Francisco Javier Estrada-Orantes[3], Liliana Avelar-Sosa[4], Noe Gaudencio Alba-Baena[5], Fabiola Hermosillo-Villalobos[6]

Abstract — **Manufacturing companies face demand fluctuations and must deliver the required quantity of parts to their customers within the required time; however, companies face different challenges in fulfilling them. One is technological advances, which make it impossible for them to compete with other countries, such as China, due to financial issues. Therefore, manufacturing companies use continuous improvement methodologies to achieve better performance in their processes. Six Sigma and Lean Manufacturing are some of the best-known approaches. This article briefly presents the application of a lean sigma approach oriented to solving problems. This research proposes a methodology based on Lean Sigma that contrasts what different authors currently do: continuous improvement projects that take up to 12 months to produce results and do not solve a problem. This implementation is conducted in a process that manufactures metal parts and fails to deliver them on time to its customers. Using tools such as the Single Minute Exchange of Die (SMED) in a production line, on-time deliveries were increased from 89 % to 96 %; at the same time, the model change times were reduced by approximately 60 %, which is required for the implementation of this methodology for only four weeks, unlike the traditional six-sigma approach that can take up to 12 months to improve the process.**

Keywords – **Problem Solution; Process Improvement; Lean-Sigma; SMED; Six-Sigma.**

Resumen — **Las empresas manufactureras presentan fluctuaciones en sus demandas y no entregan a sus clientes la cantidad de partes en el tiempo requerido. Son diferentes los retos que enfrentan estas empresas, uno de ellos son los avances tecnológicos que, por cuestiones financieras, no es posible competir con otros países, tales como China. Es por esto, que las empresas manufactureras hacen uso de metodologías de mejora continua para lograr un mayor desempeño en sus procesos. Algunos de los enfoques más conocidos son Seis Sigma y Manufactura Esbelta. En este artículo se presenta una aplicación de un enfoque Lean-Sigma, el cual se orienta a resolver problemas en un corto periodo de tiempo. El propósito de esta investigación es proponer una metodología basada en Lean-Sigma que permita contrastar lo que hacen diferentes autores en la actualidad, que básicamente son proyectos de mejora continua que tardan hasta doce meses en dar resultados y que no resuelven un problema. Esta implementación se lleva a cabo en un proceso que fabrica partes metálicas, el cual está incumpliendo con su cliente en las entregas a tiempo. Utilizando la herramienta de cambios rápidos de modelo (SMED) se lograron incrementar las entregas a tiempo de un 89 % a un 96 %. A su vez, los tiempos de cambio de modelo se reducen aproximadamente un 60 %, siendo requeridas para la implementación de esta metodología solo cuatro semanas, a diferencia del enfoque tradicional de seis sigma que puede tomar hasta doce meses para mejorar un proceso.**

Palabras Clave – Solución de Problemas; Mejoramiento de Proceso; Lean-Sigma; SMED; Six-Sigma.

I. INTRODUCTION

MANUFACTURING companies face various operational challenges, including unpredictable market changes. According to Deeb et al. [1], manufacturing businesses frequently encounter unexpected fluctuations and uncertainties caused by novel regional mandates or rules, emerging technologies and materials, new market niches, and the growing need for additional product attributes. Market fluctuations can present challenges for manufacturing organizations, requiring them to adjust their production methods, effectively managing stocks, and fulfilling client requests. Furthermore, the use of Industry 4.0 technology brings forth both advantageous prospects and obstacles for manufacturing organizations [2]. Gholami et al. [3] highlight that while Industry 4.0 can increase efficiency, customizability, and autonomy, small and medium enterprises (SMEs) in the manufacturing sector still face challenges in upgrading their manufacturing systems and adopting these technologies. This can be attributed to factors such as cost of implementation, lack of technical expertise, and resistance to change [4].

1 Omar Celis-Gracia and Fabiola Hermosillo-Villalobos receive a grant for their Ph.D. from Consejo Nacional de Humanidades Ciencia y Tecnología, CONAHCYT, under grant Agreement number 960749 & 548515, respectively.
Department of Electrical Engineering and Computer Science, Universidad Autónoma de Ciudad Juárez. Ave. Del Charro 450 North. Col. Partido Romero. Ciudad Juárez, Chihuahua, México. CP 32310. Email: al232735@alumnos.uacj.mx, ORCID: https://orcid.org/0000-0003-2061-3384

2 Department of Industrial Engineering and Manufacturing, Universidad Autónoma de Ciudad Juárez, Ave. Del Charro 450 North. Col. Partido Romero. Ciudad Juárez, Chihuahua, México, CP 32310. Email: jorge.garcia@uacj.mx, ORCID: https://orcid.org/0000-0002-7092-6963

3 Department of Industrial Engineering and Manufacturing, Universidad Autónoma de Ciudad Juárez, Ave. Del Charro 450 North. Col. Partido Romero. Ciudad Juárez, Chihuahua, México, CP 32310. Email: frestrad@uacj.mx, ORCID: https://orcid.org/0000-0002-3033-6635

4 Department of Industrial Engineering and Manufacturing, Universidad Autónoma de Ciudad Juárez, Ave. Del Charro 450 North. Col. Partido Romero. Ciudad Juárez, Chihuahua, México, CP 32310. Email: liliana.avelar@uacj.mx, ORCID: https://orcid.org/0000-0001-9490-2520

5 Department of Industrial Engineering and Manufacturing, Universidad Autónoma de Ciudad Juárez, Ave. Del Charro 450 North. Col. Partido Romero. Ciudad Juárez, Chihuahua, México, CP 32310. Email: nalba@uacj.mx, ORCID: https://orcid.org/0000-0002-3072-3248

6 Department of Electrical Engineering and Computer Science, Universidad Autónoma de Ciudad Juárez. Ave. Del Charro 450 North. Col. Partido Romero. Ciudad Juárez, Chihuahua, México. CP 32310. Email: al232734@alumnos.uacj.mx, ORCID: https://orcid.org/0000-0003-1644-7598
Manuscript Received: 11/03/2024
Revised: 17/05/2024
Accepted: 27/05/2024
DOI: https://doi.org/10.29019/enfoqueute.1027

Facing these challenges increases the need for companies to improve their flexibility [5] [6], and adaptability has become necessary for survival and success. Flexibility is a key determinant of success in the context of expectations. Consumer preferences are constantly evolving and driven by changes in lifestyle, demographics, and socioeconomic factors. Companies that can adapt their products, services, and customer experiences to align with shifting demands will be more successful in retaining and attracting customers [7]. Flexible companies can implement contingency plans, react to and solve problems quickly, diversify their offerings, and mitigate risks effectively [8] [9].

Adeodu et al. [10] state that many manufacturing companies encounter obstacles that prompt them to implement continuous improvement methodologies like Six Sigma (SS), Lean Manufacturing (LM), Lean Six Sigma (LSS), and Lean Sigma (LS). These methodologies empower regional companies to overcome their technological limitations and other shortcomings, enabling them to compete with their more advanced counterparts [11]. To improve the processes, these approaches use statistical and lean tools that improve and solve problems, such as the Single Minute Exchange of Die (SMED), a tool used in manufacturing and production processes to reduce the time it takes to perform equipment changeovers or setups. SMED aims to minimize the time required to switch a production line from producing one type of product to another, ideally achieving changeovers in less than ten minutes [12] [13].

SMED was introduced by Shigeo Shingo, a Japanese industrial engineer and one of the key contributors to the Toyota Production System (TPS). The underlying principle of SMED is to convert as many changeover tasks as possible from internal (activities that must be performed while the equipment is stopped) to external (activities that can be performed while the equipment is running) [14]. According to a study by Zhang et al. [11], SMED involves the following key steps:

1. Separation of internal and external activities
2. Convert internal tasks to external tasks
3. Streamlining internal tasks
4. Standardization
5. Continuous improvement

By implementing SMED, manufacturers can significantly reduce the downtime between production runs, increase production flexibility, and enhance overall operational efficiency. This approach is particularly beneficial in industries with frequent changes in various products or production runs [15].

In Mexico, it is crucial to use these continuous improvement methods or methodologies because of the country's ongoing establishment of foreign enterprises. By 2023, the country had 608,484 manufacturing enterprises, with 484 located in Chihuahua and 416 in Ciudad Juarez. These two cities account for almost 80 % of the state's overall manufacturing industry. These enterprises collectively created a total of 2,976,510 jobs across the country, with 503,759 jobs in Chihuahua and 326,298 jobs in Ciudad Juarez. This accounts for over 60 % of jobs at the state level and 11 % at the national level. Tijuana surpasses Ciudad Juarez and other influential industrial cities in terms of the number of IMMEX enterprises, with a total of 596. Tijuana generated 259,968 jobs, whereas Ciudad Juarez generated 326,298 jobs, making a difference of 66,330 jobs. Despite having fewer enterprises, Ciudad Juarez outperformed Tijuana in terms of job creation. This highlights the significance of conducting such research in the sector to make a beneficial contribution to the economic and social dimensions [16].

Although companies worldwide are currently using SS, LM, and LSS approaches to improve their processes and become more flexible, some issues with these approaches represent disadvantages. For example, Kulkarni et al. [17] applied SS methodology to a company dedicated to manufacturing boring tool holders. Initially, the process had many rejects owing to variations in the two critical dimensions and using the DMAIC cycle (Define, Measure, Analyze, Improve, Control) and tools such as control charts, fishbone analysis, root cause analysis, capability analysis, and control plan. Their application was focused on reducing the defects of the process; once the methodology is implemented, the sigma level of the process increases from 2.49 to 3.51, so the objective of taking the process to six sigmas is not achieved. However, the authors did not mention the analysis of the measurement system as a step in their methodology. In projects involving quality improvement, it is essential to ensure that the measurement system correctly discriminates between acceptable and nonconforming parts. Finally, this application required 240 days to achieve the results, so it can be concluded that the current approaches can take up to a year to provide company results. Given the current situation in the supply chain, it is not feasible for companies to wait a long time to see improvements in the process.

In another study, Guleria et al. [2] implemented Lean Six Sigma in an automotive company dedicated to axle manufacturing. Initially, the company had many rejects owing to problems with the components that make up the rear axle. The company decided to implement the LSS approach to find waste in the defect reduction process. The tools used during the implementation of the methodology are the Value Stream Map (VSM) and 5S, with which it is possible to reduce the material handling inside the building and the use of layout because of a better organization. Thus, the percentage of defects was reduced from 10.4 % to 3.20 %, the sigma level of the process was increased from 3.34 to 3.94, and the Lead Time was reduced from 12 to 11 days. In this implementation, it can be observed that the sigma level does not reach the six-sigma level, which is the philosophy of the SS approach. However, the author does not mention the analysis of the measurement system to ensure that it correctly discriminates between the good and bad parts. Finally, it is essential to note that the implementation of LSS, as performed by these authors, takes 240 days, which is too long for the company in terms of cost and waste.

Nallusamy et al. [18] use an approach based on Lean Manufacturing, in which they use different Lean tools to improve productivity in an automotive production process. Among the tools used are: SMED and Kaizen. Implementing this LM approach reduces the cycle time from 170 to 140 minutes and Lead Time from 6.9 to 3.6 days. During this implementation, an analysis of the Measurement System is not included to see the impact it has on the measurement of the variables used to measure the improvement; on the other hand, the implementation time of this approach, as presented by the authors, requires 180 days, which hurts the costs of the company as it requires a high investment of time and resources.

According to the previous paragraphs, the current LM approaches used to improve production systems by different authors in different industrial sectors result in medium- and long-term improvements, which is not acceptable today because companies need to find quick results that allow them to remain competitive but, above all, flexible, one of the most important qualities for customers.

The purpose of this research is to present an approach called Lean-Sigma, which aims to address this problem; it is an approach that acts at the speed of Lean "Just do it" providing results in a short period providing an advantage to companies in such a way that the benefits of improvements require less waiting time and therefore, less waste and investment. On the other hand, this approach presents a method to integrate the analysis of the measurement system and the importance of improvement projects.

This study examines the potential of lean sigma's flexibility for various applications and solutions in production systems. These applications can encompass the design phase and optimize the production process [19]. This study investigates the feasibility of utilizing Lean Sigma as a problem-solving approach rather than as a methodology centered around projects. The main objective of this study is to utilize lean-sigma synergy to efficiently complete the entire solution process within a short timeframe [20].

As mentioned, flexibility allows managers to meet customer expectations by coping with changes in demand due to external and internal factors. This was done through a case study in which the methodology was implemented, and the results were validated to demonstrate its effectiveness.

The study was conducted by a company established in the northern region of Mexico from March 6 to May 26, 2022, dedicated to manufacturing metal parts using Press Brake bending machines. The plant currently has 15 bending machines and delivers metallic subassemblies for the final assembly at another facility in the same region.

The metal area has experienced fluctuations in demand owing to increased customer demand, resulting in insufficient parts being delivered to the client to meet the current demand. In the last six months, the on-time delivery rate fluctuated between 85% and 92%, which is below the target of 96% for this process. The primary objective of this study is to improve the on-time delivery (OTD) rate using a lean sigma approach and to prove that the problem can be solved quickly.

The novelty and scientific contribution of the case study reported in this article is that quality problems are solved using the lean–sigma approach, which is based on the principle of solving them at a lean speed. This means that instead of using a traditional continuous improvement approach that takes months or even years to produce results to improve the situation, with the proposed approach, the problem is solved in a few weeks.

The advantage of this approach is that the company stops losing money for long periods owing to quality problems, which contributes to improved flexibility and efficiency in a shorter period. Additionally, the speed with which it provides results, unlike the traditional method that takes from 6 months to 12 months to start the improvement, the proposed method provides results in a matter of weeks.

The remainder of this paper is organized as follows. After a brief introduction, section two describes the methodology used to prove the proposed approach. Section three analyzes the results. Section four reports the conclusions and section five presents some limitations and future research.

II. METHODOLOGY

Lean Sigma is an approach focused on problem-solving, as opposed to Lean Six Sigma, which is more project oriented. The methodology is flexible at every stage, allowing for the utilization of engineering, lean, or statistical tools that are now accessible. This study utilized the Lean Sigma technique, which consists of five rapid improvement steps [19], as depicted in Figure 3.

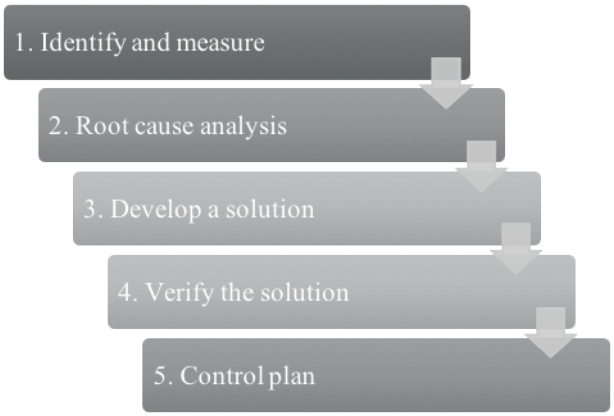

Fig. 3. Lean-Sigma approach methodology, adapted from [20].

E. Step one. Identify and Measure the Problem

The purpose of the first stage of the proposed methodology is to delimit the problem and explain its size in terms of process capability. To delimit this problem, first, a cross-functional team was formed in the process of interest; in this case, the metal-forming area. The team was composed of personnel from each of the main support teams; in this case, it was composed of Quality Engineer, Manufacturing Engineer, Process Engineer, Maintenance Engineer, Production Supervisor, and Tool Crib Engineer and involved Process Technicians who performed the model changes.

It is essential to mention that it must be sure to include all the support departments to have different points of view and opinions that vary according to the perspective of the person and the department to which they belong, this helps to eliminate the "shop blindness" and to be able to contribute ideas that enrich the solution of the problem. Once the multifunctional team was formed to work on this project, we conducted three sessions with the team performing Gemba Walk, which consists of going through the process of interest in which the project is being carried out.

For this project, one of the process machines is selected, where, based on experience, the setup has the longest time. The first day of the walk consisted of an area tour and analysis of the process metrics, mainly quality, efficiency, and on-time deliveries. The team analyzed the data and generated questions

to better understand the situation. To analyze trends, historical data were used for the metric identified as the one with the lowest performance and the one that was off-target; in this case, the on-time delivery (OTD) rate.

The second day of the Gemba walks consisted of a brief brainstorming session involving the previously formed cross-functional team to determine why the production schedule was not currently being met. Approximately 50 ideas were generated, and the team voted and identified the potential cause with the highest score that was used to solve the problem. The third and final days of the Gemba walks were used to define the problems and objectives of the project by documenting them in a Kaizen Charter.

B. Step 2. Root Cause Analysis

Two sessions were held with the team to find a solution to this problem. In the first session, a brainstorming session was generated, in which each team member contributed ideas to the potential cause identified in Step 1. Once the ideas were organized, the Nominal Group Technique tool was used, consisting of each team member evaluating and rating each idea, which was performed anonymously. Each person assigns a weight to five ideas by assigning points from 1 to 5, where 1 indicates that it has the most negligible impact on the problem and 5 indicates that it has a high impact on the problem. The moderator received anonymous weights and captured them on a spreadsheet. Using the weighted ideas, a Pareto diagram is created to prioritize the causes with the highest weighting. Finally, once the idea with the highest weighting was identified, 5 Why's technique was used to get to the root cause of the problem. In this technique, the entire team participates in the same way, asking themselves five times why the problem occurs. When the fifth reason was reached, the root cause was found, and the problem was solved by eliminating it.

C. Step 3. Develop a Solution

In the third step, based on the root cause identified in the previous step, a lean manufacturing or Six Sigma tool was selected to eliminate the root cause, including the Design of Experiments, Quick Model Changes (SMED), Kanban, and Cellular Manufacturing, among others. In this case, the SMED tool was used to reduce the model change time to less than 10 min. The SMED methodology consists of 4 four stages. In the preliminary stage, the team documents and maps the setup process, noting all the activities and times involved in each of them. In this stage, only the activities were listed with their respective times, and a video of the process was taken to analyze the micro-movements in detail and to see more specific things to be analyzed. In stage one, activities were identified as internal (performed when the equipment was completely stopped) or external (performed when the equipment was operating).

At the end of this stage, the activities were graphed to understand the proportion of internal and external activities. Subsequently, in Stage 2, the team identified those activities currently performed internally that can be transformed into external activities to prepare for all these activities before the machine stops and to have a more efficient model change. The team developed a checklist for the preparation activities and tools required before the setup. Finally, in stage 3, the team developed an action plan to reduce the time of internal activities, some of which were as follows: define a standardized work method and perform activities in parallel and fixtures that allow faster assembly and disassembly of tools, among others.

D. Step 4. Verify the Solution

Continuing with Step 4, which consists of verifying the solution, the team performs statistical tests on this part of the methodology to confirm that Step 3 solves the problem. The team collected data from on-time deliveries after implementing the SMED technique. Once the data were obtained, a 2 sample-t statistical test was performed to test the null hypothesis H_0: the OTD is the same in its initial form after implementing the proposed methodology and H_1: the OTD is lower in its initial form than after implementing the proposed methodology. Once the statistical test was performed, it was concluded that the OTD increased considerably when applying the lean–sigma.

E. Step 5. Control Plan

Finally, in Step 5, a control plan is made, which consists of deploying the work instructions and visual aids to standardize the setup process, as well as a Kaizen event with the first and second shift workers, where they were informed and trained on how to perform model changes, which were mainly asked to properly document the times of model changes to monitor the performance. Finally, an action plan is created to implement and take the lessons learned from other machines and processes.

III. RESULTS AND DISCUSSION

A. Identify and Measure the Problem

Following the Lean-Sigma approach, the team collects information on the on-time delivery rate, takes data from six months of production control reports to analyze the behavior, and records it in Table 1. A run chart of the collected information is shown in Figure 4.

Based on the data, it can be observed that the on-time delivery rate was between 85 % and 92 % during the last six months. The run graph does not show any trend, but based on the data obtained, it can be observed that 100 % of the time, the quantity of parts required by the customer is not delivered, causing line stoppages.

TABLE 1
OTD INDEX FOR THE LAST SIX MONTHS

WEEK	OTD %	WEEK	OTD %
WK 40	90 %	WK 50	88 %
WK 41	92 %	WK 51	85 %
WK 42	92 %	WK 52	87 %
\0WK 43	86 %	WK 01	88 %
WK 44	86 %	WK 02	90 %
WK 45	90 %	WK 03	87 %
WK 46	88 %	WK 04	86 %
WK 47	87 %	WK 05	86 %
WK 48	86 %	WK 06	89 %
WK 49	85 %	WK 07	88 %

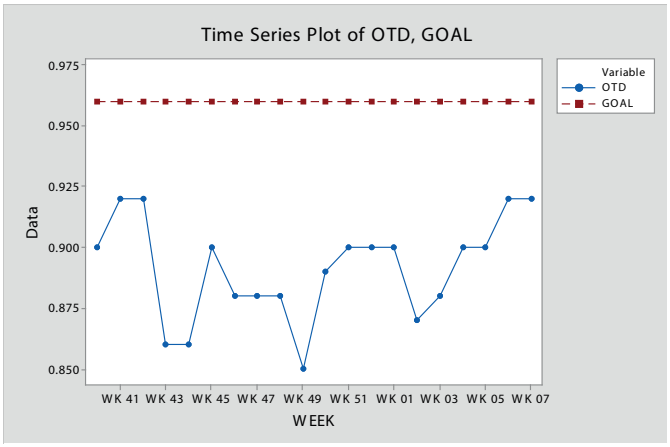

Fig. 4. Run chart of the OTD index under the initial conditions.

B. Root Cause Analysis

Once the information has been reviewed and analyzed, essential quality tools are used to determine the root cause of the problem. First, we gathered a multifunctional team from an area composed of a production supervisor, setup technician, quality engineer, manufacturing engineer, and tool crib technician to conduct a brainstorming session.

The session aims to identify the factors that team groups believe affect the on-time delivery indicator and their possible causes. After generating over 50 ideas, reviewing them, and debugging, the potential causes were reduced to three: high setup times, lack of tools, and sudden changes in production plan priorities due to a lack of materials.

Once the three potential causes were identified, the team concluded that the lack of materials could not be controlled and that the lack of tools was caused by not returning them to the tool crib for preventive maintenance; therefore, these causes were discarded.

The team decided to focus on high setup times. Subsequently, data on model changes or setup times were collected from the document control area. The data are plotted and shown in Figure 5, where the model changed over time in the last six weeks, ranging from 20 to 115 min, with an average setup time of 68 min.

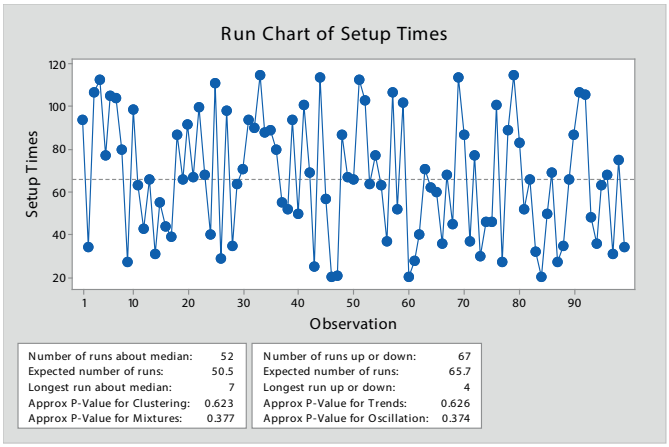

Fig. 5. Run chart of changeover time duration under the initial conditions.

C. Develop a Solution

The team used the SMED technique to reduce model changes over time. A four-step methodology was used to achieve this, as illustrated in Figure 6.

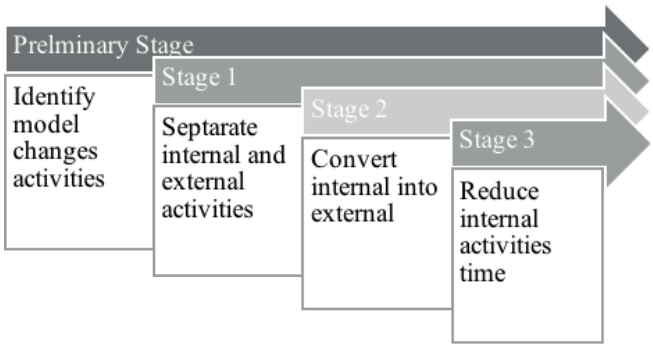

Fig. 6. SMED phases.

The purpose of the preliminary stage was to identify all the activities that constitute the setup of the process. In this case, recording during the process and listing activities is recommended. To this point, only the activities have been listed, and they were all visualized as the set of activities necessary to perform a model change. Table 2 shows the activities identified during the analysis of model changes. It can be seen that 30 activities comprised the model change, taking 78 minutes.

Many transfers were visualized during the analysis between different departments, such as tool crib, quality, and production.

In Stage One, the team identifies and classifies each activity according to how it is currently being executed. The activities were classified into two categories: internal and external. Internal activity was performed while the machine was stopped, whereas external activity was performed while the machine was still running. Figure 7 shows that under the current conditions, 100 % of the 30 activities identified were performed internally.

TABLE 2
ACTIVITIES IDENTIFIED DURING THE CHANGEOVER

No.	Activity	Time (Sec)
1	Remove tools	64
2	Request folder	117
3	Get drawing	90
4	Request tools to tool crib	60
5	Fill out the form to request fabric	57
6	Request fabric	286
7	Assemble the tolos	76
8	Introduce parameters for adjustments	12
9	Review the dimensions on the drawing	39
10	Enter dimensions for fitting	9
11	Z-axis adjustment	73
12	Upper tool mounting	156
13	Retainer adjustment	51
14	Raise the curtain to place the fabric	73
15	Origin point adjustment	78
16	Get measuring equipment	37
17	Adjust measurements and angles	13
18	Adjust piece	40
19	Measure the first bend	2.4
20	Adjustments to the first bend	31
21	Review part against the drawing	116
22	Adjust the first piece	668
23	Review part against drawing	36
24	Adjustments	267
25	Request critical dimensions	511
26	Measure and fill documentation	450
27	Go and get supervisor authorization	43
28	The supervisor signs the documentation	6
29	Take the first piece to quality	110
30	Quality release of the first piece	1089
	Production starts after:	4660

In Stage Two, the team identified activities that, under the current conditions, were performed internally but could be performed externally. This stage aimed to reduce the proportion of internal activities to such a level that the internal activities were close to 1/3 of the total number of activities. From the identified activities, Table 3 determines which of the 30 activities can be converted to internal, which is a fundamental principle of SMED. As shown in Figure 8, 50 %, that is, 15 of the 30 activities, can be converted to internal. This reduces the model changeover time from 78 to 27 minutes, representing a 66 % reduction just by converting the activities to external ones. During this stage, the team developed a checklist with all the necessary materials, documentation, and elements that must be ready before starting the change, thus ensuring that all external activities were ready during the model change.

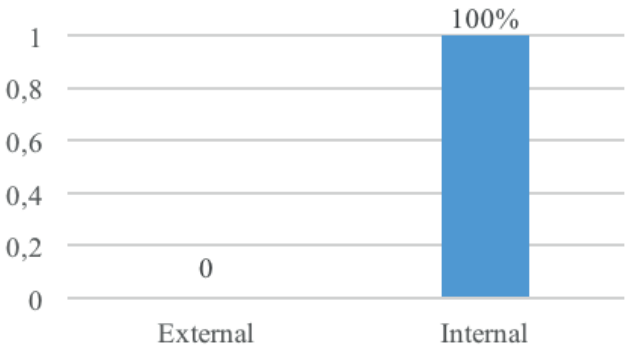

Fig. 7. Identification of Internal and External Activities.

TABLE 3
IDENTIFICATION OF INTERNAL AND EXTERNAL ACTIVITIES

No.	Activity	E/I	No.	Activity	E/I
1	Remove tools	I	16	Get measuring equipment	E
2	Request folder	E	17	Adjust measurements and angles	I
3	Get drawing	E	18	Adjust piece	I
4	Request tools to tool crib	E	19	Measure the first bend	I
5	Fill out the form to request fabric	E	20	Adjustments to the first bend	I
6	Request fabric	E	21	Review part against the drawing	E
7	Assemble the tools	I	22	Adjust the first piece	I
8	Introduce parameters for adjustments	I	23	Review part against drawing	E
9	Review the dimensions on the drawing	E	24	Adjustments	I
10	Enter dimensions for fitting	I	25	Request critical dimensions	E
11	Z-axis adjustment	I	26	Measure and fill documentation	E
12	Upper tool mounting	I	27	Go and get supervisor authorization	E
13	Retainer adjustment	I	28	The supervisor signs the documentation	E
14	Raise the curtain to place the fabric	I	29	Take the first piece to quality	E
15	Origin point adjustment	I	30	Quality release of the first piece	E

E: External, I: Internal

In the final stage, the team developed activities to reduce the time required for internal activities. To achieve this, the team created an action plan and followed it up. Some of the activities to be carried out included standardization of the model change time by performing activities in parallel to reduce the time of internal activities. However, standard measurement tools were proposed for purchase so that tools for different model changes could be grouped.

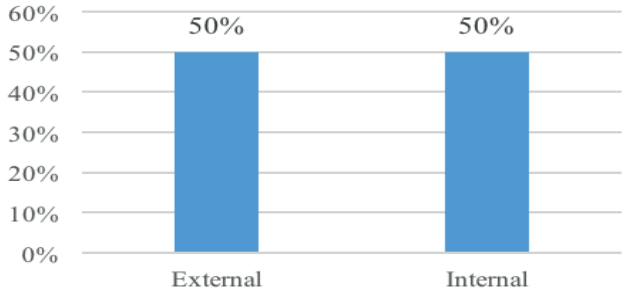

Fig. 8. Conversion of internal to external activities.

D. Verify the Solution

To test the solution, six weeks of data were taken from the time of model change and on-time deliveries after the implementation of the SMED tool; a control chart was made before vs. after.

There is an increase in the OTD after implementing the Lean-Sigma methodology, with an approximately 8 % increase in the on-time delivery rate and an average of 96.15 % after the implemented improvements.

The model changeover times were compared before and after the implementation of the methodology; approximately 60 % of the model changeover time was reduced in the four weeks following the implementation of SMED.

A Two-Sample test was carried out to probe the hypothesis that the change over time is minor under the initial conditions. As shown in Figure 9, using a p-value of 0, the changeover time was reduced after improvements were applied.

Two-Sample T-Test and CI: Before, After

Two-sample T for Before vs. After

	N	Mean	StDev	SE Mean
Before	99	66.8	28.2	2.8
After	30	28.83	9.47	1.7

Difference = μ (Before) - μ (After)
Estimate for difference: 37.98
95% lower bound for difference: 32.49
T-Test of difference = 0 (vs >): T-Value = 11.45 P-Value = 0.000 DF = 125

Fig. 9. Two-sample-t for changeover time before vs. after.

E. Control Plan

As the last step of the methodology, a work instruction was developed to standardize the process of model changes for the bending machines and update the inventories of the maximum and minimum tool cribs. By contrast, a Kaizen event was held to train those involved in the new work method.

V. CONCLUSIONS

The initial information of the process shows an average on-time delivery rate of 89 %, which is outside the company's minimum goal of 96 %, equivalent to a performance of 0.1 sigma. After applying the Lean Sigma methodology, we can statistically demonstrate an increase in the on-time delivery rate of 8 %; that is, on average, after the proposed improvements, it is 96.5 % above the company's minimum goal, representing a performance of 2.5 sigmas. Concerning the model changes, a reduction of approximately 60 % was achieved using the SMED approach.

Implementing the lean sigma methodology is carried out in four weeks, fulfilling the requirements of rapid improvement. In summary, using the lean–sigma methodology oriented toward problem-solving instead of focusing on developing improvement projects can achieve the objectives and solve the problem at a low speed.

It can be concluded that using the approach proposed in this study differs from the current approaches in the time it takes to solve a problem; while using Six Sigma can take up to 12 months, using the proposed approach took only 4 to 5 weeks to solve the problem. This helps the company to have more flexibility.

Nowadays, companies cannot afford to continue having losses for not delivering parts on time or for having high scrap rates. This implies that organizations must change the way they are acting to improve processes, they must focus on actually solving the problem quickly. Using current approaches means that the company will continue to lose, become less efficient, less flexible, negatively impacting quality, cost and delivery, variables that are key to be a competitive company in this globalized world we live in today,

IV. LIMITATIONS AND FUTURE RESEARCH

It should be noted that this application is carried out in a metal manufacturing process, and it is possible to use it in any sector. Some of the limitations during implementation are that it requires high commitment from management and the formation of a multidisciplinary team that invests a significant amount of time and effort to solve the problem in a short period. Developing this approach for automotive and medical processes is recommended for future research to demonstrate that the results obtained can be the same or better for other types of processes. It is essential to mention that the projects should be led by a Black Belt knowledgeable in lean manufacturing and Six Sigma tools.

REFERENCES

[1] S. Deeb, H. B. El Haouzi, A. Aubry and M. Dassisti, "A generic framework to support the implementation of six sigma approach in SMEs," Elsevier B.V., Jan. 2018, pp. 921–926. https://doi.org/10.1016/j.ifacol.2018.08.490

[2] P. Guleria, A. Pathania, S. Sharma and J. C. Sá, "Lean six-sigma implementation in an automobile axle manufacturing industry: A case study," *Mater Today Proc*, vol. 50, pp. 1739–1746, Jan. 2022, https://doi.org/10.1016/J.MATPR.2021.09.177

[3] H. Gholami, N. Jamil, M. Z. Mat Saman, D. Streimikiene, S. Sharif and N. Zakuan, "The application of Green Lean Six Sigma," *Bus Strategy Environ*, vol. 30, no. 4, pp. 1913–1931, May 2021, https://doi.org/10.1002/bse.2724

[4] R. S. Barot, J. Patel, B. Sharma, B. Rathod, H. Solanki and Y. Patel, "Lean six sigma feasibility and implementation aspect in cast iron foundry," *Materials Today: Proceedings*, Elsevier Ltd, 2019, pp. 1084–1091. https://doi.org/10.1016/j.matpr.2020.01.087

[5] R. Rathi, M. Singh, A. K. Verma, R. S. Gurjar, A. Singh and B. Samantha, "Identification of Lean Six Sigma barriers in automobile part manufacturing industry," in *Materials Today: Proceedings*, Elsevier Ltd, 2021, pp. 728–735. https://doi.org/10.1016/j.matpr.2021.05.221

[6] J. Singh, H. Singh and S. Kumar Gandhi, "4 7 Assessment of Implementation of Six Sigma DMAIC Approach in a Casting Unit: A Case Study Assessment of Implementation of Six Sigma DMAIC Approach in a Casting Unit: A Case Study," 2018.

[7] A. Aytekin *et al.*, "Critical success factors of lean six sigma to select the most ideal critical business process using q-ROF CRITIC-ARAS technique: Case study of food business," *Expert Syst Appl*, vol. 224, Aug. 2023, https://doi.org/10.1016/j.eswa.2023.120057

[8] J. P. Costa, I. S. Lopes, and J. P. Brito, "Six Sigma application for quality improvement of the pin insertion process," in *Procedia Manufacturing*, Elsevier B.V., 2019, pp. 1592–1599. https://doi.org/10.1016/j.promfg.2020.01.126

[9] M. S. Carrillo Landazabal, J. T. Peralta Ordosgoitia, C. A. Severiche Sierra, V. P. Ortega Vélez, and L. E. Vargas Ortiz, "Reducción de ruido industrial en un proceso productivo metalmecánico: Aplicación de la metodología DMAIC de Lean Seis Sigma," *Entre ciencia e ingeniería*, vol. 15, no. 30, pp. 41–48, Dec. 2021, https://doi.org/10.31908/19098367.1819.

[10] A. Adeodu, M. G. Kanakana-Katumba and M. Rendani, "Implementation of lean six sigma for production process optimization in a paper production company," *Journal of Industrial Engineering and Management*, vol. 14, no. 3, pp. 661–680, 2021, https://doi.org/10.3926/jiem.3479

[11] A. Mittal, P. Gupta, V. Kumar, A. Al Owad, S. Mahalwat, and S. Singh, "The performance improvement analysis using Six Sigma DMAIC methodology: A case study on Indian manufacturing company," *Heliyon*, p. e14625, Mar. 2023, https://doi.org/10.1016/j.heliyon.2023.e14625

[12] D. Zhang, S. Chen and Y. Xu, "Study on the Improvement of Single Minute Exchange of Die Based on Lean Production," 2022, https://doi.org/10.1117/12.2645572

[13] M. Tekin, M. Arslandere, M. Etlioğlu, Ö. Koyuncuoğlu and E. Tekin, "An application of SMED and Jidoka in lean production," in *Proceedings of the International Symposium for Production Research 2018 18*, Springer, 2019, pp. 530–545. https://doi.org/10.1007/978-3-319-92267-6_45

[14] P. Ondra, "The Impact of Single Minute Exchange of Die and Total Productive Maintenance on Overall Equipment Effectiveness," *Journal of Competitiveness*, 2022, https://doi.org/10.7441/joc.2022.03.07.

[15] D. Agung and H. Hasbullah, "Reducing the product changeover time using SMED and 5s methods in the injection molding industry," *Sinergi*, 2019, https://doi.org/10.22441/sinergi.2019.3.004

[16] "Index." Accessed: Jan. 29, 2024. [Online]. Available: https://index.org.mx/

[17] S. D. Kulkarni *et al.*, "Enhancing the process capability of machining process of boring tool holder by application of six sigma methodology," *Mater Today Proc*, vol. 52, pp. 329–338, 2022, https://doi.org/10.1007/978-3-319-92267-6_45

[18] S. Nallusamy and V. Saravanan, "Lean tools execution in a small scale manufacturing industry for productivity improvement-A case study," *Indian J Sci Technol*, vol. 9, no. 35, pp. 1–7, 2016. https://doi.org/10.17485/ijst/2016/v9i35/100162

[19] F. Estrada-Orantes and N. Alba-Baena, "Creating the lean-sigma synergy," in *Lean manufacturing in the developing world: methodology, case studies and trends from Latin America*, 2014, pp. 117–134. https://doi.org/https://doi.org/10.1007/978-3-319-04951-9_6.

[20] O. C. Gracia, F. J. E. Orantes and F. H. Pérez, "Aplicación de la metodología Lean-Sigma en la solución de problemas en procesos de manufactura: Caso de Estudio," *Cultura Científica y Tecnológica*, no. 57, 2016.

Intensity-Duration-Frequency Curves for Manicaragua city, Cuba

Roberto Luis López Ferras[1], Carlos Lázaro Castillo García[2], Ismabel Domínguez Hurtado[3], José Alejandro Solis[4] y Lisdelys González Rodríguez[5]

***Abstract* — The Intensity-Duration-Frequency (IDF) curves are a way to visualize and represent extreme hydrometeorological rainfall events. In this article, an analysis of convective rainfall events recorded at the La Piedra Meteorological Station, Villa Clara, Cuba, was conducted. To develop IDF curves, the 2006-2019 time series was analyzed. A partial duration series was generated, including intervals from 20 minutes to 4320 minutes, subjected to an outlier detection process. The series was divided into two categories: one for durations ≤ 720 minutes and another for durations > 720 minutes. The resulting series underwent non-parametric tests to assess their independence, randomness, homogeneity, and seasonality. Subsequently, they were fitted to the Generalized Pareto probability distribution and to a parametric equation of the Montana model, and then the curves were plotted for return periods of 10, 50 and 100. The Montana model led to obtaining correlation coefficients greater than 0.90 compared to the other methods used, significantly improving the quality of the fit in both categories. This research provides information to understand and plan the management of intense climatic phenomena and adequate risk management in an area where such studies are lacking, facilitating access to crucial data essential in the design and execution of hydraulic engineering projects in the region.**

***Keywords* – partial duration series, rainfall intensity, threshold, curves, precipitation.**

***Resumen* — Las curvas de Intensidad-Duración-Frecuencia (IDF) son una manera de visualizar y representar los eventos hidrometeorológicos extremos de lluvia. En este artículo se llevó a cabo un análisis de eventos de lluvias convectivas registrados en la Estación Meteorológica La Piedra, Villa Clara, Cuba. Para desarrollar curvas IDF se analizó la serie temporal 2006-2019. Se generó una serie de duración parcial que incluyó intervalos de 20 minutos hasta 4320 minutos, sometiéndola a un proceso de detección de datos anómalos. La serie se dividió en dos categorías: una para duraciones ≤ 720 minutos y otra para duraciones > 720 minutos. Las series resultantes se sometieron a pruebas no paramétricas para evaluar su independencia, aleatoriedad, homogeneidad y estacionalidad. Posteriormente, se procedió a ajustarlas a la distribución probabilística Generalizada de Pareto y a una ecuación paramétrica del modelo de Montana. Luego se grafica la representación de las curvas para períodos de retorno de 10, 50 y 100 años. El modelo de Montana condujo a la obtención de coeficientes de correlación superiores a 0.90 y a los demás métodos utilizados, mejorando significativamente la calidad del ajuste en ambas categorías. Esta investigación aporta información para comprender y planificar la gestión de fenómenos climáticos intensos, así como para una adecuada gestión de riesgos en una zona donde no se cuenta con este tipo de estudios. Asimismo, facilita el acceso a datos cruciales que resultan fundamentales en el diseño y ejecución de proyectos de ingeniería hidráulica en la zona.**

***Palabras claves* – series de duración parcial, intensidad de la lluvia, umbral, curvas, precipitación.**

I. INTRODUCTION

IN water resources management and engineering projects, Intensity-Duration-Frequency (IDF) curves are often needed. According to [1], the IDF curve establishes how the maximum annual average intensity varies in relation to the duration of a specific event. IDF curves are a widely used tool in hydrological design of maximum flows, when rainfall-runoff models such as unit hydrographs or the rational method are used [2]. Using this data, a large number of hydrological projects, such as flood discharge designs, bridge construction, and drainage network construction, are defined in relation to the maximum precipitation that could be expected for a given return period [2]. The parameters storm duration and intensity of the IDF curve are of great importance in the field of hydrology, as they are the basic elements when it comes to hydrological risk analysis [3]. According to [4], constructing the IDF relationship of rainfall is one of the main applications of Extreme Value Theory (EVT). IDF relationships are developed based on historical data from time series of rainfall by fitting a theoretical probability distribution to series of annual maximum values [5] (that is, maximum values per blocks with a block size of one year) or partial duration series (PDS), also known as peak over threshold series.

In the PDS approach, rainfall events with intensity exceeding the defined high threshold value are considered as the extreme rainfall series and are typically modeled using the Generalized Pareto Distribution (GPD) [6]. However, [7] in Israel analyzed IDF

1 A. Roberto Luis López Ferras is with the Central University Marta Abreu de Las Villas. Email: rlferraz@uclv.cu, ORCID: https://orcid.org/0009-0001-4756-6496

2. B. Carlos Lázaro Castillo García is with the Central University Marta Abreu de Las Villas. Email: ccgarcia@uclv.cu, ORCID: https://www.orcid.org/0000-0002-6430-2775

3. C. Ismabel Domínguez Hurtado is with the Provincial Meteorological Center Villa Clara, Santa Clara, Cuba. Email: ismabel.dominguez@vcl.insmet.cu, ORCID: https://www.orcid.org/0000-0002-7841-8031

4. D. José Alejandro Solis is with the Central University Marta Abreu de Las Villas. Email: jsolis@uclv.cu, ORCID: https://orcid.org/0009-0003-4777-605X

5. E. Lisdelys González Rodríguez is with the Faculty of Engineering and Business, University of the Americas, Concepción Campus, Concepción 4030000, Chile. Email: lgonzalezr@udla.cl ORCID: https://orcid.org/0000-0002-7892-4604

Manuscript Received: 25/03/2024
Revised: 15/05/2024
Accepted: 30/05/2024
DOI: https://doi.org/10.29019/enfoqueute.1046

curves based on partial duration series and used both the Generalized Pareto Distribution (GPD) and the Generalized Extreme Value (GEV) distribution, in addition to Gumbel and Log normal distributions, finding that there are not many differences in the results. On the other hand, the extreme rainfall series obtained by extracting the maximum value in each calendar year is generally modeled using the Generalized Extreme Value (GEV) distribution, as seen in works by authors such as [8], [9], [10], and [11].

The annual maximum series (AMS) model shows a significant limitation as it does not consider secondary events within a year that may exceed the annual maxima of other years. The PDS overcomes the limitations of AMS by extracting all maximum values that exceed a particular discharge level, called a threshold [12]. When the threshold is appropriately selected, it can lead to reasonable variability in quantile estimates [13]. [14] demonstrated in their research that for records of less than 15 years, the PDS method is superior to the AMS method. On the other hand, [15] states that PDS is used when the data set is small (< 12 years) or when using return periods less than 5 years. [16] confirm this information when stating that for modeling return periods less than 10 years (2 and 5 years), PDS tends to produce higher values. This is supported by [17] in a comparison between PDS and AMS methodologies, demonstrating that for obtaining design storms, PDS is more effective than those imposed by the AMS Methodology since the rainfall exceeds by 4 to 10 %, and therefore is more conservative, and higher results are obtained for return periods between 2 and 5 years.

Despite the advantages shown by the PDS method, the difficulty in determining the appropriate threshold for PDS is a significant obstacle to its widespread use. As expressed by [18], there is no general recommendation for choosing a suitable threshold.

In their work, [19] present an equation that shows the relationship between the return period for AMS and PDS, as shown in the following expression (Eq. 1).

$$T_P = -\frac{1}{\ln\left(1-\frac{1}{T_A}\right)} \quad (1)$$

Where TP is the return period of the PDS analysis and TA is the return period obtained from AMS. Even for return periods greater than 10 years, this expression can be reduced to TA=TP+1/2, which makes both results, for both PDS and AMS, relatively equal.

On the other hand, another aspect to consider is the variability in data series trends. [20] state that most efforts to develop future IDF curves are limited to individual cities or regions that assume stationarity in precipitation, works by [21] and [22] apply this methodology. Ganguli himself observes that for longer return periods (i.e., 25 years), detectable changes occur in the design storm considering a non-stationary model than the stationary ones. Studies conducted in Malaysia by [23] demonstrate that for non-stationary models with generalized extreme value functions, there are no clear advantages over similar stationary models.

The selection of the threshold in PDS is the main question that arises, there are several methods for this, but one has not yet been established that applies as a defined law for all cases. [24] estimated a value of peaks per year (λ) ranging from 3 to 15 for homogeneous regions in Italy. Rosbjerg and Madsen (2004) cited in [25] conducted a frequency analysis based on rainfall data using a Bayesian framework in Denmark and suggested a value of λ between 2 and 3. Deidda (2010) cited by [26] developed a multiple threshold method, which is based on parameter estimates within a range of thresholds $u>u*$ and provides a robust fit of the GPD regardless of data resolution or rounding. Regarding the choice of the optimal threshold $u*$, it should be noted that it should be selected large enough to reliably consider that the distribution of exceedances approaches a GPD, but low enough to keep the estimation variance small. [27] conducted a comparison between PDS and AMS methods, where for obtaining the threshold they choose the minimum value of each duration from the AMS dataset to extract the PDS data. According to [28], since the selection of the threshold is an iterative process, one could easily choose any higher or even lower threshold value, but the lower threshold offers some advantages in terms of sample size. In their study, the author himself states that the results of statistical tests were considerably better if more data points are added. [29] predetermined the threshold values during the selection of rainfall data.

Human errors, such as data entry mistakes, can lead to the presence of outliers or atypical values in the data. Despite the ambiguity in providing a clear definition, an outlier is generally considered to be a data point that significantly differs from other data points or does not fit the expected normal pattern of the phenomenon it represents [30]. According to [31], they are data points that are extremely distant from the majority of other data points.

There are three types of outliers that a researcher may encounter [1]:

- Vertical outliers: These are extreme observations in the dependent variable.
- Good leverage points: These are extremes in both dependent and independent variables but fall on or near the regression line.
- Bad leverage points: These are outliers in the independent variables.

There is no solid theoretical basis to justify the choice of a specific probability distribution function, nor a theoretical procedure to define a probabilistic model as the best one in a frequency analysis contrasted with different probabilistic models [32]. The author himself established a definitive conclusion, stating that the competence of a probabilistic model in fitting hydrological data is directly related to the flexibility and form of the probability distribution function. Moreover, the more parameters a model contains, the more versatile its probability distribution function will be, adapting to the data.

The formulation proposed by Sherman in (1931), cited by [33], has universalized the mathematical and graphical representation for calculating intensity (i)-duration (d)-frequency (T) curves worldwide.

In Cuba, [34] conducted a study and proposed a methodology for creating IDF curves in our country. Subsequent research has been conducted, such as that by [35] and [36], both focusing on AMS. In this case, a different methodology is intended to be employed, as there is a small dataset of pluviographic records, specifically 13 years of records. The literature consulted

previously affirms that for return periods of less than 15 years, the PDS methodology is superior to AMS. With this, the aim is to establish a new methodology to apply in Cuba for meteorological stations with few years of records.

II. MATERIALS AND METHODS

A. Study Area

The "La Piedra" Meteorological Station (Code 78308) is located in Manicaragua, a municipality belonging to the province of Villa Clara, Cuba (Figure 1). This municipality is situated at latitude 22°9'0.8'' N and longitude 79°58'43.2'' W, nestled in the Escambray Mountains in the southern part of Villa Clara, bordering the provinces of Cienfuegos to the west and Sancti Spíritus to the east. It covers an area of 1066.0 km^2, making it the largest municipality in terms of surface area in the province, encompassing the southern portion, resembling a triangle with one of its vertices pointing south, at the intersection point of the provincial boundaries of Villa Clara, Cienfuegos, and Sancti Spíritus. Due to its geographical location, it experiences the influence of a warm humid tropical climate. Precipitation is regulated by the regime of the Northeast Trade Winds, which interact perpendicularly with the moist air masses from higher altitude regions, leading to intense processes with a marked increase in precipitation.

Fig. 1. a) Geographical location of the central region of Cuba, **b)** Area where the La Piedra Meteorological Station is located.

An analysis of the pluviographic data recorded during the period 2006-2019 (13 years) was conducted. A study of the maximum precipitation values at the La Piedra Meteorological Station was performed. The results are presented in the form of partial series, considering different time ranges: 20, 40, 60, 90, 120, 150, 240, 300, 720, 1440, 2880, and 4320 minutes.

It is important to mention that there are some limitations due to the lack of records for the year 2018, as the data recording sheets were lost. Additionally, records are occasionally interrupted for short periods due to breakdowns, maintenance, and instrument malfunctions. Another major limitation is the scarcity of recorded years, resulting from the few years the meteorological station has been in operation.

B. Flow Chart

The methodological scheme shown in Figure 2 can be applied to the development of IFD curves in stations that have analog and/or digital data records. It is divided into five stages and 14 phases.

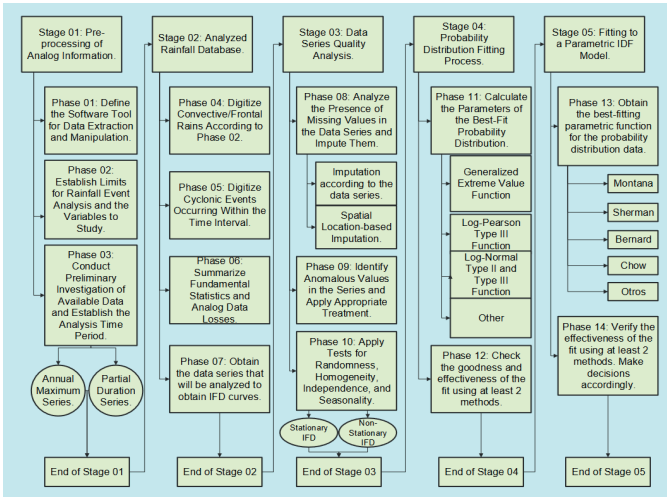

Fig. 2. Methodological scheme used in this study.

Stage 01. The partial duration series of precipitation were collected from the rainfall data recorded at the La Piedra Meteorological Station. Prior to this, the necessary conditions for the analysis of rainy events were established. To process the analog/digital information volumes, Excel, SPSS, and R software were employed.

Stage 02. The database of the selected rainfall parameters to be analyzed was designed with the aim of summarizing the essential components of the IFD analysis in each event, as well as other variables that may be of interest in other research. Since rainfall could be described in various ways as a completely random phenomenon, data were extracted from precipitation hyetographs or mass curves that reflect the statistical behavior of the rainfall shape, as reflected by [36]. It was necessary to select a threshold, for which a value was chosen in such a way as to satisfy the condition of independence of the series. A higher threshold value allows us to ensure greater probability of independence, but reduces the number of events in the series, which means a loss of valuable information. On the other hand, a lower threshold value provides a greater number of events in the series, thus allowing for a more reliable parameter estimation, but at the same time increases the possibility of independence. Therefore, a threshold was used that satisfies the condition of independence, while also allowing us to have the largest amount of data possible from the series. The procedure was carried out in such a way that a λ value between 2 and 3 was obtained. An attempt was made to obtain a number of peaks as close to 3 as possible in order to have a larger sample of data considering the limited number of years, as there are only thirteen years of records available.

Stage 03. Demonstrating the quality of the data obtained in the analysis of rainfall events was crucial to ensure the reliability of the predictions. In this regard, the treatment of anomalous data played a fundamental role in avoiding biases in the predictions. The application of sensitivity analysis methods in the analysis of outliers became an essential tool to reduce the uncertainty associated with an IFD curve study. For the analysis of anomalous hydrological data, the US-WRC (United States-Water Resources Council) method was employed. This method

is recommended by [37] and [38], where it is cautioned that to apply it, it is necessary to assume that the logarithms or another function of the hydrological series are normally distributed, as the test is only applicable to samples obtained from a normal population. Therefore, to implement the test, equations 2 and 3 are calculated:

$$X_H = \exp(\bar{x} + K_N s) \quad (2)$$

$$\boldsymbol{X_L = \exp(\bar{x} - K_N s)} \quad (3)$$

Where, $\bar{x}$ y s represent the mean and standard of the natural logarithms of the sample, respectively. The K_N statistic refers to the Grubbs and Beck table, which is tabulated for different sample sizes and levels of significance, and N denotes the sample size, while X_H is the upper limit of the test and X_L is the lower limit [37].

If 5≤N≤150, KN can be calculated using equation 4 (Stedinger and others, 1993 cited in [37]):

$$K_N = -0.9043 + 3.345\sqrt{\log(N)} - 0.4046\log(N) \quad (4)$$

For the frequency analysis results to be valid, the dataset must meet the statistical criteria of randomness, independence, homogeneity, and stationarity [37]. Table 1 shows the test performed for each statistical criterion.

TABLE I
NON-PARAMETRIC TESTS FOR THE ANALYSIS OF DATA QUALITY OF LA PIEDRA METEOROLOGICAL STATION

Statistical Criteria	Recommended Test	Confidence Interval (%)
Randomness	Run Test	95
Homogeneity	Mann-Withney test	
Independence	Wald-Wolfowitz test	
Seasonality	Mann- Kendall, Sen´s Slope test	

The analysis of extreme hydrological data frequencies, such as floods, droughts, winds, and maximum daily precipitation, is based on accepting that the maximum annual data in the available sample are independent and come from a stationary random process [7]. The author himself expresses that due to some factors such as changes in land use and impacts of global warming, hydrological data series exhibit trends, which would indicate that they are not stationary. Therefore, it is necessary to check the existence of seasonality in the data series.

The Mann-Kendall test was developed to identify trends and analyze seasonality in data sets. This test, considered non-parametric, was designed to evaluate the presence of non-linear trends and change points in time series. It is commonly used in detecting trends and spatial variations in data related to climate, hydrology, and agrometeorology, as highlighted by [39].

The null hypothesis of trend, denoted as H0, holds that a sample of data arranged in chronological order is independent of each other and follows the same distribution at all time points. [40] defines the statistic S as presented in equations 5 and 6:

$$S = \sum_{i=1}^{n-1}\sum_{j=i+1}^{n} \operatorname{sgn}(x_j - x_i) \quad (5)$$

Where:

$$\operatorname{sgn}(x) = \begin{cases} 1 \text{ si } x > 0 \\ 0 \text{ si } x = 0 \\ -1 \text{ si } x < 0 \end{cases} \quad (6)$$

When the sample size (n) is equal to or greater than 40, the statistic S follows an approximately normal distribution. In this case, the mean of that distribution is zero and the variance can be calculated using equation 7:

$$\operatorname{Var}\{S\} = \frac{1}{18[n(n-1)(2n+5) - \sum_t t(t-1)(2t+5)]} \quad (7)$$

Where t is the size of a given tied group and ∑ is the sum of the set of all tied groups in the data sample. The normalized test statistic K is calculated using the equation 8:

$$\boldsymbol{K = \frac{S-1}{\sqrt{Var(S)}}; 0; \frac{S+1}{\sqrt{Var(S)}} \text{ para: } S > 0,\ S = 0, S < 0,} \quad (8)$$

The statistic K follows a standard normal distribution, which means it has a specific distribution shape with a mean of 0 and a variance of 1. To find the probability (P) associated with the statistic K in your sample data, you can use the cumulative distribution function of the normal distribution, in the form of equation 9:

$$P = \frac{1}{\sqrt{2\pi}} \int_{-\infty}^{z} e^{\frac{t^2}{2}} dt \quad (9)$$

When analyzing sets of independent data without showing any trend, the value of P should hover around 0.5. In situations where the data exhibit a clear trend towards increasing values, the value of P tends to approach 1. On the other hand, if the trend is marked in a downward direction, the value of P approaches 0. If the sample data are serially correlated, it will be necessary to whiten the data beforehand and apply a correction to calculate the variance [37].

When we are seeking linear trend in a dataset, we commonly use the least squares estimation technique via linear regression to calculate the slope. However, this approach is reliable only if there is no systematic correlation between consecutive observations (serial correlation). Additionally, it is important to note that this method can be heavily influenced by outliers in the data, meaning that an unusual data point can have a significant impact on the slope estimation. Sen (1968) developed a more robust method [36], [37].

The slope of the trend was calculated as equation 10:

$$\beta = mediana\left(\frac{x_i - x_j}{i - j}\right);\ \forall j < i \quad (10)$$

The trend slope β was estimated using the formula where Q is the resulting value and xi and xj represent the data values at

times i and j. If β is positive, it indicates an upward trend, while if it is negative, it signals a downward trend.

The Sen's slope estimator is simply the median of the N' values of β. This approach is applied in the same way, whether we have one or multiple observations per time period.

Sen (1968) proposed a non-parametric method to calculate a confidence interval for the slope. However, in practice, a simpler method based on the normal approximation is more commonly used. To calculate this, we require the standard deviation of the Mann-Kendall statistic, S [37]. In simpler terms, we need to know how much the Mann-Kendall statistic S varies in order to perform calculations related to its distribution and statistical significance.

Stage 04. Identifying the probability function best fitting the data for the evaluated conditions and the proposed significance level was essential. Fit was assessed using analytical and probabilistic methods to ensure the correct choice of the distribution function and the results of its parameters.

In the field of hydrology, probability distributions are essential tools used to analyze precipitation amounts and patterns in time series. To describe rainfall events, three distributions were employed: (1) Generalized Extreme Value (GEV), (2) Generalized Pareto [29], (3) Johnson SB. Equations 11, 12, and 13 show the probability density function of GEV, the Generalized Pareto distribution, and the probability density function (Johnson, 1949), [34], respectively:

$$F(x;\ \mu,\sigma,\xi) = \exp\left[-\left(1+\xi^{*}\left(\frac{x-\mu}{\sigma}\right)^{\frac{1}{\xi}}\right)\right] \tag{11}$$

Where μ is the location parameter, σ is the scale parameter, and ξ is the shape parameter. When ξ=0, the GEV reduces to the type I extreme value distribution (Gumbel). When ξ>0, the tail of the distribution is heavier, and when ξ<0, the tail is lighter.

$$\mathrm{FX(x)} = 1 - [1 - \kappa(x-\xi)/\alpha]^{1/\kappa} \tag{12}$$

Where κ is a shape parameter, ξ is the location parameter, and α is the scale parameter.

$$f(x) = \frac{\delta}{\sqrt{2\pi}}\frac{\lambda}{(x-\varepsilon)(\varepsilon+\lambda-x)}\ e^{\frac{1}{2}\left[\gamma+\delta\ln\left(\frac{x-\varepsilon}{\varepsilon+\gamma-x}\right)\right]^{2}} \tag{13}$$

ε, λ: Location and scale parameters.

γ, δ: Shape parameters representing skewness and kurtosis, respectively.

Parameter estimation A very tempting method from a statistical point of view is the maximum likelihood method. It consists of selecting the parameters that give a fitting distribution the greatest statistical coherence possible with the observed sample.

The method of maximum likelihood is the most commonly used method to find the parameter values that make the observed data most probable under the proposed model, as affirmed by Millar (2011) and Pawitan (2001), both cited by [24]. The author himself expresses that the method provides biased estimates, hence researchers strive to develop nearly unbiased estimators for the parameters of various distributions.

Goodness of fit [30] stated that many of the problems observed in numerous research studies stem from the incorrect use of test statistics, which occurs when they are applied inappropriately. This can be due to various factors:

- Lack of knowledge of both descriptive and inferential statistics.
- Limited understanding of research methodology.
- Shortage of research-oriented faculty members.

Inadequate familiarity with statistical software.

These four aspects directly influence the conduct of research. If any of them is not understood or applied properly, the research would exhibit significant deficiencies. [37] explains that in hydrology, there are various rigorous and effective statistical tests to evaluate whether it is plausible to conclude that a specific set of observations comes from a particular distribution. These tests are called Goodness of Fit Tests. The Kolmogorov-Smirnov test allows for obtaining bounds for each of the observations on a probability plot when the sample has been effectively drawn from the assumed distribution.

This procedure is a non-parametric test that allows testing whether two samples come from the same probabilistic model. Suppose we have two samples of total size N=m+n composed of observations x1, x2, x3, …, xn e y1, y2, y3,…, ym. The test assumes that the variables x e y are mutually independent and that each x comes from the same continuous population P1 and each y comes from another continuous population P2. The null hypothesis is that both distributions are identical, meaning they are two samples from the same population [36].

The Kolmogorov-Smirnov test was used due to its ability to reasonably assume that observations could follow the specific distribution in question. It is straightforward to calculate and apply, and it does not require data grouping, unlike the Chi-square test. Additionally, it has the advantage of being applicable to samples of any size, unlike the Chi-square test, which requires a minimum sample size.

Stage 05. The results of the probability function were parameterized into mathematical models of the form *f(I)=[D]* for different T, or *f(I)=[D; T]*, in order to verify the effectiveness of the fits. If necessary, a point of inflection in the data series was identified, contributing to obtaining more precise results with less margin of error. Models for Intensity-Frequency-Duration curves: In this study, we focused on fitting the models proposed by Montana, Sherman, Bernard, and Chow according to [33], [36], equations 14-17.

$$\mathrm{i_d^T} = \frac{\mathrm{kT^m}}{\mathrm{d^{\theta}+C}} \tag{14}$$

$$\mathrm{i_d^T} = \frac{\mathrm{kT^m}}{\mathrm{(d+C)^n}} \tag{15}$$

Where: i_d^T It represents the maximum precipitation intensity, measured in mm/min or mm/h. T is the return period in years, d is the duration of precipitation in minutes, and k, m, θ and n are the parameters that must be estimated to fit the curve.

III. RESULTS AND DISCUSSION

The Table II shows the selection of thresholds is shown below, indicating the threshold and the number of resulting peaks in each of the time series.

TABLE II
RESULTS OF THRESHOLD SELECTION
AND NUMBER OF PEAKS FOR EACH SERIES

Series min	Threshold mm/min	N° of peaks per year
20	1	2.92
40	0.75	2.77
60	0.55	2.69
90	0.43	2.85
120	0.33	3.0
150	0.28	2.92
240	0.185	3.0
300	0.15	3.0
720	0.069	3.0
1440	0.038	2.92
2880	0.025	3.0
4320	0.0185	3.0

The data processing was done with the assistance of the R software. The US-WRC method was applied, which extracts the outlier data from each series. Table III displays these outlier data.

TABLE III
ANOMALOUS DATA EXTRACTED FROM EACH OF THE SERIES

Series (min)	Anomalous Data (mm/min)	Date
20	3.5	23/07/2019
40	2.46	23/07/2019
60	1.5	07/04/2019
	1.83	23/07/2019
90	1.02	30/06/2006
	2.01	24/05/2012
	1.27	07/04/2019
	1.31	23/07/2019
120	0.76	30/06/2006
	0.67	09/09/2008
	1.5	24/05/2012
	1.17	07/04/2019
	0.99	23/07/2019
150	0.61	30/06/2006
	0.58	09/09/2008
	1.2	24/05/2012
	1.1	07/04/2019
	0.79	23/07/2019
240	0.51	09/09/2008
	0.75	24/05/2012
	0.72	07/04/2019
	0.49	23/07/2019
300	0.49	09/09/2008
	0.6	24/05/2012
	0.57	07/04/2019
	0.39	23/07/2019
720	0.386	09/09/2008
	0.258	24/05/2012
	0.423	09/09/2017
	0.238	07/04/2019
1440	0.193	09/09/2008
	0.129	24/05/2012
	0.212	09/09/2017
	0.158	28/05/2018
2880	0.145	09/09/2008
	0.149	09/09/2017
	0.143	28/05/2018
4320	0.1068	09/09/2008
	0.0678	24/05/2012
	0.1176	09/09/2017
	0.1255	28/05/2018

The data shown in Table III were removed from the series for exceeding 10 % above the upper limits of the US-WRC model for a 95 % confidence level.

The results of the quality tests conducted on the partial duration series as recommended by the [36] included Runs, Mann-Whitney (M-W), Wald-Wolfowitz (W-W), and Mann-Kendall (M-K) tests and are summarized in Table IV. The expression 'OK' means that the null hypothesis is accepted, and the word 'NO' means that the null hypothesis is not accepted, indicating that:

1. The series is random at a significance level of 5 % (Runs Test).
2. The series is independent at a significance level of 5 % (Wald-Wolfowitz Test).
3. The series is homogeneous at a significance level of 5 % (Mann-Whitney Test).
4. The series is seasonal at a significance level of 5 % (Mann-Kendall Test).

TABLE IV
RESULTS OF QUALITY TESTS FOR EACH DATA SERIES

Series (min)	Rachas	M-W	W-W	M-K
20	OK	OK	OK	NO
40	OK	OK	OK	NO
60	OK	OK	OK	NO
90	OK	OK	OK	NO
120	OK	OK	OK	NO
150	OK	OK	OK	NO
240	OK	OK	OK	NO
300	OK	OK	OK	NO
720	OK	OK	OK	NO
1440	OK	OK	OK	NO
2880	OK	OK	OK	NO
4320	OK	OK	OK	NO

According to the results obtained in the quality tests, it has been demonstrated that the data series collected for the La Piedra Meteorological Station are suitable for use in the development of Intensity-Duration-Frequency (IDF) curves. These results highlight the data's capability to be used in probabilistic analyses, suggesting the suitability of applying non-stationary models in the processing and interpretation of such information, in order to understand and predict climate patterns with greater accuracy and relevance.

Figure 3 shows the results of the analysis using the Generalized Pareto distribution, which has been adjusted using the nearest neighbor method. The results are presented for intervals of 1h, 2h, 4h, and 12h. The adjustment corresponding to the previously mentioned durations is illustrated using the cumulative probability function graph.

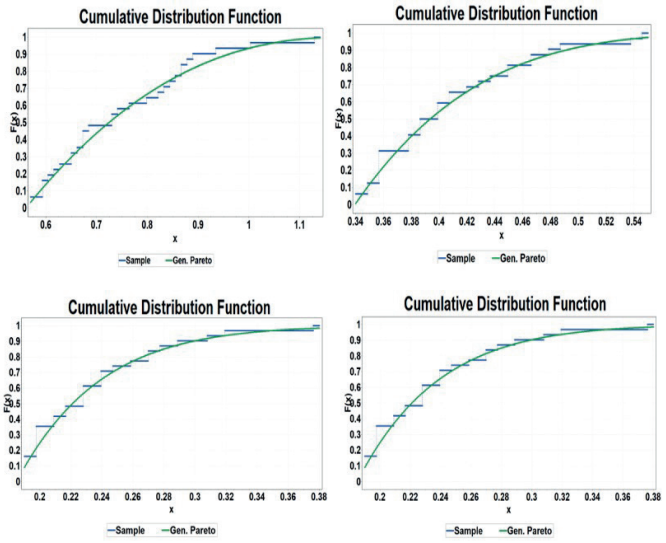

Fig. 3. Fit to the Generalized Pareto cumulative probability function for intervals of a) 1h, b) 2h, c) 4h, d) 12h.

In Table V, the results of the position and scale parameters derived from this analysis are detailed.

TABLE V
PARAMETERS OF THE GENERALIZED PARETO PROBABILITY DISTRIBUTION OBTAINED FOR THE 1H, 2H, 4H, 12H SERIES

Series	Location parameter μ	Scale parameter σ	Shape parameter k
1 hora	0.56029	0.27309	-0.42739
2 horas	0.33943	0.08459	-0.2314
4 horas	0.18496	0.05312	-0.06513
12 horas	0.06739	0.02166	-0.0024

The Kolmogorov-Smirnov goodness-of-fit test is conducted to assess the suitability of the (1) Generalized Pareto, (2) Generalized Extreme Value (ξ=0), (3) Johnson SB functions in obtaining the optimal probability function. With a significance level of 95 %, the test results indicate that the fit by the Generalized Pareto is statistically more effective.

The application of the Montana, Sherman, Bernard, and Chow models to fit the results of the Pareto probability function in a partial duration series did not yield favorable results. In this context, we rely on the Pearson correlation coefficient, detailed in Table VI, along with the values of k, m, θ, C, and n associated with each model.

TABLE VI
PARAMETERS OBTAINED AND PEARSON CORRELATION RESULTS FOR THE APPLIED MODELS

Model	k	m	θ	c	n	Pearson
Montana	77.823	0.111	1.055	36.949	-	0.6581
Sherman	75.725	0.111	-	29.262	1.045	0.6969
Bernard	9.894	0.111	-	-	0.669	0.6875
Chow	26.101	0.124	-	0.123	-	0.6652

As a result, the suggestion is to divide the series into two segments: the first covering up to 12 hours and the second beyond 12 hours. By implementing this modification in the models, Table VII presents new values for k, m, θ, C, and n, along with a new Pearson correlation coefficient.

TABLE VII
PARAMETERS OBTAINED AND PEARSON CORRELATION RESULTS FOR THE APPLIED MODELS WITH DURATIONS LESS THAN AND GREATER THAN 12 HOURS

Model	k	m	θ	c	n	Pearson
Montana (-12 h)	93.946	0.111	1.09	46.734	-	0.9250
Montana (+12h)	$3.1*10^{10}$	0.261	3.28	$7.4*10^{11}$	-	0.9863
Sherman (-12h)	108.149	0.111	-	34.12	1.111	0.9236
Sherman (+12h)	2.351	0.258	-	$-5*10^{-5}$	0.553	0.9519
Bernard (-12 h)	9.749	0.111	-	-	0.664	0.9108
Bernard (+12 h)	2.351	0.258	-	-	0.553	0.9519
Chow (-12h)	24.125	0.132	-	0.182	-	0.6480
Chow (+12h)	35.532	0.367	-	0.018	-	0.9354

According to the data presented in Table VII, it is concluded that the Montana model proves to be the most suitable for fitting the results of the Generalized Pareto probability distribution. This analysis supports the choice of the Montana model as the one that best fits the data of the series in question, and Equation 18 represents the conclusive formula used for the analysis at the corresponding station.

$$I = \begin{cases} \dfrac{93.946T^{0.111}}{(D^{1.093}+46.734)} & \text{for } D \leq 720 \text{ min} \\ \dfrac{30993903192.321T^{0.261}}{(D^{3.280}+737208928517.207)} & \text{por } D > 720 \text{ min} \end{cases} \quad (18)$$

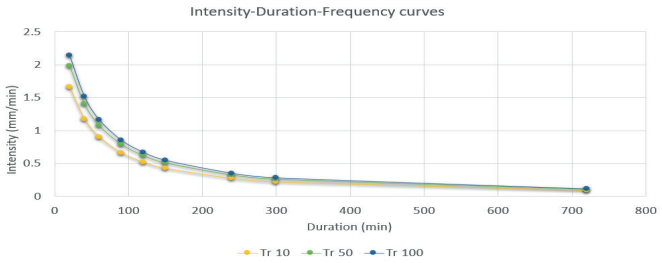

Fig. 4. Graph of Intensity-Duration-Frequency (IDF) curves for the La Piedra Meteorological Station.

Table VIII shows the numerical percentage difference between the values obtained using the Montana method and the values from NC 1239-2018. For this purpose, the results of the Montana method were compared with those of NC 1239-2018, calculating the difference between both sets of data.

TABLE VIII
COMPARISON BETWEEN THE RESULTS OBTAINED BY THE MONTANA METHOD AND NC 1239-2018

Series (min)	Return period		
	10 years	30 years	100 years
20	41.2 %	98 %	139 %
40	27.4 %	69 %	102 %
60	27 %	63 %	92 %
90	28 %	59 %	86 %
120	29 %	57 %	81 %
150	30 %	55.3 %	78.2 %
240	29 %	50.2 %	70 %
300	27 %	47 %	65.9 %
720	22 %	36 %	49.6 %

The difference was expressed as a percentage to clearly identify the maximum deviation between the compared values. It was determined that the greatest discrepancy, 139 %, was observed for a return period of 100 years and a rainfall duration of 20 minutes.

IV. CONCLUSIONS

After conducting the study and analysis of the data obtained throughout this research, the following conclusions are drawn:

- The collected data cover a period of 13 years of pluviographic records from the La Piedra Meteorological Station. During the processing of this data, series representing partial duration for intervals of 20, 40, 60, 90, 120, 150, 240, 300, 720, 1440, 2880, and 4320 minutes were generated.
- Pluviographic records for the year 2018 were not available due to total loss.
- 41 values considered outliers were identified using the US-WRC method. These values were excluded from our analysis due to the lack of information about their origin or source.
- The data series underwent analysis to verify their randomness, independence, homogeneity, and seasonality. As a result of this analysis, the hypotheses were corroborated, and it was concluded that a non-stationary IDF model would accurately represent the studied phenomenon.
- The Pareto distribution was applied to the data series, and it was verified, through the Kolmogorov-Smirnov method, that this distribution fits the data adequately. This fit was highlighted when compared to the Johnson SB and Generalized Extreme Value distributions, with the Pareto distribution yielding the most favorable results in comparison.
- The Montana model achieved parameterization with a more significant correlation when applied to data from the probability distribution. It is important to note that this was achieved by dividing the series into two categories: durations less than 720 minutes and durations greater than this figure. This division led to the formulation of a Montana model with two equations presenting different parameters.
- The results of this research present data developed through the Montana method, which, when compared with NC 1239-2018, showed a difference in values exceeding 100 %.

ACKNOWLEDGMENTS

The authors would like to express their sincere gratitude to the Provincial Meteorological Center of Villa Clara for their invaluable collaboration in the development of this research. The support provided has been exceptional and deserves special recognition.

REFERENCES

[1] R. Balbastre Soldevila, *Análisis comparativo de metodologías de cálculo de tormentas de diseño para su aplicación en hidrología urbana*. [Tesis de Maestría, Universitat Politècnica de València], 2018. Available: http://hdl.handle.net/10251/100090

[2] P. L. Martínez Rodas, Curvas de Intensidad-Duración-Frecuencia para la ciudad de Cuenca. [Magíster en Hirosanitaria, Universidad del Azuay], 2023. Available: http://dspace.uazuay.edu.ec/handle/datos/12941

[3] A. G. Yilmaz, H. Safaet, F. Huang and B. J. C. Perera, "Time-varying character of storm intensity frequency and duration curves," Australasian Journal of Water Resources, vol. 18, no. 1, 15-26, 2014, https://doi.org/10.7158/W12-017.2014.18.1

[4] V. Agilan, and N. V. Umamahesh, "What are the best covariates for developing non-stationary rainfall Intensity-Duration-Frequency relationship?," Advances in Water Resources, vol. 101, 11-22, 2017c. https://doi.org/https://doi.org/10.1016/j.advwatres.2016.12.016

[5] M. Noor, T. Ismail, E.-S. Chung, S. Shahid and J. H. Sung, "Uncertainty in Rainfall Intensity Duration Frequency Curves of Peninsular Malaysia under Changing Climate Scenarios," Water, vol. 10, no. 12, 2018, https://doi.org/https://doi.org/10.3390/w10121750

[6] V. Agilan and N. V. Umamahesh, "Non-Stationary Rainfall Intensity-Duration-Frequency Relationship: a Comparison between Annual Maximum and Partial Duration Series," Water Resources Management, vol. 3, no. 6, 1825-1841, 2017b, https://doi.org/10.1007/s11269-017-1614-9

[7] D. F. Campos-Aranda, "Ajuste con momentos L de las distribuciones GVE, LOG y PAG no estacionarias en su parámetro de ubicación, aplicado a datos hidrológicos extremos," Agrociencia, vol. 52, no. 2, 169-189, 2018. Available: https://www.scielo.org.mx/scielo.php?pid=S1405-31952018000200169&script=sci_arttext

[8] S. Emmanouil, A. Langousis, E. I. Nikolopoulos and E. N. Anagnostou, 2020. Quantitative assessment of annual maxima, peaks-over-threshold and multifractal parametric approaches in estimating intensity-duration-frequency curves from short rainfall records. Journal of Hydrology, vol. 589, 125151, https://doi.org/https://doi.org/10.1016/j.jhydrol.2020.125151

[9] P. Coelho Filho, J. Alexandre, D. C. de Rezende Melo and M. de Lourdes Martins Araújo, Estudo de chuvas intensas para a cidade de Goiânia/GO por meio da modelação de eventos máximos anuais pela aplicação das distribuições de Gumbel e Generalizada de Valores Extremos. Ambiência, vol. 13, no. 1, 2017. Available: https://core.ac.uk/download/pdf/230459134.pdf

[10] C. Montesinos, W. Lavado, N. Quijada, L. Gutierrez and O. Felipe, Desarrollo de curvas pluviométricas Intensidad-Duración-Frecuencia (IDF) en Perú. Servicio Nacional de Meteorología e Hidrología del Perú– SENAMHI, 2023. Available: https://repositorio.senamhi.gob.pe/handle/20.500.12542/2825

[11] J. L. Ng, S. K. Tiang, Y. F. Huang, N. I. F. M. Noh and R. A. Al-Mansob, "Analysis of annual maximum and partial duration rainfall series," IOP Conference Series: Earth and Environmental Science, vol. 646, no. 1, 012039, 2021, https://doi.org/10.1088/1755-1315/646/1/012039

[12] S. Swetapadma and C. S. P. Ojha, "Chapter 9 - A comparison between partial duration series and annual maximum series modeling for flood frequency analysis," in K. S. Kasiviswanathan, B. Soundharajan, S. Patidar, J. He and C. S. P. Ojha (eds.), Developments in Environmental Science, vol. 14, 173-192, Elsevier, 2023, https://doi.org/https://doi.org/10.1016/B978-0-443-18640-0.00007-9

[13] C. Leys, M. Delacre, Y. L. Mora, D. Lakens and C. Ley, "How to classify, detect, and manage univariate and multivariate outliers, with emphasis on pre-registration," International Review of Social Psychology, vol. 32, no.1, 2019, https://doi.org/http://doi.org/10.5334/irsp.289

[14] W. Martín Rosales, A. Pulido Bosch, Á. Vallejos and M. López Chicano, "Precipitaciones máximas en el Campo de Dalias y vertiente meridional de la Sierra de Gador (Almería)," Geogaceta, vol. 20, no. 6, 1251-1254, 1996. Available: https://dialnet.unirioja.es/servlet/articulo?codigo=8115318

[15] G. Zucarelli, N. Piccoli, M. Pittau and M. Gallo, "Curvas intensidad-duración-frecuencia en la Región Litoral de la República Argentina," Cuadernos del CURIHAM, vol. 15, no. 0, 69-76, 2009, https://doi.org/10.35305/curiham.v15i0.71

[16] A. G. Yilmaz, H. Safaet, F. Huang and B. J. C. Perera, "Time-varying character of storm intensity frequency and duration curves," Australasian Journal of Water Resources, vol. 18, no. 1, 15-26, 2014, https://doi.org/10.7158/W12-017.2014.18.1

[17] S. Vrban, Y. Wang, A. McBean Edward, A. Binns and B. Gharabaghi, Evaluation of stormwater infrastructure design storms developed using partial duration and annual maximum series models," Journal of Hydrologic Engineering, vol. 23, no. 12, 04018051, 2018, https://doi.org/10.1061/(ASCE)HE.1943-5584.0001712

[18] N. Guru and R. Jha, "A Framework for the Selection of Threshold in Partial Duration Series Modeling," In R. Jha, V. P. Singh, V. Singh, L. B. Roy and R. Thendiyath (eds.), Hydrological Modeling: Hydraulics, Water Resources and Coastal Engineering (pp. 69-84), 2022. Springer International Publishing. https://doi.org/10.1007/978-3-030-81358-1_7

[19] W. Martín Rosales, A. Pulido Bosch, Á. Vallejos and M. López Chicano, "Precipitaciones máximas en el Campo de Dalias y vertiente meridional de la Sierra de Gador (Almería)," Geogaceta, vol. 20, no. 6, 1251-1254, 1996. Available: https://dialnet.unirioja.es/servlet/articulo?codigo=8115318

[20] P. Ganguli and P. Coulibaly, Assessment of future changes in intensity-duration-frequency curves for Southern Ontario using North American (NA)-CORDEX models with nonstationary methods. Journal of Hydrology: Regional Studies, vol. 22, 100587, 2019, https://doi.org/https://doi.org/10.1016/j.ejrh.2018.12.007

[21] M. T Vu, V. S. Raghavan and S. Y. Liong, "Deriving short-duration rainfall IDF curves from a regional climate model," Natural Hazards, vol. 85, no. 3, 1877-1891, 2017, https://doi.org/10.1007/s11069-016-2670-9

[22] J. Li, J. Evans, F. Johnson and A. Sharma, "A comparison of methods for estimating climate change impact on design rainfall using a high-resolution RCM," Journal of Hydrology, vol. 547, 413-427, 2017, https://doi.org/https://doi.org/10.1016/j.jhydrol.2017.02.019

[23] M. Noor, T. Ismail, E.-S. Chung, S. Shahid and J. H. Sung, "Uncertainty in Rainfall Intensity Duration Frequency Curves of Peninsular Malaysia under Changing Climate Scenarios," Water, vol. 10, no. 12, 2018, https://doi.org/https://doi.org/10.3390/w10121750

[24] P. Claps and F. Laio, "Can continuous streamflow data support flood frequency analysis? An alternative to the partial duration series approach," Water Resources Research, vol. 39, no. 8, 2003, https://doi.org/https://doi.org/10.1029/2002WR001868

[25] N. Guru and R. Jha, "A Framework for the Selection of Threshold in Partial Duration Series Modeling," In R. Jha, V. P. Singh, V. Singh, L. B. Roy and R. Thendiyath (eds.), Hydrological Modeling: Hydraulics, Water Resources and Coastal Engineering (pp. 69-84), 2022. Springer International Publishing. https://doi.org/10.1007/978-3-030-81358-1_7

[26] S. Emmanouil, A. Langousis, E. I. Nikolopoulos and E. N. Anagnostou, 2020. Quantitative assessment of annual maxima, peaks-over-threshold and multifractal parametric approaches in estimating intensity-duration-frequency curves from short rainfall records. Journal of Hydrology, vol. 589, 125151, https://doi.org/https://doi.org/10.1016/j.jhydrol.2020.125151

[27] V. Agilan and N. V. Umamahesh, "Non-Stationary Rainfall Intensity-Duration-Frequency Relationship: a Comparison between Annual Maximum and Partial Duration Series," Water Resources Management, vol. 3, no. 6, 1825-1841, 2017b, https://doi.org/10.1007/s11269-017-1614-9

[28] F. Karim, M., Hasan and S. Marvanek, "Evaluating Annual Maximum and Partial Duration Series for Estimating Frequency of Small Magnitude Floods," Water, vol. 9, no. 7, 4812017, https://doi.org/10.3390/w9070481

[29] J. L. Ng, S. K. Tiang, Y. F. Huang, N. I. F. M. Noh and R. A. Al-Mansob, "Analysis of annual maximum and partial duration rainfall series," IOP Conference Series: Earth and Environmental Science, vol. 646, no. 1, 012039, 2021, https://doi.org/10.1088/1755-1315/646/1/012039

[30] H. Wang, M. J. Bah and M. Hammad, 2019, Progress in Outlier Detection Techniques: A Survey. IEEE Access, 7, 107964-108000, https://doi.org/10.1109/ACCESS.2019.2932769

[31] C. Leys, M. Delacre, Y. L. Mora, D. Lakens and C. Ley, "How to classify, detect, and manage univariate and multivariate outliers, with emphasis on pre-registration," International Review of Social Psychology, vol. 32, no.1, 2019, https://doi.org/http://doi.org/10.5334/irsp.289

[32] W. T. Hernández Guarín and P. X. Moreno Vivas, Regionalización de sequía hidrológica en la cuenca del río Bogotá a partir del método de l-momentos, 2017. Available: http://hdl.handle.net/11634/9266

[33] A.,Gutiérrez-López and R. Barragán-Regalado, "Ajuste de curvas IDF a partir de tormentas de corta duración," Tecnología y ciencias del agua, vol. 10, no. 6, 1-24. 2019. https://doi.org/10.24850/j-tyca-2019-06-01

[34] Y. Rodríguez López, N. Marrero de León and A. León Méndez, "Consideraciones practicas sobre las curvas IFD," Ingeniería Hidráulica y Ambiental, vol. 30, no. 1, 2009. Available: https://link.gale.com/apps/doc/A304466968/IFME?u=anon~91a3f3a4&sid=googleScholar&xid=c12dbfc5

[35] S. Barcia Sardiñas and O. González, "Determinación de la curva de intensidad-duración-frecuencia de Cienfuegos," Revista Cubana De Meteorología, 19(1), 3-12, 2013. Available: http://rcm.insmet.cu/index.php/rcm/article/view/140

[36] C. Castillo-García, I. Domínguez-Hurtado, Y. Martínez-González and D. Abreu-Franco, "Curvas de intensidad-duración-frecuencia para la ciudad de Santa Clara, Cuba," Tecnología y Ciencias del Agua, vol. 15, no.1, 361-408, 2024, https://doi.org/10.24850/j-tyca-15-01-09

[37] OMM, Guía de prácticas hidrológicas, Gestión de Recursos hídricos y aplicación de prácticas hidrológicas, 2011, Sexta edición ed., Vol. II. Available: https://library.wmo.int/doc_num.php?explnum_id=10038

[38] M. Naghettini, Fundamentals of statistical hydrology. Springer, 2017. https://doi.org/https://doi.org/10.1007/978-3-319-43561-9

[39] S. F. A. Xavier Júnior, J. d. S. Jale, T. Stosic, C. A. C. d Santos and V. P. Singh, "Precipitation trends analysis by Mann-Kendall test: a case study of Paraíba, Brazil," Revista Brasileira de Meteorología, vol. 35, 2020, https://doi.org/https://doi.org/10.1590/0102-7786351013

[40] R Maity. Statistical methods in hydrology and hydroclimatology. Springer Singapore, 2018, https://doi.org/https://doi.org/10.1007/978-981-16-5517-3